STUDY OF THE CAPABILITIES OF ELECTROWETTING ON DIELECTRIC DIGITAL MICROFLUIDICS (EWOD DMF) TOWARDS THE HIGH EFFICIENT THIN-FILM EVAPORATIVE COOLING PLATFORM

by

JAGATH B. YADDESSALAGE

Presented to the Faculty of the Graduate School of

The University of Texas at Arlington in Partial Fulfillment

of the Requirements

for the Degree of

DOCTOR OF PHILOSOPHY

THE UNIVERSITY OF TEXAS AT ARLINGTON

August 2013

Copyright © by JAGATH B. YADDESSALAGE

All Rights Reserved

ACKNOWLEDGEMENTS

First of all, I would like to thank my research advisor Professor Hyejin Moon, who provided me the opportunity to work in her Integrated Micro and Nanofluidics Systems Lab (IMNF Lab) and offered me to work on challenging research projects. I joined with her research group in spring 2009. She helped me to gain skill in microfabrication, writing manuscripts for paper publications and doing oral presentations at academic conferences. Her suggestions opened the path for me to think independently and improve my creativity and diligence. I admire her regular encouragement and patient supervisions. I enjoyed the weekly lab meeting very much where I had academic conversation with her and other lab members.

Second, I would like to thank my co-advisor professor Seung M. You and other committee members Professor Albert Y. Tong, Professor Cheng Luo and Professor Ankur Jain. Their comments, suggestions and guidance were very helpful for me to be successful in this research project.

Next, I would also like to thank all the faculty and staff in the Department of Mechanical and Aerospace Engineering at University of Texas at Arlington for their kind help and assistance. My especial thanks go to the staff in the Nanofabrication facility who trained and helped me with microfabrications and to the students who worked with me collaboratively.

Special thanks to my lab members Pawithra Wijethunga and Subin mac George for constructing LabVIEW program and the control board. Further I wish to thank Alex Yin Guan and Shailesh Mala with whom I carried out collaborative research work. Finally, I would like to express my gratitude to my family members for their help and support to my research work.

July 18, 2013

ABSTRACT

STUDY OF THE CAPABILITIES OF ELECTROWETTING ON DIELECTRIC DIGITAL MICROFLUIDICS (EWOD DMF) TOWARDS THE HIGH EFFICIENT THIN-FILM EVAPORATIVE COOLING PLATFORM

Jagath B.Yaddessalage, PhD

The University of Texas at Arlington, 2013

Supervising Professor: Hyejin Moon

With the current technological advancement, the size of the electronic components is being reduced to smaller and compact sizes. In the meantime, the packaging density and power consumption is ever increasing. To tackle this challenge, an efficient cooling technology is required.

Thin-film evaporation is a very efficient cooling technology. A practical application using thin-film evaporation is a spray cooling which is known as the cooling method that can handle very high heat flux. However, a random spray of coolant cannot guarantee a thin coolant film, therefore either local dry-out or flooding may occur, which hampers cooling efficiency significantly. Moreover, bulky spraying system is not suitable for cooling of small electronic devices.

As solving the drawbacks of spraying cooling, it has been suggested making thin liquid films by delivering nanoscale liquid drops to the superhydrophilic nanoporous coating (SHNC). As soon as a nanoscale liquid drop arrives to the SHNC on a hotspot, it spontaneously spreads,

forms very thin liquid film, and quickly evaporates. Electrowetting on dielectric (EWOD) digital microfluidics (DMF) is properly suited for this purpose, since it handles liquids in the form of droplets by controlling only electric fields without any bulky mechanical pumps or valves.

This dissertation reports an experimental study of three essential requirements of the EWOD DMF towards the thin-film evaporative cooling platform: (1) the high accuracy and consistency in volume of coolant nanodrops dispensed from the reservoir, (2) the fast motion of coolant nanodrops to the hotspot to avoid dry-out, and (3) the simultaneous achievement of both small volume and high frequency of nanodrop that arrives to the hotspot. In this investigation, glass-based EWOD DMF and silicon-based EWOD DMF were developed, fabricated and tested. Deionized (DI) water was used as coolant due to its high heat of vaporization.

To increase the volume accuracy of nanodrop, various electrode geometries of the reservoir were designed to control drop pinch-off point. A simple force balance was taken into account for the design. The minimum average volume error of 0.083 % for fifty drops of repeatable drop generation was achieved. The experimental results agreed with the numerically simulated results.

To increase the speed of drop motion, three major parameters that affect the speed of drop motion were investigated: The effects of electrode size, electrode geometry and surface roughness were tested. Ten times faster speed (400 mm/s) of drop motion was achieved by modifying the electrode geometry.

To achieve simultaneously high frequency and small volume of nanodrops that arrive to the hotspot, a new electrode geometry was designed to split a droplet into two while it moves toward the hotspot. Using this method, the droplet arrival frequency to the heated section was increased 4 times while the droplet volume that arrives to the heated section is 4 times smaller than the volume of droplet generated from the reservoir.

By combining all of the above results, fully completed and automated EWOD DMF was designed, fabricated and characterized to deliver liquid in small volume (down to 50 nL) with high accuracy (< 5 %) and high frequency of arrival to heated zone (over 200 Hz).

TABLE OF CONTENTS

ACKNOWLEDGEMENTS ..... ……..iii

ABSTRACT iv

LIST OF ILLUSTRATIONS..... xi

LIST OF TABLES xx

Chapter Page

1. INTRODUCTION……..…….….. 1

1.1 Electrowetting-On-Dielectric (EWOD).....2

1.2 Overview of this dissertation:
Toward EWOD in Heat Transfer Applications.....5

2. EXPERIMENT AND TESTING… 12

2.1 Reagents and Materials 12

2.2 Experimental Description (Device Fabrication).....13

2.2.1 Type-1: PCB Based EWOD Device 13

2.2.2 Type-2: Glass Based EWOD Device 17

2.2.3 Type-3: Silicon based EWOD Device 20

2.3 Testing Setup 23

2.3.1 The Fixture System of the EWOD Setup 23

2.3.2 Test Setup 1: Droplet Generation
with Volume Consistency.....25

2.3.3 Test Setup 2: Enhancing
Speed of Droplet Motion 27

3. VOLUME PRECISION AND CONSISTANCY OF DROPLETS
DISPENSED BY EWOD 29

3.1 Droplet Generation in EWOD Device.....29

3.2 Review on Droplet Generation in EWOD Device 30

3.3 New Electrodes Designs: TCC Electrodes 37

3.3.1 TCC Reservoir 37

3.3.2 How TCC Reservoir Works 38

3.3.3 Comparison of TCC Reservoir with Conventional Reservoir Design 40

3.4 Enhanced TCC Reservoir Design 42

3.4.1 TCC Reservoir with Angular Generating Site 42

3.5 Performance Tests 44

3.5.1 Device Preparation 44

3.5.2 Testing Procedure 47

3.6 Results and Discusion 48

3.6.1 Volume Precision Associated with the Conventional Reservoir: Circular Reservoir Drop 48

3.6.2 Volume Precision Associated with the Conventional Reservoir: Rectangular Reservoir Drop 52

3.6.3 Volume Precision Associated with the TCC Reservoir with Rectangular Drop generating Site 55

3.6.4 Volume Precision Associated with the TCC Reservoir with Circular and Angular Drop generating Site 59

3.7 Conclusion 67

4. STUDYING MAJOR PARAMETERS THAT AFFECT THE SPEED OF DROP MOTION 68

4.1 Parameter 1: Surface Roughness 68

4.2 Parameter 2: Electrode Size of the Square Electrodes 70

4.3 Parameter 3: Electrode Geometry 72

4.3.1 Solid Electrodes (Square Electrodes) 72

4.3.2 Stripped Electrodes (Rectangular Electrodes) 73

4.4 Results and Discussion 75

4.4.1Surface Roughness of the PCB-Based and Glass-Based EWOD Substrates 75

4.4.2 Electrode Size of the Solid Electrodes 76

4.4.3 Electrode Geometry: Solid Electrodes (Square Electrodes) 78

4.4.4 Electrode Geometry: Stripped Electrodes (Rectangular Electrodes) 86

4.4.5 Speed Enhancement: Solid electrodes 92

4.4.6 Speed Enhancement: Stripped Electrodes 93

4.5 Conclusion 97

5. SIMULTANEOUS ACHIVEMENT OF INCREASING FREQUENCY AND DECREASING VOLUME OF DROPLETS TO THE HEATED SECTION 99

5.1 Generation of Multiple Droplets: Droplet Splitting at C-Junction 100

5.1.1 Application of C-Junction to a High-Frequency Droplet Delivery System 102

5.1.2 Future Work: Complete Test Vehicle for Thin-Film Evaporative Characterization 103

5.2 Reduction of Time to Dispense a Droplet: Droplet Dispensing at L-Junction 104

5.3 Combined Method: Multiple Drop Dispensing at Y-Junction 106

5.4 Results and Discussion 108

5.4.1 Droplet Splitting at the C-Junction 135

5.4.2 Droplet splitting and delivery using Double C-junction 110

5.4.3 Reduction of time to dispense a drop: Dispensing at L-Junction 113

5.4.4 Comparing L-Junction with the Conventional Design 117

5.4.5 Multiple Drop Dispensing at the Y-Junction 119

5.4.6 Comparing C-Junction with the Y-Junction 124
5.5 Conclusion 125
6. COUCLUSION AND SUMMARY 126
REFERENCES 129
BIOGRAPHICAL INFORMATION 133

LIST OF ILLUSTRATIONS

Figure Page

1.1 Illustration of electrowetting on dielectric (EWOD) (a) before applying an electric potential, (b) after applying an electric potential 2

1.2 Illustration of drop motion by EWOD in the parallel plate configuration (a) both electrodes are grounded; drop is at equilibrium on the first electrode, (b) electric potential is applied to the second electrode; reduction in contact angle generates a pressure gradient across the liquid drop, (c) liquid drop has moved to the second electrode; both electrodes are grounded 4

1.3 Comparing two methods for making thin films in heat transfer applications; (1) Thin-films by spray cooling, (2) Thin-films by EWOD DMF and SHNC 8

1.4 Coolant delivery using EWOD DMF to the heated region which is coated with SHNC 9

1.5 Making thin-films of liquid over the superhydrophilic nanoporous coating (SHNC) by EWOD DMF coolant delivery 9

2.1 PCB based EWOD chip design (a) layout of the top layer: electrodes and vias which are placed at the middle of each electrode, (b) layout of the bottom layer: conducting lines and vias 13

2.2 Manufactured PCB based EWOD chip through the vendor (a) copper (Cu) electrodes covered with Tin/Lead plating, (b) copper (Cu) connecting lines covered with Tin/Lead plating 14

2.3 Schematic top view of the PCB based EWOD plate after filling Via holes and polishing the surface of the PCB substrate 15

2.4 Schematic side view of the PCB based complete EWOD system 16

2.5 Mask used to fabricate the glass based EWOD plate, (b) electrode geometry and dimensions 18

2.6 Schematic side view of the glass based complete EWOD system 19

2.7 The electrode pattern obtained on the Silicon substrate with to the mask shown above 21

2.8 Schematic side view of the Silicon based complete EWOD system 22

2.9 The fixture system that holds the EWOD setup and provides electrical wiring 23

2.10 Sandwiched drop of DI water in between the bottom plate and the cover plate 24

2.11 Schematic of the test setup for droplet generation with volume consistency 26

2.12 The high speed camera (FASTEC, TS3), lenses and extensic tubes used for the test 27

2.13 Schematic of the test setup for enhancing speed of drop motion 28

3.1 Top view of the cutting droplet. The droplet is stretched out along the longitudinal direction and squeezed at the middle along the orthogonal direction enhancing the neck formation 30

3.2 Sequence of dispensing a liquid droplet from the conventional reservoir. 31

3.3 Schematic of the drop dispensing system by capacitive metering 33

3.4 Dispensing droplets with consistent volume using side electrodes 34

3.5 Layout of the TCC reservoir with rectangular drop generating site 37

3.6 The sequence of drop dispensing from the TCC reservoir with rectangular drop generating site, OFF electrode is shown in Green, ON electrode is shown in Red 38

3.7 Comparing design and operational differences of the conventional and the TCC reservoirs affecting for the volume precision of the dispensing droplets, OFF electrode is shown in Green, ON electrode is shown in Red 40

3.8 Layout of the TCC reservoir with circular and angular drop generating site 42

3.9 The sequence of drop dispensing from the TCC reservoir with circular and angular drop generating site 43

3.10 Geometry and dimensions of the conventional reservoir used in the experiment for computing volume precision of the dispensing droplet 45

3.11 Geometry and useful dimensions of the modified TCC reservoir with rectangular drop generating site 46

3.12 Geometry and useful dimensions of the modified TCC reservoir with circular and angular drop generating site 47

3.13 Video frame image of the circular reservoir drop 49

3.14 Video frame image of the extruded liquid column from the reservoir 49

3.15 Video frame image of the liquid column which is subjected to the neck formation and pinch-off. A larger tail has formed behined the already formed liquid drop 50

3.16 Video frame image of the dispensed droplet. The size of the dispensed droplet is bigger than the size of the electrode 50

3.17 Volume precision and consistency of the droplets dispensed from the conventional reservoir with a circular reservoir drop. Black curve represents the experimentally obtained results. Red curve represents the numerically simulated results 51

3.18 Video frame image of the reservoir drop and the extruded liquid column from the reservoir drop 52

3.19 Video frame image of the liquid column which is subjected to the neck formation and pinch-off. A larger tail is formed behined the already formed liquid droplet 53

3.20 Volume error of the droplets dispensed from the conventional reservoir with a rectangular reservoir drop. Black curve represents the experimentally obtained results. Red curve represents the numerically simulated results 54

3.21 Video frame image of the initial reservoir drop. Both T-electrode and the drop generating site are wetting 55

3.22 Video frame image showing the motion of the menisci on the de-wetting T-electrode at the beginning of droplet dispensing 55

3.23 Video frame image of the dispensing droplet. Menisci align along the edges *a,b* and *c* of the drop generating site and the front edges y_{1B} and y_{2B} of the first C-electrode and stop their motion 56

3.24 Video frame image of the dispensing droplet. Pinch-off happens at the point the two menisci meet each other 57

3.25 Video frame image of the dispensing droplet. De-wetting meniscus of the reservoir drop is moving back to the reservoir 57

3.26 Video frame image of the dispensed droplet. Volume of the dispensed droplet is almost equal to the volume occupied by the drop generating site. Front boundary of the reservoir drop is aligned over the front edge of the first C-electrode 58

3.27 Volume precision and consistency of the droplets dispensed from the conventional reservoir with a rectangular reservoir drop. Black curve represents the experimentally obtained results. Red curve represents the numerically simulated results 59

3.28 Video frame image of the initial reservoir drop. Both T-electrode and the drop generating site are wetting 60

3.29 Video frame image showing the motion of the meniscus on the de-wetting T-electrode at the beginning of droplet dispensing. The meniscus starts to align over the front circular edge of the drop generating site and the front edges y_{1B} and y_{2B} of the first C-electrode 60

3.30 Video frame image of the dispensing droplet. Liquid meniscus has perfectly aligned along the front circular edge of the drop generating site. Liquid meniscus is still aligning along the front edge of the first C-electrode 61

3.31 Video frame image of the dispensing droplet. At the reservoir side, liquid moves parallel along the vertical edge of the first C-electrode. At the drop generating site, liquid follows the angular edge of the drop generating site 61

3.32 Video frame image of the dispensing droplet. At the reservoir side, liquid moves parallel along the horizontal edges x_{1B} and x_{2B} of the first C-electrode. At the drop generating site, liquid follows the remaining halfway of the angular edge towards the tip of the angle 62

3.33 Video frame image of the dispensed droplet. Volume of the dispensed droplet is equal to the volume occupied by the drop generating site. Front boundary of the reservoir drop is aligned over the front edge of the first C-electrode 63

3.34 Volume precision and consistency of the droplets dispensed from the TCC reservoir with circular and angular drop generating site 64

3.35 Volume of the droplets dispensed from the different reservoirs: The area of the drop generating site is the same (4.00 mm^2) 65

3.36 Percentage volume precision of the droplets dispensed from the different reservoirs: The area of the drop generating site is the same (4.00 mm^2) 66

4.1 Electrode arrays with two different electrode sizes to study effect of electrode size on the speed of drop motion 71

4.2 In each electrode array, arrangements between two adjacent electrodes are different; 1st row: square electrodes only without any interdigitating fingers as a reference, 2nd row: many interdigitating fingers, and 3rd row: a few fingers 71

4.3 Motion of a droplet over the solid electrodes 72

4.4 Motion of a droplet over the stripped electrodes 73

4.5 Comparison of drop motion on solid and stripped electrodes 74

4.6 Surface irregularities on the surface of the PCB substrate over the filled via hole 75

4.7 Surface irregularities on the surface of the PCB substrate besides the via hole 75

4.8 Surface roughness of the glass substrate 76

4.9 Studying the effect of electrode size for the speed of drop motion on the glass-baes EWOD device. Video frame image shows higher speed of drop motion for larger electrode 76

4.10 Studying the effect of electrode size for the speed of drop motion on the Si-based EWOD device. Video frame image shows higher speed of drop motion for larger electrodes 77

4.11 Video frame image of the droplet siting on the right electrode just before it starts the motion (time: $t = 0$) 78

4.12 Video frame image of the moving droplet (time: $t = 4\ ms$) 78

4.13 Video frame image of the moving droplet (time: $t = 8\ ms$) 79

4.14 Video frame image of the moving droplet (time: $t = 11\ ms$) 79

4.15 Video frame image of the moving droplet (time: $t = 21\ ms$) 80

4.16 Video frame image of the moving droplet (time: $t = 25\ ms$) 80

4.17 Video frame image of the moving droplet (time: $t = 30\ ms$) 81

4.18 Video frame image of the moving droplet (time: $t = 33\ ms$) 81

4.19 Video frame image of the moving droplet (time: $t = 36\ ms$) 82

4.20 Video frame image of the moving droplet (time: $t = 40\ ms$) 82

4.21 Predicted $V - t$ trajectory of head and tail by using equation [4.4]. 84

4.22 Instantaneous velocity of the droplet motion. Red curve represents the head motion. Black curve represents the tail motion. Electrode size: $2 \times 2\ mm^2$, applied voltage: 125 V, switching time 100 ms 85

4.23 Video frame image of the droplet siting on the electrodes E_3-E_7 just before it starts the motion (time: $t = 0$) 86

4.24 Video frame image of the moving droplet (time: $t = 1\ ms$) 87

4.25 Video frame image of the moving droplet (time: $t = 2\ ms$) 87

4.26 Video frame image of the moving droplet (time: $t = 3\ ms$) 88

4.27 Video frame image of the moving droplet (time: $t = 4\ ms$) 88

4.28 Video frame image of the moving droplet (time: $t = 5\ ms$) 89

4.29 Video frame image of the moving droplet (time: $t = 6\ ms$) 89

4.30 Video frame image of the moving droplet (time: $t = 7\ ms$) 90

4.31 Instantaneous velocity of the droplet motion. Red curve represents the motion H. Black curve represents the motion of T. Electrode size: $0.4 \times 2\ mm^2$, applied voltage: 125 V, switching time 20 ms Both H and T reach to a maximum velocity (~ 140 mm/s) and then decelerates 91

4.32 Instantaneous velocity of the head motion on solid electrodes corresponding to two different switching times. Red curve represents the motion of T at 66 ms. Black curve represents the motion of H at 100 ms. Electrode size: $2 \times 2\ mm^2$, applied voltage: 125 V 92

4.33 Instantaneous velocity of the motion of H on stripped electrodes corresponding to two different switching times. Black curve represents the motion of Tat 10 ms. Red curve represents the motion of H at 20 ms. Electrode size: $2 \times 2\ mm^2$, applied voltage: 125 V 94

4.34 Instantaneous velocity of the motion of H on stripped electrodes corresponding to two different switching times. Black curve represents the motion of H at 8 ms. Red curve represents the head motion at 10 ms. Electrode size: $2 \times 2\ mm^2$, applied voltage: 125 V 95

4.35 Instantaneous velocity of the motion of H on stripped electrodes corresponding to two different switching times. Black curve represents the motion of H at 5 ms. Red curve represents the head motion at 8 ms. Electrode size: $2 \times 2\ mm^2$, applied voltage: 125 V 96

5.1 C-junction splitting, 1) Before starting the actuation, liquid column is on the activated rectangular electrode. Both square electrodes are grounded, 2) Liquid column undergoes a neck formation; inner boundary has a fixed radius of curvature (R_1), outer boundary is approaching towards the inner boundary with increasing radius of curvature (R_2), 3) After separation, two droplets with equal volume are created 101

5.2 Drop delivery system with decreased droplet volume and increased delivery frequency. Electrode path starting at the TCC reservoir is branching out at the C-junction. Four TCC reservoirs together with C-junction splitting mechanism were placed at the four sides from the heated region 103

5.3 Schematic diagram of the proposed method of delivering coolant to the SHNC to make thin-film of liquid 104

5.4 Dispensing a droplet from the L-junction reservoir. Reservoir drop does not supply any backward force to cause pinch-off 105

5.5 Dispensing two droplets at the Y-junction simultaneously. Droplet splitting happens at the same speed it moves on the stripped electrodes 107

5.6 Droplet dispensed from the TCC reservoir. The size of the square electrode on which droplet occupies is $2 \times 2\ mm^2$ 108

5.7 Fine liquid column on the rectangular electrode. Electrode size: $0.96\ \times 4.24\ mm^2$ 109

5.8 Liquid column undergoes a neck formation; inner boundary has a fixed radius of curvature, outer boundary is approaching towards the inner boundary with increasing radius of curvature 109

5.9 After pinch-off, two droplets with equal volumes are created. Electrode size: (E_1, E_2 = $1.41\ \times 1.41 mm^2$) 110

5.10 Droplet dispensed from the TCC reservoir. Electrode size on which the droplets exists is $2 \times 2\ mm^2$ 110

5.11 Splitting at the 1st C-junction. Electrode size: $1.41\ \times 1.41 mm^2$ 111

5.12 Splitting at the 2nd C-junction. Electrode size: $1.0\ \times 1.0\ mm^2$ 111

5.13 Resulted four droplets at the end of the splitting process. Electrode size: $1.0 \times 1.0\ mm^2$ 112

5.14 Volume precision of the liquid droplet moving from the TCC reservoir to the spreading zone in the Figure 5.16 112

5.15 At the beginning of forming a droplet. De-wetting occurs on the stripped electrode E_{11} and pinch-off starts. Stripped electrodes E_1-E_{10}:wetting, E_{11}: de-wetting, E_{12}-E_{15}: wetting, E_{16},E_{17},…de-wetting 113

5.16 Droplet is on electrodes E_{13}-E_{17}. De-wetting occurs on both E_{11} and E_{12}. Neck formation is becoming narrower 114

5.17 Droplet is on electrodes E_{14}-E_{18}. De-wetting occurs on electrodes E_{11}-E_{13}. Neck formation is becoming narrower 114

5.18 Square shaped droplet has already formed on electrodes E_{15}-E_{19}. De-wetting occurs on electrodes E_{11}-E_{14}. Neck formation is becoming narrower 115

5.19 Already formed droplet before pinch-off 115

5.20 Comparison of L-junction drop dispensing with the conventional method 117

5.21 Droplet dispensed from the L-junction has arrived to the Y-junction. Stripped electrodes 24-28 are wetting 119

5.22 Liquid droplet at the beginning of Y-junction splitting 119

5.23 Formation of two droplets 120

5.24 Already formed two droplets before the separation: fixed radius of curvature at the middle of the front meniscus 121

5.25 Pinch-off of the two droplets 121

5.26 Created two droplets after separation 122

5.27 Volume precision of one liquid droplet moving from the L-junction to the spreading zone 123

5.28 Comparison of droplet splitting at the Y-junction with the droplet splitting at the C-junction 124

LIST OF TABLES

Table Page

1.1 Different cooling techniques, corresponding heat fluxes and heat transfer coefficients 5

5.2 Comparison of speed of drop dispensing and reproducibility of TCC reservoir and L-junction, Supplied voltage is 125 V for both cases 116

5.3 Comparing the capability of drop splitting at both C-junction and Y-junction 122

CHAPTER 1

INTRODUCTION

Surface tension forces show interesting wonders in the natural world associating small volume of liquid [1]. For an example smaller liquid drops are in spherical shapes. A steel needle which is denser than water can be floated on the water surface. When the size of the liquid handling system shrinks down to the micro scale, which is much less than one millimeter, surface tension becomes dominant over most other forces, such as gravity, viscosity and inertia [2]. This dominant surface tension can be utilized in verity of practical microfluidics applications such as thermocapillarity and electrocapilarity [3].

Thermocapillarity refers to the change in surface tension at the fluid-fluid interface between two immiscible media under a temperature gradient [4]. This phenomenon can be utilized to induce motion of liquid drops or bubbles immersed in a second phase. Sammarco et al studied the motion of a drop of mineral oil in a microchannel under a temperature gradient [5]. They showed that the velocity of the drop in the microchannel is linearly proportional to the temperature deference at either side of the drop. Pratap et al studied the motion of drops of decane on PDMS- coated glass surface under a temperature gradient [4]. They measured the velocity of the drop for different applied temperature gradients and the drop sizes. However, liquid handling in microfluidics deices based on thermocapillary principle has such disadvantages as use of high power, evaporation of the liquid due to heat generation, and low speed of drop motion [3].

Electrocapillarity refers to the change in surface tension at the fluid-fluid interface between two immiscible media under externally applied electrical potential [6]. Liquid actuation in microfluidics devices using electrocapillary effect has very attractive features over the thermocapilary effect such as low power consumption, higher speed of drop motion and no

heating of the liquid drop [3]. Piston motion of a mercury droplet confined in a microhole is reported by Wan et al [7] and was actuated by electrocapillary effect. They have achieved larger displacements of the droplet with very low voltages. Berge et al used electrocapillary effect to change the contact angle at the liquid-liquid interface of a transparent liquid drop in order to achieve variable focal length [8]. However, liquid handling in microfluidics deices based on electrocapillary principle is limited to the systems that contains a liquid metal as an electrode and a electrolyte solution.

Electrowetting (EW) [9] and Electrowetting on Dielectric (EWOD) [10] which are similar to the electrocapillarity, can be used to actuate liquid in micro scale using only a single phase of liquid [3], thus allow more flexibilities in the selection of materials and the device design.

1.1 Electrowetting-On-Dielectric (EWOD)

Electrowetting-On-Dielectric (EWOD) refers to the modification of wettability of a liquid drop placed on a hydrophobic and dielectric coated solid surface with an applied electric potential [11, 12]. There are two configurations in EWOD, the single- plate configuration [13] and the parallel-plate configuration [14, 15]. Figure 1 illustrates the basic operation of the single plate configuration (i.e. sessile drop configuration).

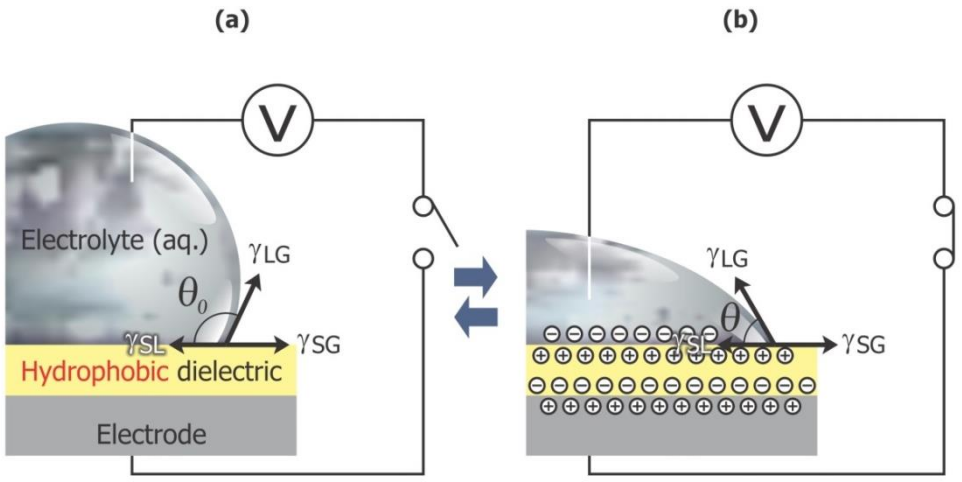

Figure 1.1 Illustration of electrowetting on dielectric (EWOD), (a). Before applying an electric potential, (b). After applying an electric potential

In the single plate configuration, a drop of electrolyte (polarizable or conducting) is placed on a solid electrode which is coated with layers of dielectric and hydrophobic. This dielectric layer insulates the liquid drop from the electrode and prevents any electric current passing through the system. Without any electric potential applied between the electrode and the electrolyte, the charge build-up over the surfaces is negligible (Figure 1.1 (a)).

An electric potential applied between the electrolyte and the solid electrode, induces charges over the surfaces (Figure 1.1 (b)) [12]. This charge redistribution makes the interfacial energy between the solid surface and the electrolyte decrease [12, 16]. This interfacial energy is related to the contact angle (θ) between the solid surface and the electrolyte [12, 16]. This decrease in interfacial energy results a decrease in contact angle [12, 16].

In the parallel plate configuration, a drop of electrolyte is sandwiched between two plates assembled in a parallel structure. The cover plate consists of a grounding electrode coated with a layer of hydrophobic insulation. The bottom plate consists of array of distinct electrodes that can be actuated independently from an outside source. This plate is covered by thin layers of dielectric and hydrophobic insulation. A uniform spacer gap is maintained between the top plate and the bottom plate. A precisely controlled volume of liquid is generated from a reservoir such that the footprint of the liquid drop is approximately equal to the top surface area of the electrode. The gap between two electrodes is controlled to be very small such that the liquid drop is in contact with the neighboring electrodes. The surrounding medium around the liquid drop is air. Initially, all the electrodes in the bottom plate are grounded (Figure 1.2a). When an electric potential is applied to a neighboring electrode, the decrease in contact angle generates a pressure gradient across the liquid drop [3] (Figure 1.2b). This pressure difference moves the liquid drop from the existing electrode to the neighboring electrode (Figure 1.2c).

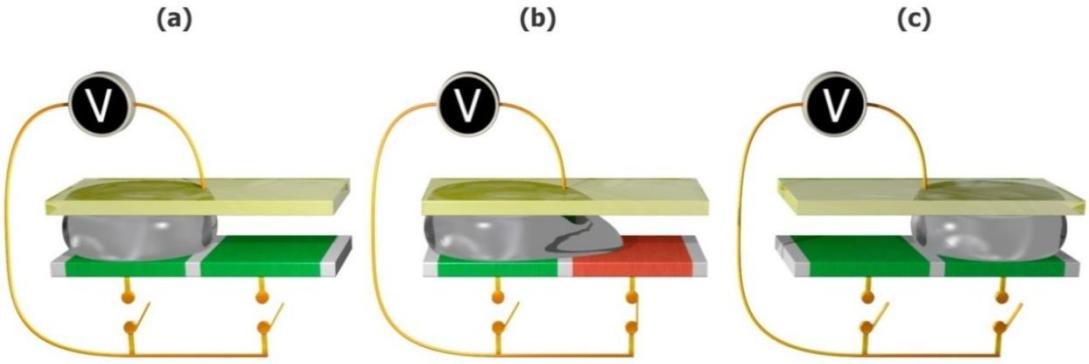

Figure 1.2 Illustration of drop motion by EWOD in the parallel plate configuration, (a). Both electrodes are grounded; drop is at equilibrium on the first electrode. (b). Electric potential is applied to the second electrode; reduction in contact angle generates a pressure gradient across the liquid drop. (c). Liquid drop has moved to the second electrode; both electrodes are grounded.

The liquid drop can be moved in any direction along an array of electrodes by sequentially actuating individual electrodes one by one. A well-defined speed of drop motion can be archived by varying the actuating switching time. In addition to generating and moving the liquid drop, EWOD can be used to perform more digital microfluidic operations such as cutting and merging [17]. Since any current does not pass through the EWOD system, it indicates lower power consumption with no heat generation and no evaporation of the liquid drop. The unique feature of this EWOD system is that it consists of microfluidic device and the control board without any outside mechanical connections except electrical connections [15, 18]. Further, the design and fabrication of the EWOD system is much simpler since the system does not need any pressure source like microchannels, micropumps, or microvalves to drive the liquid drop [19]. Today EWOD based microfluidic devises have been executed in a wide range of applications such as chemical synthesis in Chemistry, extraction of proteins in Biology, sample clean-up and extraction in Medicine [20, 21].

1.2 Overview of this dissertation: Toward EWOD in Heat Transfer Applications

Table 1.1 Different cooling techniques, corresponding heat fluxes and heat transfer coefficients (Glassman, 2005 [22])

Mechanism	Cooling Method	Heat Transfer Coefficient ($W/cm^2 \cdot K$)	Highest Heat Flux (W/cm^2)	Reference
Single Phase	Free Air Convection	0.0005-0.0025	15	(Mudawar, 2001; Azar, 2002)
Single Phase	Forced Air Convection, (Heat Sink with a fan)	0.001-0.025	35	(Mudawar, 2001)
Single Phase	Natural Convection with FC	0.1	0.1-3	(Anderson et al., 1989)
Single Phase	Natural Convection with water	0.08-0.2	5-90	(Mudawar, 2001)
Two Phase	Heat Pipes (water)	-NA-	250	(Zuo et al., 2001)
Single Phase	Micro-channel	-NA-	790	(Tukerman et al., 1981)
Electrical	Peltier Cooler	-NA-	125	(Riffat et al., 2004)
Two phase	Pool boiling with porous media	3.7	140	(Rainey et al., 2003a)
Two Phase	Sub-cooled Flow Boiling	2	129	(Sturgis and Mudawar, 1999)
Two Phase	Micro-channel Boiling	10-20	275	(Faulkner et al., 2003)
Two Phase	Spray Cooling	20-40	1200	(Pais et al., 1992)
Two Phase	Jet Impingement	28	1820	(Overholt et al., 2005)

With the recent advancement of semiconductor technology, the size of the electronic components has decreased while the package densities have increased to achieve higher performance. Hence, the power consumption of the component increases proportionately. As a result of that, heat generation of components continue to increase creating non uniform temperature distributions within the components. To maintain the stability of these components, the generated heat should be removed from the system and satisfactory temperature range

should be maintained throughout the component. To accomplish this requirement, higher heat flux cooling techniques are needed to address the growing thermal profiles of the components.

As a solution for the above issue, various research groups from around the world reported a number of cooling techniques for the electronics cooling. The table 1.1 shows some of the selected cooling techniques, corresponding heat fluxes and heat transfer coefficients [22]. According to the table 1.1, forced air convection by a heat sink with a fan has the lowest cooling capability. Higher cooling performance was achieved by liquid cooled heat pipes and micro channels.

Very recently, EWOD has been proposed as a promising technique for electronic hotspot cooling [23, 24, 25]. Paik et al have used EWOD to cool the hotspot with water as the coolant [22]. They investigated essential parameters that can affect for heat transfer applications such as response of droplet actuating frequency, response of heat flux density at the hot-spot and the response of the drop volume. However, the cooling potential of this method was limited due to dry-out of the coolant at the hot-spot. Thus, coolant with higher thermal stability were needed at higher temperatures above 100 ^{0}C. To tackle dry-out problem, Moon et al introduced a cooling system based on EWOD DMF that uses Room temperature Ionic Liquids (RTILs) as the coolant [24]. Unlike water, ionic liquid has the property of being thermally stable at higher temperatures resulting in no evaporation during the cooling process [26]. However, the thermal conductivity values of ILs are lower than that of the water [27]. As a result of that, the cooling performance of ILs is poor at the hot-spot [24]. Nikapitiya et al showed that thermal conductivity of ILs can be enhanced by mixing multiwall carbon nanotubes (MWCNT) with the base fluids (ILs) [28]. They reported a thermal conductivity enhancement of 16 % by mixing CNT with a particle concentration of 0.25 mol. dm^{-3} with the IL (trihexyl (tetradecyl) posphonium dicyanamide). They further enhanced the thermal conductivity up to 20 % under externally applied strong magnetic field (1530 Gauss). Although single phase droplet-base cooling is

promising for the applications in small electronics with relatively low heat flux, phase change cooling is highly sought for very high heat flux applications.

Spray cooling can be introduced as such high efficient two phase cooling technique which utilizes evaporation through liquid boiling. The main functionality of ideal chip cooling system is providing higher rate of heat transfer uniformly over a larger area [29]. Spray cooling is properly suited for this purpose since it cools hot surfaces of high performance electronic devices in a compact volume [29]. Spray cooling uses a discharge of tiny liquid droplets injected by atomization nozzle on to the heated surface to enhance the rate of heat removal as a cooling technique with phase change [29, 30]. The droplets already hit the surface are spread over large surface area by the continually injecting flow of droplets. Thus, the hot surface is regularly wetted by the impinging droplets and a thin film of liquid is formed over the hot surface [29]. The rate of heat removal is enhanced as a result of latent heat absorbed by the liquid droplets during the evaporation process. This enhancement of heat transfer is related to number of mechanisms such as conduction, convection, nucleation, de-saturation of the gas, and secondary nucleation entrainment [29, 31].

However, several practical problems are anticipated with spray cooling to make thin coolant films in heat transfer applications. First, the volume of the tiny droplets in the spray cannot be precisely controlled. Next, the frequency of the droplets impinging on a heated surface is not well defined. Therefore either local dry-out or flooding may occur, which hampers cooling efficiency significantly. Further, the evaporated vapor flow is obstructed by the coolant droplets sprayed towards the hot surface. Some of the impinged coolant droplets are re-bounced from the hot surface without evaporation (Figure 1.3). Therefore, random spray of coolant cannot guarantee a well-defined and properly controllable thin coolant film.

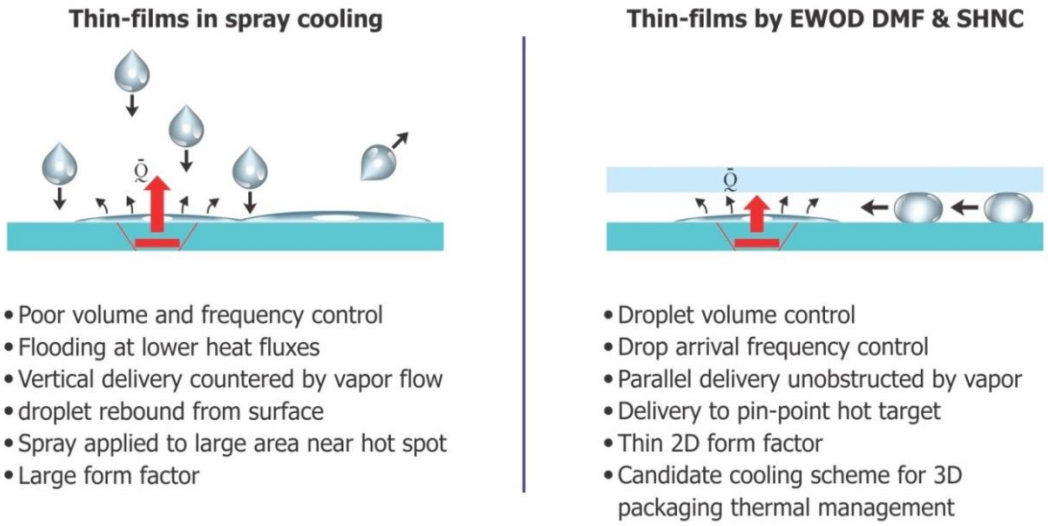

Figure 1.3 Comparing two methods for making thin films in heat transfer applications; (1) Thin-films by spray cooling, (2) Thin-films by EWOD DMF and SHNC

As solving the drawbacks of spraying cooling, it has been suggested making thin liquid films by delivering nanoscale liquid drops by EWOD DMF to the superhydrophilic nanoporous coating (SHNC). Electrowetting on dielectric (EWOD) digital microfluidics (DMF) is properly suited for this purpose since it handles liquids in the form of droplets by controlling only electric fields without any mechanical pumps or valves. As soon as a nanoscale liquid drop arrives to the SHNC on a hotspot, it spontaneously spreads, forms very thin liquid film, and quickly evaporates. Not like in the spray cooling, the volume of the coolant droplet can be precisely controlled by EWOD. The speed of coolant droplet motion and their arrival frequency to the designated spot can be properly controlled depending on the application. The parallel delivery of the coolant droplets does not interfere the vapor evaporated from the hot surface. Therefore, EWOD DMF is properly suited for delivering tiny droplets to the hotspot to make thin coolant films.

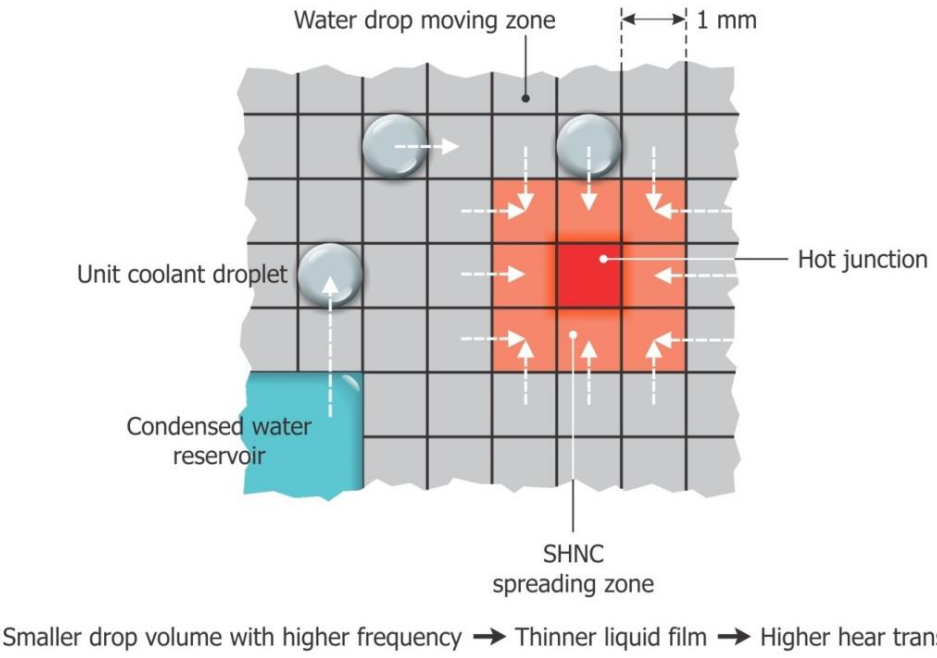

Figure 1.4 Coolant delivery using EWOD DMF to the heated region which is coated with SHNC

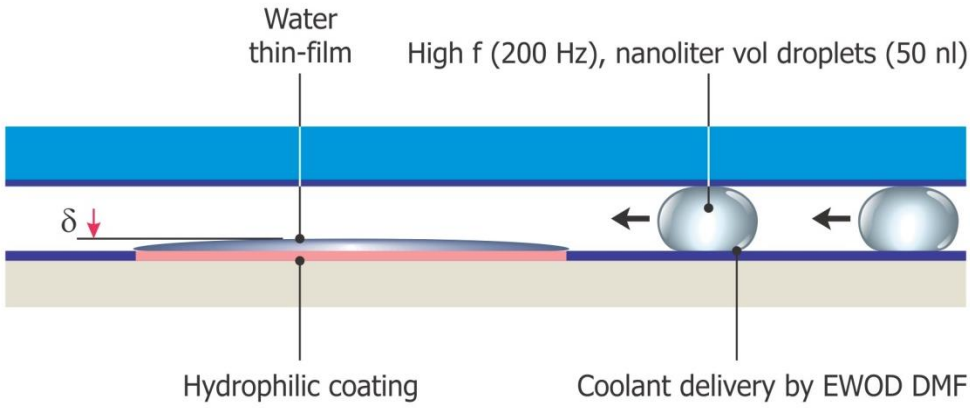

Figure 1.5 Making thin-films of liquid over the superhydrophilic nanoporous coating (SHNC) by EWOD DMF coolant delivery.

In this present dissertation, we study the liquid delivery capabilities of EWOD DMF towards high efficient cooling technology based on thin-film evaporative cooling platform. The major challenges of the liquid delivery part are, (1) generating coolant drop from the reservoir

with higher accuracy in volume, (2) the fast motion of coolant drops to the hotspot to avoid dry-out (3) increasing the droplet arrival frequency to the heated section while decreasing the droplet volume that arrives to the heated section.

Chapter 3 deals with the challenge of the accuracy in volume of a unit drop. The volume accurady is crucial to maintain steady state operation of thin-film evaporation. To meet this requirement, a new reservoir called TCC reservoir was designed and tested. In the TCC reservoir, the point of pinching off is consistent with a very short tail formation. Volume of the generated drop does not depend on the volume of the reservoir drop. Identical volume of drop generation was achieved for repeatable drop generation with a very minimum error (~ 3 %). Experimental results agreed with the numerically simulated results validating the design. To further reduce the volume error of the generated drop, this TCC reservoir was modified and optimized to completely remove the tail formation of the generated drop. According to the experimental results, very small volume error (~ 0.083 %) was achieved that is much less than that of the previous value.

In Chapter 4, enhancing the speed of drop motion is demonstrated. In the actual combined device with higher heat flux densities, droplets with nanoliter volumes must be transported at higher speeds to the hotspot area to avoid dry out problem. The maximum speed of drop motion on conventional solid electrodes (~ 40 mm/s) is lower due to smaller EWOD force acting on the drop and higher inertia resisting the drop motion. To increase the speed of drop motion, three major parameters that affect the speed of drop motion were investigated. The effect of electrode size, electrode geometry and surface roughness were tested. By modifying the electrode geometry and actuating methodology, a new electrode geometry called stripped electrodes was designed to enhance the speed of drop motion. In stripped electrodes, the EWOD force acting on the drop is much higher than in the case of solid electrode. Further, the inertia resisting the drop motion is much less than compared to the solid electrodes. As a

result of that, ten times faster speed (400 mm/s) of drop motion was achieved in stripped electrodes.

In Chapter 5, the bottleneck to high frequency of drops arriving a hotspot is tackled. Not only the higher speed of drop motion but the higher frequency of droplet arrival to the heated section is also a crucial requirement to avoid dry out at the hotspot. To increase the droplet arrival frequency to the heated section, new multiple drop generating technique called C-junction splitting was developed to split a droplet into two with consecutive electrodes. Using this method, the droplet arrival frequency to the heated section was increased while the droplet volume that arrives to the heated section was decreased to a value that is 4 times smaller than the volume of the generated drop from the TCC reservoir.

By combining all of the above results, fully completed and automated EWOD DMF was designed, fabricated and characterized to deliver liquid in small volume (down to 50 nL) with high accuracy (< 5 %) and high frequency of arrival to heated zone (over 200 Hz). In future, to further improve the drop delivery system, a new reservoir called T-junction reservoir with stripped electrodes and a new multiple drop generating technique called Y-junction splitting with stripped electrodes were introduced. The T-junction reservoir with stripped electrodes shows eighteen times faster speed of drop generation than the previously mentioned TCC reservoir with solid electrodes. The Y-junction splitting with stripped electrodes demonstrates eight times faster speed of multiple drop generation than the previously mentioned C-junction splitting with solid electrodes.

CHAPTER 2

EXPERIMENT AND TESTING

This chapter presents detailed procedures of EWOD devices fabrication on different types of substrates and the integrated testing setup used in this work. It is noted that the same fabrication methods and testing setup described in this chapter were commonly used for parametric studies described in following chapters. Therefore, in each of following chapters will not repeat the device fabrication unless the parameters of interest needs to be described separately.

The first section explains the fabrication procedure of EWOD device on a printed circuit board (PCB). The second and the third section introduce the fabrication details of EWOD devices based on glass and silicon substrates, respectively. Finally, the last section demonstrates the fabricated EWOD device testing setups and facilities.

2.1 Reagents and Materials

Indium tin oxide (ITO) coated glass wafers were purchased from Delta Technologies, LTD. Stillwater, MN. The thickness of the ITO layer of these wafers ranges1,200 - 1,600 Å, and sheet resistance ranges 8-12 Ω-cm. Test quality Silicon wafers with 4" in diameter, P type, <100> orientation and 0.5 mm thickness were purchased from Nova Electronic Materials, LLC, Flower Mound, TX. Teflon solution was prepared by dissolving 4% (w/v) of Teflon AF1600 (E.I. du Pont de Nemours and Company, Wilmington, DE) in Fluoroinert FC-40 solvent (SIGMA-ALDRICH, Atlanta,GA). DI water (Resistivity at 25 °C -18.0 MΩ•cm) was obtained from Nanofabrication facility at the University of Texas at Arlington. Clean room reagents including S1813 and SU-8-5 photoresists, MF-319 developer, 1165 remover from MicroChem Corp (Newton MA) and CR-7 Chrome Mask Etchant from OMG Cyantek (Fremont, CA) were used to fabricate EWOD devices.

2.2 Experimental Description (Device Fabrication)

2.2.1 Type-1: PCB Based EWOD Device

As mentioned in the introduction, in the EWOD digital microfluidics device, droplets of nanoliter volume can be transported along an array of discrete electrodes. The number of electrodes and electrode arrangement depend on the predefined microfluidic protocol. These electrodes are accessed from conducting lines coming from exterior control circuit. When the number of electrodes in the system becomes higher and the device becomes more complex, the access lines must run through the electrode gap. Leaving space for access lines in between the electrode gap increases the electrode gap and that decreases the efficiency of the EWOD system [32].

As a solution, Gong et al reported a multilayered Printed Circuit Board (PCB) based EWOD device that simplify the fabrication [32]. In this PCB based EWOD device, surface mounting solder pads are patterned on the top layer of the PCB while the connecting lines are pattered in the bottom layer. These solder pads are used as the electrodes for EWOD actuation. Underlying connecting lines access these electrodes directly and independently through vias placed at the middle of the each electrode. Since its simplicity of manufacturing and easier handling, firstly, we used multilayered PCB as the EWOD substrate. The detailed procedure of developing PCB based EWOD device is given below.

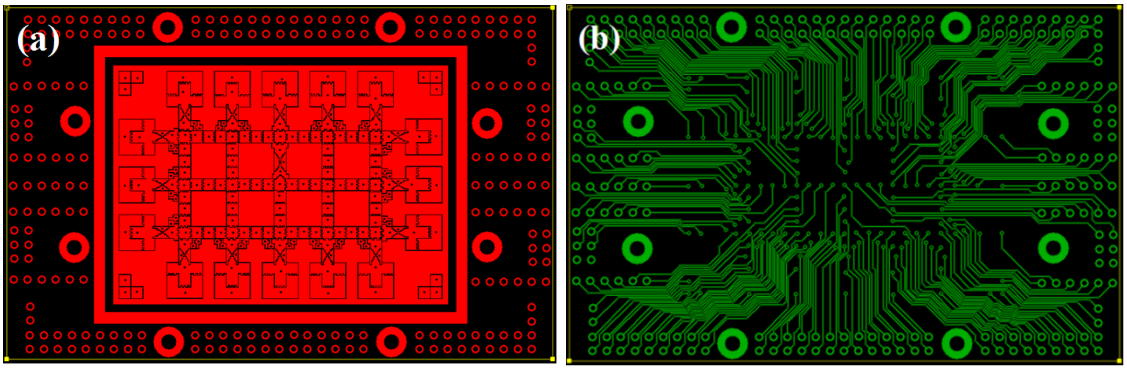

Figure 2.1 PCB based EWOD chip design (a) Layout of the top layer: electrodes and vias which are placed at the middle of each electrode. (b) Layout of the bottom layer: conducting lines and vias

Electrode pattern was designed in Express PCB, a layout drawing software. The top layer of this PCB design consists of solder pads (electrodes) which is represented Red in color (Figure 2.1.a). The bottom layer of the PCB design consists of connecting lines (conducting lines) which are represented Green in color (Figure 2.1.b).

The chip was got manufactured through the vendor Express PCB. The gap between two electrodes is 179 µm. The diameter of the connecting via is 356 µm. The thickness of the surface mounted electrode is 43 µm. Electrodes and connecting wires are manufactured with Copper (Cu) and they are covered with the Tin/Lead plating (Figure 2.2).

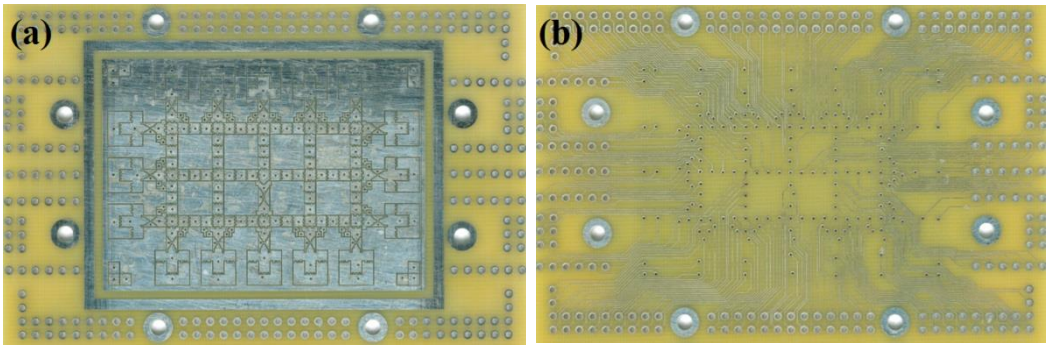

Figure 2.2 manufactured PCB based EWOD chip through the vendor. (a). Copper (Cu) electrodes covered with Tin/Lead plating. (b). Copper (Cu) connecting lines covered with Tin/Lead plating

The current PCB substrate, as we receive from the vendor, has higher surface topography and it prevents droplet dispensing by EWOD. Therefore, this PCB substrate requires additional post process to reduce its surface topography and improve EWOD performance. First, the via holes placed at the middle of the each electrode exerts resistive force on the moving liquid drop on the PCB surface and prevents the drop motion. To reduce this resistive force, via holes were filled with lead. Further, the trench between the electrodes also exerts resistive force on the moving liquid drop and prevents the droplet to spread to the adjacent electrode. To reduce this resistive force, this trench was filled with SU-8-5. Moreover, the higher surface roughness of the PCB surface adds additional resistive force to the moving

drop and slows down the drop motion. To reduce this higher surface topography, the PCB surface was smoothened with Chemical Mechanical Polishing (CMP) (Figure 2.3).

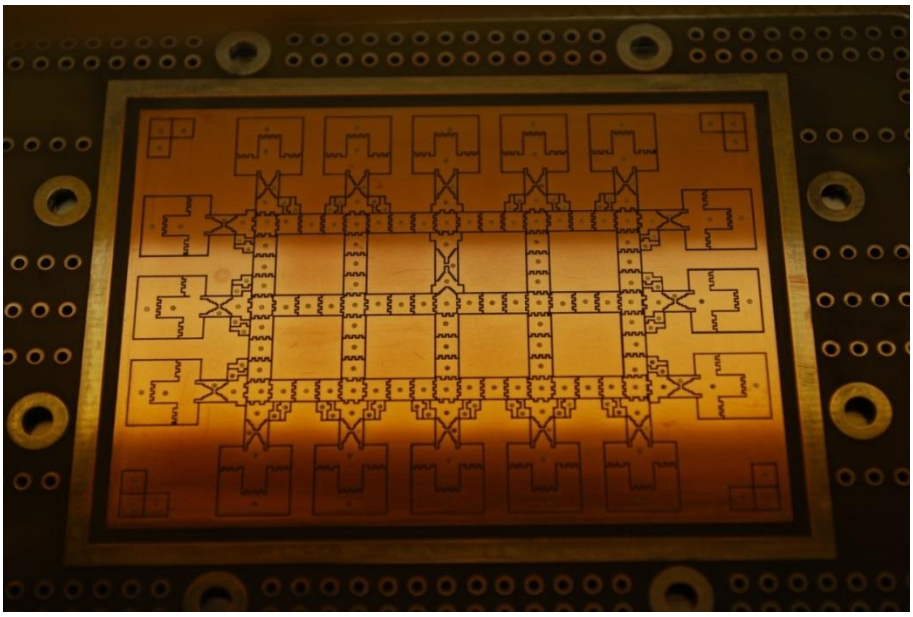

Figure 2.3 Schematic top view of the PCB based EWOD plate after filling Via holes and polishing the surface of the PCB substrate

After this post-PCB process, the surface of the PCB substrate was coated with dielectric (SU-8-5) and hydrophobic (Teflon) materials at the Nanofabrication facility, the University of Texas at Arlington according to the following procedure. The PCB substrate was first cleaned thoroughly with non-halogenated hydrocarbons: Acetone, Methanol, Isopropanol and then rinsed with DI water. The PCB substrate was then dehydrated at 150 ^{0}C for 2 minutes. A layer of dielectric (SU-8-5, Microchem) was spin coated on the PCB surface with following recipe; spin speed was ramped up to 500 rpm with 100 rpm/s for 5s; ramping with 900 rps/s to 2000 rpm for 30s. This resulted in 5 μm thick uniform dielectric layer. The PCB substrate with the coated dielectric layer was baked to harden the layer at 65 ^{0}C for 1 min and then 95 ^{0}C for 3 min.

Photo Lithography was done for this PCB substrate with a light dose of 140 mJ/cm^2 on the Backside-Aligner (OAI 806MBA). The PCB substrate was then baked at 65 ^{0}C for 1 min, 95 ^{0}C for 1 min and 150 ^{0}C for 5 min.

A layer of Teflon was spin coated on the dielectric coated PCB surface to provide hydrophobicity with following recipe; spin speed was ramped up to 1000 rpm with 300 rpm/s for 30s. This resulted in 300 nm thick uniform hydrophobic layer. After that, dielectric and hydrophobic layer coated PCB substrate was annealed at 150 ^{0}C for few hours to increase surface uniformity. Finally, the ITO coated cover plate was first cleaned thoroughly with non-halogenated hydrocarbons: Acetone, Methanol, Isopropanol and then rinsed with DI water. The cover plate was then dehydrated at 150 ^{0}C for 2 minutes. A layer of Teflon with a thickness 300 nm was spin coated on the cover plate to provide hydrophobicity, and annealed at 150 ^{0}C for few hours to increase surface uniformity.

A drop of DI water (~ 0.4 µl) was dispensed onto the reservoir using a pipette and the top plate was positioned to provide a uniform spacer gap between the bottom plate and the cover plate (Figure 2.4).

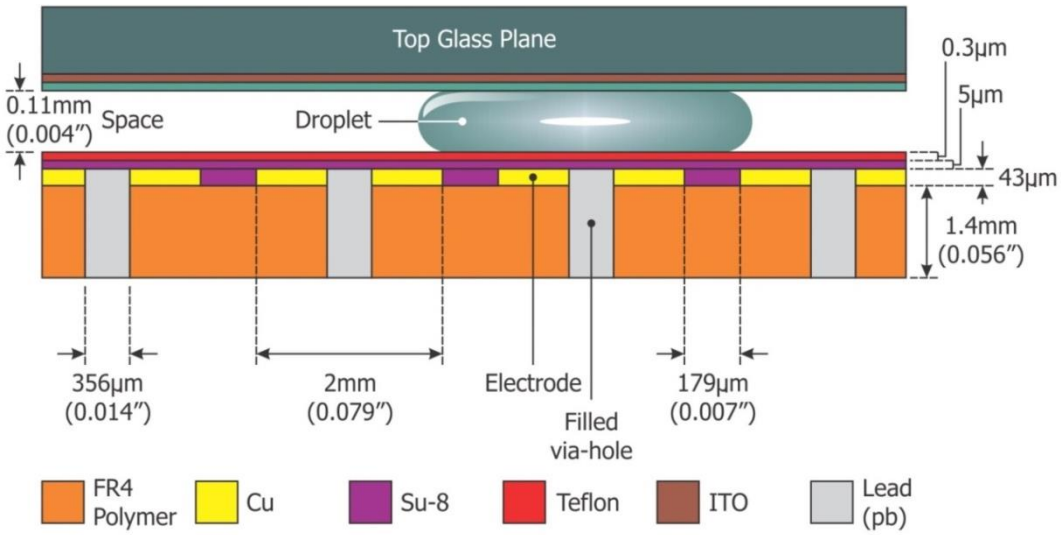

Figure 2.4 Schematic side view of the PCB based complete EWOD system

The PCB based EWOD device is capable of performing essential microfluidics operations such as droplet generation from the bulk liquid reservoir, drop motion along specific electrode array, merging with other drops and splitting into smaller drops. However, the irregularities on the PCB surface and the surface roughness slow down the drop motion at high speed. Therefore, glass based EWOD device was proposed to remove those factors.

2.2.2 Type-2: Glass Based EWOD Device

Digital microfluidic device was fabricated at the Nanofabrication facility, the University of Texas at Arlington. The ITO wafer was first cleaned thoroughly with non-halogenated hydrocarbons: Acetone, Methanol, Isopropanol and then rinsed with DI water. The wafer was then dehydrated at 150 ^{0}C for 2 minutes. A thin layer of HMDS was spin coated on the wafer to provide good adhesion capabilities to the Photo Resist (PR) with following recipe; spin speed was ramped up to 500 rpm with 100 rpm/s for 5s; ramping with 900 rps/s to 4000 rpm for 30s. This resulted in a very thin and uniform adhesive layer. The glass substrate with the coated adhesive layer was then baked to harden the layer at 150 ^{0}C for 1.5 min.

A positive PR (Microchem S1813) was spin coated on the wafer with following recipe; spin speed was ramped up to 500 rpm with 100 rpm/s for 5s; ramping with 900 rps/s to 3000 rpm for 30s. This resulted in 1.2 µm thick uniform PR layer. The glass substrate with the coated PR layer was baked to harden the PR at 115 ^{0}C for 1 min. Photo Lithography was done for this glass substrate with a light dose of 140 mJ/cm^2 on the Backside-Aligner (OAI 806MBA). The wafer was then soft baked at 110 ^{0}C for 1 min. One of the masks used in this lithography is shown in the Figure 2.5 (designed in LEdit and manufactured through the vendor CAD Art Services, Inc, Bandon, OR). Other masks are shown in the Appendix. After developing in a developer (Microchem, MF-319) and dehydrating at 115 ^{0}C for 2 min, the projected electrode pattern onto the PR layer was observed under the microscope for accuracy. The wafer was then agitated in mixture of Hydrogen Chloride (HCL) acid, Nitric (HNO_3) acid and DI water (H_2O) (wt

%- 20% HCl, 5% HNO_3, 75% H_2O or vol %- 8:1:15, HCl: HNO_3: H_2O) for 2.5 min at 55 ^{0}C to etch ITO layer. After PR stripping (Remover 1165, Microchem), The wafer was dehydrated at 150 ^{0}C for 2 min.

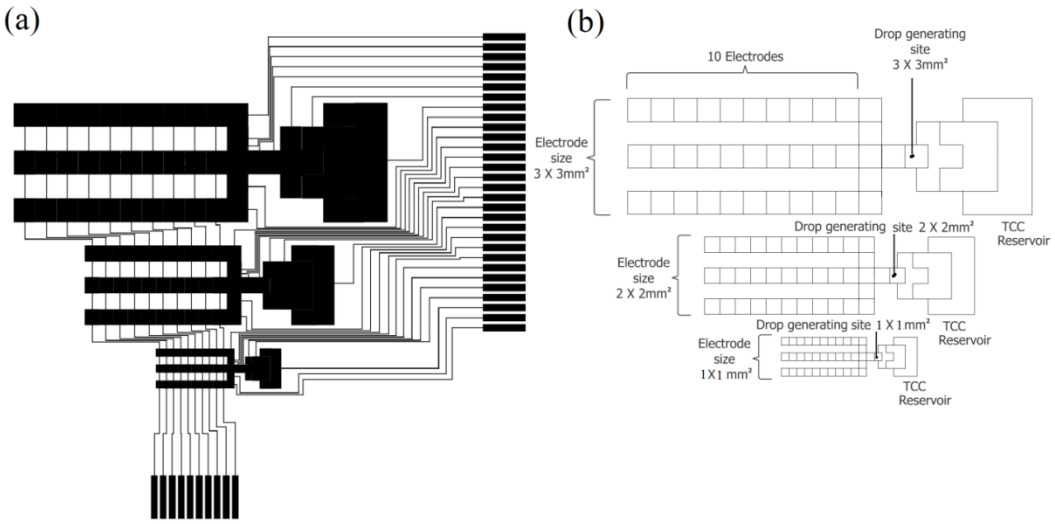

Figure 2.5 (a) Mask used to fabricate the glass based EWOD plate, (b) electrode geometry and dimensions

After that, a layer of dielectric (SU-8-5, Microchem) was spin coated on the wafer with following recipe; spin speed was ramped up to 500 rpm with 100 rpm/s for 5s; ramping with 900 rps/s to 2000 rpm for 30s. This resulted in 5 µm thick uniform dielectric layer. The glass substrate with the coated dielectric layer was then baked to harden the layer at 65 ^{0}C for 1 min and then 95 ^{0}C for 3 min.

Photo Lithography was done for this dielectric layer coated glass substrate with a light dose of 140 mJ/cm^2 on the Backside-Aligner (OAI 806MBA). The glass substrate was then soft baked at 65 ^{0}C for 1 min, 95 ^{0}C for 1 min and hard backed at 150 ^{0}C for 5 min. A layer of Teflon was spin coated on the dielectric coated glass surface to provide hydrophobicity with following recipe; spin speed was ramped up to 1000 rpm with 300 rpm/s for 30s. This resulted in 300 nm thick uniform hidrophobic layer. After that, dielectric and hydrophobic layer coated glass substrate was annealed at 150 ^{0}C for few hours to increase surface uniformity. Finally, the ITO

coated cover plate was first cleaned thoroughly with non-halogenated hydrocarbons: Acetone, Methanol, Isopropanol and then rinsed with DI water. The cover plate was then dehydrated at 150 ^{0}C for 2 minutes. A layer of Teflon with 300 nm thick was spin coated on the cover plate to provide hydrophobicity, and annealed at 150 ^{0}C for few hours to increase the surface uniformity. A drop of DI water (~ 0.4 µl) was dispensed onto the reservoir using a pipette and the top plate was positioned to provide a uniform spacer gap between the bottom plate and the cover plate (Figure 2.6).

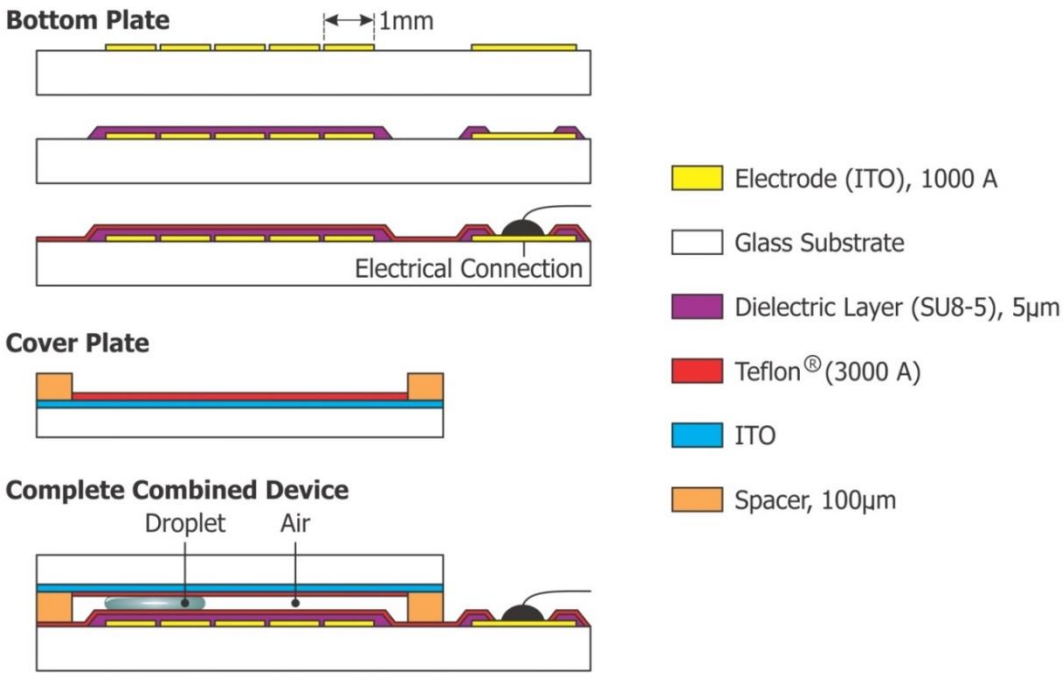

Figure 2.6 Schematic side view of the glass based complete EWOD system

The glass based EWOD device successfully demonstrates all the essential microfluidics operations mentioned above. When comparing with the PCB substrate, the glass substrate has much less surface roughness. As a result of that, much higher speed of drop motion was achieved in the glass based EWOD device. However, the EWOD system we are developing finally has to be combined with the modern Silicon (Si) based Integrated Circuits (ICs). Therefore, Si surface was proposed as the EWOD substrate.

2.2.3 Type-3: Silicon based EWOD Device

Digital microfluidic device was fabricated at the Nanofabrication facility, the University of Texas at Arlington. The Si wafer was first cleaned thoroughly with non-halogenated hydrocarbons: Acetone, Methanol, Isopropanol and then rinsed with DI water. The wafer was then dehydrated at 150 ^{0}C for 2 minutes. A layer of SiO_2 with a thickness of 1 µm was deposited on the Si wafer using Plasma Enhanced Chemical Vapor Deposition (PECVD) at 300 °C with the deposition rate of 450 ^{0}A/min. After depositing a layer of SiO_2, to check the uniformity of the deposition, the thickness of the SiO_2 layer was measured using the NanoCalc Thin Film Reflectometry System. A layer of Chromium (Cr) with a thickness of 0.1 µm was then deposited on the SiO_2 deposited Si surface using Ebeam Evaporator (CHA) with the deposition rate of 2.5 ^{0}A/s.

After that, a thin layer of HMDS was spin coated on the Si substrate to provide good adhesion capabilities to the Photo Resist (PR) with following recipe; spin speed was ramped up to 500 rpm with 100 rpm/s for 5s; ramping with 900 rps/s to 4000 rpm for 30s. This resulted in a very thin and uniform adhesive layer. The Si substrate with the coated adhesive layer was then baked to harden the layer at 150 ^{0}C for 1.5 min. A positive PR (Microchem S1813) was spin coated with following recipe; spin speed was ramped up to 500 rpm with 100 rpm/s for 5s; ramping with 900 rps/s to 3000 rpm for 30s. This resulted in 1.2 µm thick uniform PR layer. The Si substrate with the coated PR layer was then baked to harden the PR at 115 ^{0}C for 1 min.
Photo Lithography was done for this Si substrate with a light dose of 140 mJ/cm^2 on the Backside-Aligner (OAI 806MBA). The wafer was then soft baked at 110 ^{0}C for 1 min. The mask used in this lithography is shown in the Figure 2.5. After developing in the developer (Microchem, MF-319) and dehydrating at 115 ^{0}C for 2 min, the projected electrode pattern onto the PR layer was observed under a microscope for accuracy. The wafer was then agitated in Chrome Mask Etchant (OMG Cyantek, CR-7) to etch the Cr layer. After PR stripping (Remover 1165, Microchem), the wafer was dehydrated at 150 ^{0}C for 2 min.

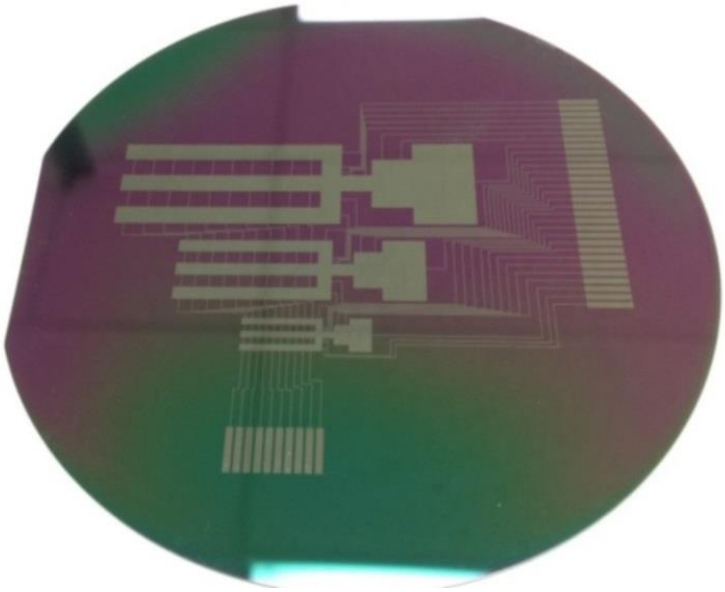

Figure 2.7 The electrode pattern obtained on the Silicon substrate with to the mask shown above.

After that, a layer of dielectric (SU-8-5, Microchem) was spin coated on Si substrate with following recipe; spin speed was ramped up to 500 rpm with 100 rpm/s for 5s; ramping with 900 rps/s to 2000 rpm for 30s. This resulted in 5 μm thick uniform dielectric layer. The Si substrate with the coated dielectric layer was then baked to harden the layer at 65 ^{0}C for 1 min and then 95 ^{0}C for 3 min.

Photo Lithography was done for this dielectric layer coated Si substrate with a light dose of 140 mJ/cm^2 on the Backside-Aligner (OAI 806MBA). The Si substrate was then soft baked at 65 ^{0}C for 1 min, 95 ^{0}C for 1 min and hard backed at 150 ^{0}C for 5 min. A layer of Teflon was spin coated on the dielectric coated Si surface to provide hydrophobicity with following recipe; spin speed was ramped up to 1000 rpm with 300 rpm/s for 30s. This resulted in 300 nm thick uniform hidrophobic layer. After that, dielectric and hydrophobic layer coated Si substrate was annealed at 150 ^{0}C for few hours to increase surface uniformity. Finally, the ITO coated cover plate was first cleaned thoroughly with non-halogenated hydrocarbons: Acetone,

Methanol, Isopropanol and then rinsed with DI water. The cover plate was then dehydrated at 150 ^{0}C for 2 minutes. A layer of Teflon with 300 nm thick was spin coated on the cover plate to provide hydrophobicity, and annealed at 150 ^{0}C for few hours to increase the surface uniformity. A drop of DI water (~ 0.4 µl) was dispensed onto the reservoir using a pipette and the top plate was positioned to provide a uniform spacer gap between the bottom plate and the cover plate (Figure 2.8).

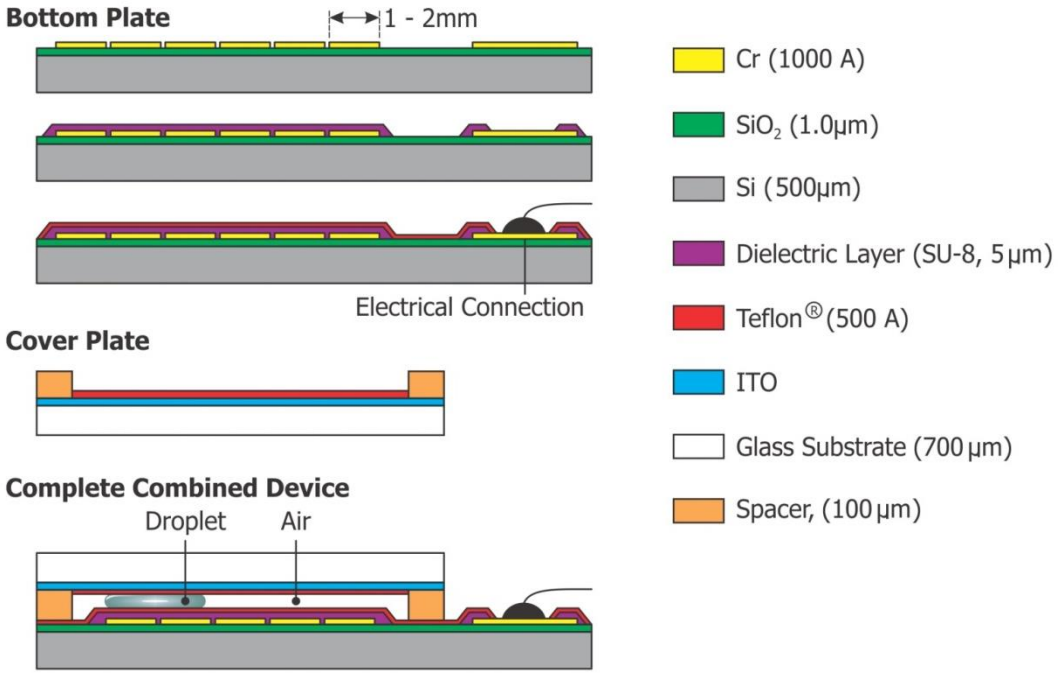

Figure 2.8 Schematic side view of the Silicon based complete EWOD system

The Silicon based EWOD device successfully demonstrates all the essential microfluidics operations mentioned above. Specially, two tests were performed using the EWOD devices as explained in the above; 1). droplet generation with volume consistency, 2).speed of droplet motion. According to the experimental results, the speed of drop motion on Si-based EWOD device is lower than that of the glass based EWOD deice. The reason for lower speed on Si-based EWOD device will be investigated in future.

To carry out the droplet dispensing in the above EWOD devices with automation, a custom-built fixture system for the EWOD setup was constructed using Lexan sheets and PCB. This fixture system can fix the EWOD setup on a horizontal plane while providing electrical wiring to the EWOD setup. This fixture system was then interfaced to the computer through a data acquisition (DAC) system and a control board. This DAC system and the control board enabled controlling the drop dispensing by a custom-built LabVIEW program.

2.3 Testing Setup

2.3.1 The Fixture System of the EWOD Setup

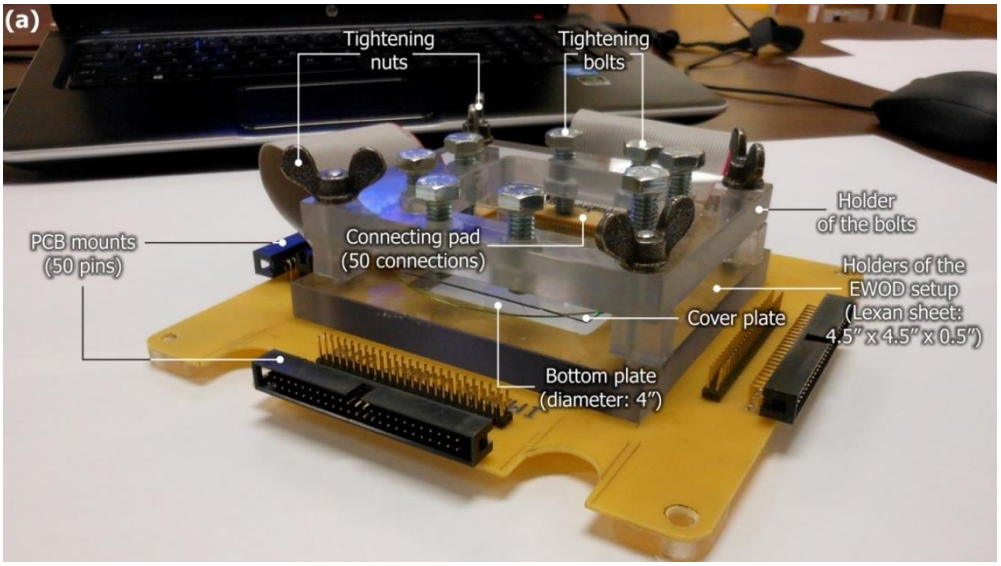

Figure 2.9 The fixture system that holds the EWOD setup and provides electrical wiring

This home-built fixture system mainly consists of three components: 1). the holder of the EWOD setup. This holder is made of a transparent Lexan sheet with dimensions $4.5" \times 4.5" \times 0.5"$. It provides a stable and strong rest for the bottom plate of the EWOD setup without any bending deformation. 2). the holder of the bolts that supports for the electrical wiring to the EWOD setup. This holder is made of a transparent Lexan sheet with dimensions $4.5" \times 4.0" \times 0.5"$ with a square cut in the middle with dimensions $2.5" \times 2.5"$ which is the field of view of drop dispensing of the EWOD setup. This cut helps to capture clear images of the droplets by the

CCD camera mounted at the top of EWOD setup. 3). customized connecting pads with spring-loaded contact pins that provide electrical connections to the EWOD setup.

Each connecting pad has fifty flexible springs attached to the bottom surface of the pad. This spring arrangement of the connecting pad helps to establish a solid electrical connection between the EWOD setup and the connecting pad. This connecting pad is eventually connected to the external control board through the PCB mount connected at the edge of the PCB (Figure 2.9). This PCB has a square cut in the middle with dimensions $2.5" \times 2.5"$ which is the field of view of drop dispensing of the EWOD setup. This square cut allows illuminating the liquid drops in the EWOD setup by the LED light sources placed at the bottom of the PCB.

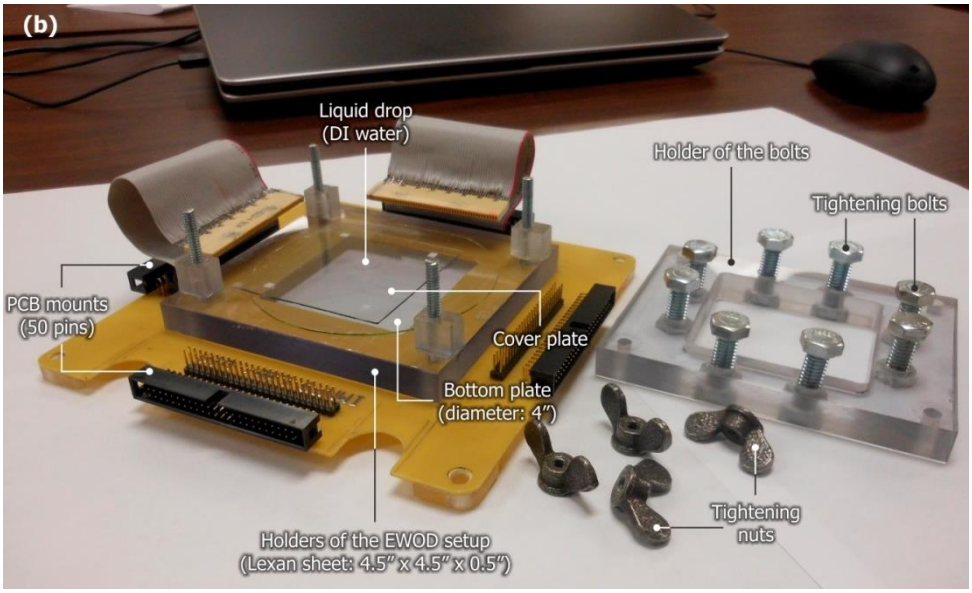

Figure 2.10 Sandwiched drop of DI water in between the bottom plate and the cover plate

To study the droplet dispensing in the EWOD setup by automated LabVIEW program, firstly, dielectric and hydrophobic coated bottom plate was placed on the holder of the EWOD setup (Figure 2.10). In this example, the bottom plate is made of an ITO coated glass wafer ($4"$ in diameter) while the square shaped cover plate is cut out of an ITO coated glass wafer. A drop of DI water (~ 4µl) was dispensed into the reservoir by a pipette. This drop was

sandwiched by a cover plate with a uniform spacer gap (~ 100 µm) in between the bottom plate and the cover plate. After that, the holder of the bolds was placed on the holder of the EWOD setup and fixed with tightening nuts (Figure 2.9). To form electrical connections, the connecting pad was placed on the contact pad of the bottom plate and pressed down by rotating the tightening bolts until a solid connection established between the bottom plate and the connecting pad. Next, the connecting pad was connected to the external control board through the PCB mount. Finally, the conducting ITO layer of the cover pate was grounded.

Mainly, two tests were carried out using this test setup: 1). generating drops with higher accuracy in volume, 2). enhancing speed of drop motion. In the first test, multiple drops were generated from the reservoir and their 2D images were captured digitally by the PC interfaced optical system. To calculate the foot print area of these liquid drops, these images were image-processed using a custom-written MATLAB program. Since the spacer gap between the bottom plate and the cover plate is known, the volume of the generated liquid drops was calculated to check the volume accuracy of the generated drops. In the second test, a liquid drop was moved along an array of electrodes with a higher speed. This high speed motion was recorded by a high speed camera (FASTEC, TS3). These high speed camera videos were analyzed to check the maximum speed of drop motion.

2.3.2 Test Setup 1: Droplet Generation with Volume Consistency

The fixture system of the EWOD setup was mounted on the rest and liquid drop was illuminated with LED light sources adjusted from the bottom (Figure 2.11). Clear and enlarge view of this droplet was taken into the computer desktop using optical system (Hiro-USA,Inc, RiverEdge, new Jersey) consisting of a zoom lens, a white light semi-flexible fiber optical source and a USB CCD camera. A sinusoidal signal (frequency 1 *kHz*) was generated from the waveform generator (Model 2720 A, Tegam) which is connected to the high-voltage amplifier (Model 2340, Tegam) to provide high enough AC voltage (~ 100 *V*) for testing.

To generate a liquid drop from the reservoir drop, a control signal (digital 1/0) was generated by the custom-built LabVIEW interface (developed by Wijethunga, P. and George, S.) with a Data Acquisition Device (High-Density Industrial Digital I/O for USB – 96-Channel, 5 V TTL/CMOS, National Instrument Inc). This control signal was transformed into amplified high voltage signal by the control board (developed by George, S.) and supplied to the required electrode in the EWOD device. This LabVIEW program is capable of controlling many electrodes (96) simultaneously according to any desired actuating pattern.

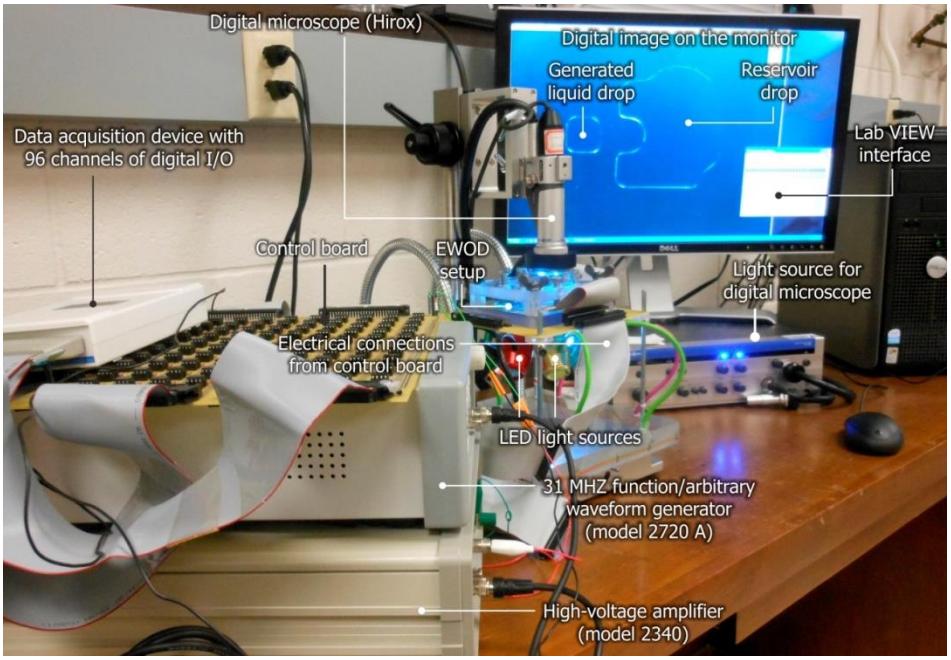

Figure 2.11 Schematic of the test setup for droplet generation with volume consistency

Fifty drops were generated from the reservoir drop and tested for volume consistency. The PC monitor shows the enlarged images of one generated drop and the remaining drop left in the reservoir. All the measurements were carried out under ambient atmospheric conditions at room temperature. More details of reservoirs that generate droplets with consistent volumes and their volume accuracy results are given in the chapter 3.

2.3.3 Test Setup 2: Enhancing Speed of Droplet Motion

There are several parameters in the EWOD setup that affect the speed of drop motion. Among these parameters, electrode size, electrode geometry and surface roughness play notable role in enhancing speed of drop motion. For an example, as mentioned in the above, much higher speed of drop motion can be achieved on the glass based EWOD device than that of the PCB based EWOD device since glass has much less surface roughness compared to the PCB. To study the maximum speed of drop motion in each case, a single droplet was oscillated over all ten electrodes by reducing the switching frequencies. The switching frequency denotes the rate at which the droplet is relocated across two electrodes, thus it measures the effective speed of drop motion.

Figure 2.12 The high speed camera (FASTEC, TS3), lenses and extensic tubes used for the test

This high speed motion of the liquid drop was recorded by the high speed camera (FASTEC, TS3, Fastec Imaging Corporation, San Diego, CA) and analyzed in Sine Viewer Application (CV 2.14b, Phantom, www.visionresearch.com) to check the maximum speed of

drop motion (Figure 2.12). This camera can capture clear images of drop motion with higher resolution with a maximum frame rate of 1250 fps. Depending on the field of view of the test, specific lenses and specific extensic tubes have to be used to focus the required region.

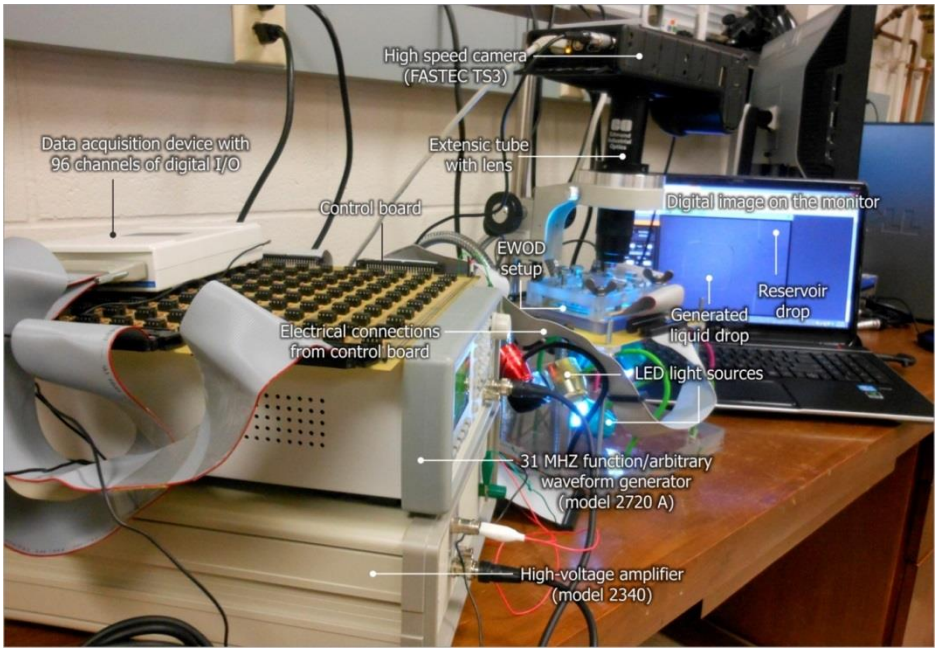

Figure 2.13 Schematic of the test setup for enhancing speed of drop motion

The test setup 2 is similar to the previous test setup 1 except the optical system (Figure 2.13). As in the first case, the fixture system of the EWOD setup was mounted on the rest and liquid drop was illuminated with LED light sources adjusted from the bottom. Clear and enlarge view of the droplet was taken into the PC screen by adjusting the mounting height of the high speed camera and focusing the lens. The fast motion of the liquid drop was recorded with a frame rate of 1000 fps and saved in a storage device connected to the high speed camera externally.

All the measurements were carried out under ambient atmospheric conditions at room temperature. More details about parametric study for enhancing speed of drop motion and corresponding results are given in the chapter 4.

CHAPTER 3

VOLUME PRECISION AND CONSISTANCY OF DROPLETS DISPENSED BY EWOD

This chapter presents the enhancement of volume precision and consistency of droplets generated solely by EWOD operation. Previous studies by other researchers reported various parameters that affect the droplet volume, however, in this work, we mainly focused geometry of electrodes and developed new reservoir designs that dispense droplets with higher volume precision and consistency. Volume precision of drop dispensing is defined by the difference between the dispensed drop volume and the volume subtended by the drop dispensing electrode. Volume precision is important to dispense predefined volumes and control of the volumes. Volume consistency is defined by the random uncertainty associated with dispensed volumes. Volume consistency is important to dispense the same volume from the reservoir repeatedly. The first section of the chapter describes traditional method of drop generation from the conventional reservoir. The second section discusses various efforts of the previous research groups made to generate droplets with volume consistency. The third section explains the design and operational mechanisms of the newly introduced TCC reservoir that has a higher volume accuracy of drop dispensing. Finally, the last section compares experimentally obtained volume accuracy results for the TCC reservoir with that of the conventional reservoir. All the experimental results agreed with the numerically simulated results. Glass based EWOD device with DI water was used in this study.

3.1 Droplet Generation in EWOD Device

Before the droplet generation from the reservoir, let's consider splitting a droplet into two. Hydrodynamic instability must be developed to achieve successful splitting. Figure 3.1 illustrates the method of splitting a droplet by EWOD. Initially, the droplet exists on the middle

electrode (E_2). At the same time, droplet is in contact with the neighboring electrodes (E_1 and E_3). To start the cutting, E_1 and E_3 are activated while deactivating E_2. This activation creates a decrease in contact angle on the activated electrode. Thus, it creates positive pressure in the droplet (P_1) while negative pressure occurs on the E_2 due to non-wetting (e.g. hydrophobic) contact angle. For a successful pinch-off a droplet, the negative meniscus (or neck) at point 1 should develop and meet each other. This can be done only when $|P_1| > |P_2|$. P_1 and P_2 vary with several parameters such as gap between top and bottom plates, electrode geometry and surface hydrophobicity etc.

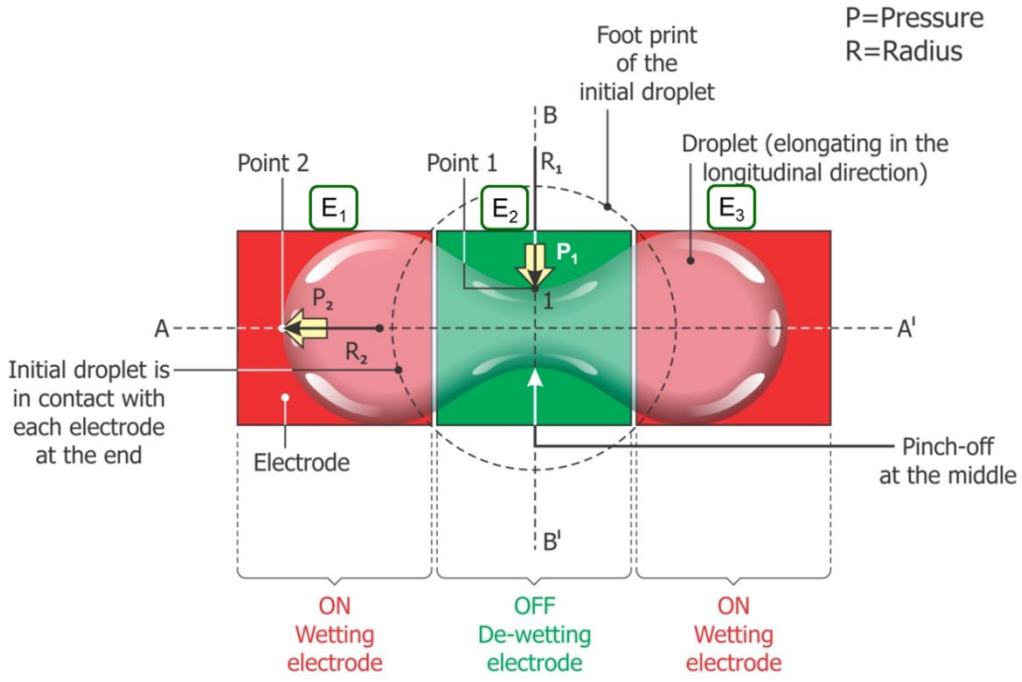

Figure 3.1 Top view of the cutting droplet. The droplet is stretched out along the longitudinal direction and squeezed at the middle along the orthogonal direction enhancing the neck formation

3.2 Review on Droplet Generation in EWOD Device

Droplet generation in EWOD device refers to the process of creating a smaller droplet, which is typically less than one microliter, from a larger reservoir droplet. The traditional drop dispenser pattered on the EWOD substrate consists of a larger reservoir electrode and a path of

smaller electrodes emanating from the reservoir. These electrodes are designs in such a way that one electrode is overlapping with the neighboring electrodes to allow the droplet to spread to the neighboring electrode and improve the EWOD actuation. To conduct an experiment, a drop of DI water which is few microliters (1-5 µl) in volume is manually dispensed onto the reservoir using a pipette. The reservoir drop is then sandwiched between the parallel plates and mounted on the fixture system to connect electrical wiring. After that, the testing setup is assembled as explained in the Chapter 2.

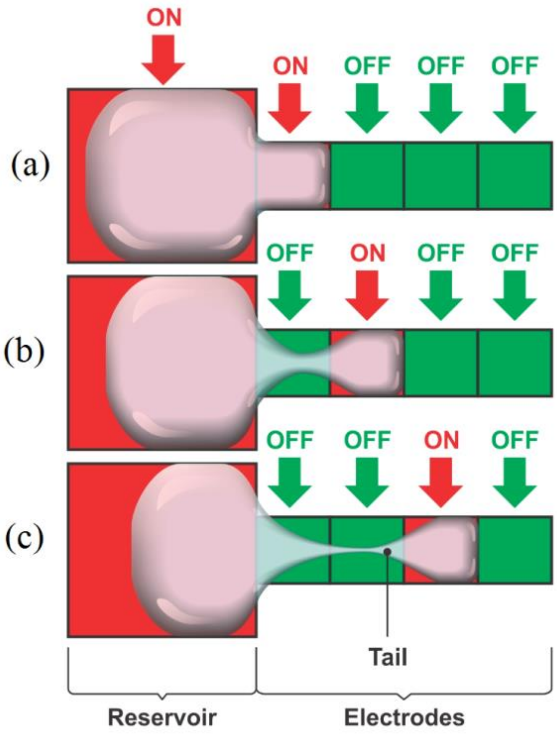

Figure 3.2 Order of dispensing a liquid droplet from the conventional reservoir, (a,b) pulling out a liquid column from the reservoir, (c) Inducing the liquid pinch-off: the electrode at the right and the reservoir electrode are activated while deactivating the electrodes in between, the liquid tail formed behind the liquid drop before pinch-off. OFF electrode is shown in Green, ON electrode is shown in Red.

To generate a liquid drop, similar to droplet splitting, a liquid column has to be pulled out from the reservoir and moved away from the reservoir by sequentially activating the electrodes from left to right (Figure 3.2) [17,33]. At a certain location of this pulling out process,

the liquid column becomes unstable, a drop is pinched off and some of the liquid is being drawn back to the reservoir. In another words, to induce the liquid pinch-off, the electrode at the right and the reservoir electrode have to be activated while deactivating the electrodes in between (Figure 3.2) [34]. Cho et al investigated the drop generating mechanism by pulling a liquid column out from the reservoir [17]. They reported two major drawback of this method of drop generation. First, the length of the liquid column that has to be extruded from the reservoir to generate a droplet is inconsistent. Next, the point of pinch-off is unpredictable. As a result of that, the conventional reservoir results inconsistent volumes of the generated drops.

The liquid tail, which is the smaller liquid region formed behind the drop before separation, is a major factor affecting to the droplet volume variation [34]. After separation, this liquid tail adds some extra amount of liquid to the already dispensed droplet. As a result of that, the volume of the dispensed liquid drop is usually somewhat larger than the volume occupied by the square electrode [34, 35].

Precise liquid handling in EWOD digital microfluidics is crucial for many applications. For an example, in drug discovery (chemical syntheses, screening of compounds), precision of the test fully depend on the portion selected from the testing agent [37, 38]. Further, in our current application, the volume precision of a unit drop is crucial to maintain a steady-state operation of thin-film evaporation. To improve the volume precision and consistency, various research groups around the world have performed extensive research and introduced several precise and consistent drop dispensing techniques.

First, Ren et al introduced a consistent drop dispensing technique by capacitive metering [8]. In this method, the built-in capacitance of the EWOD device is measured to estimate the droplet volume and to control the dispensing process. A needle with very small diameter (300 μm) is inserted into EWOD device through the spacer gap in between the bottom plate and the cover plate in such a way that the needle is at a right angle to the path of the electrode. Liquid is delivered onto the electrode through the needle with the help of an electric

pump. When the liquid drop becomes larger, the capacitance in between the liquid drop and the electrode becomes higher. By measuring this growing capacitance, the amount of liquid collected on the electrode is computed. When the necessary drop volume is achieved, the droplet is dispensed by EWOD actuation and separated from the inlet. A liquid drop with any desired volume is dispensed by controlling the ending capacitance (Figure 3.3).

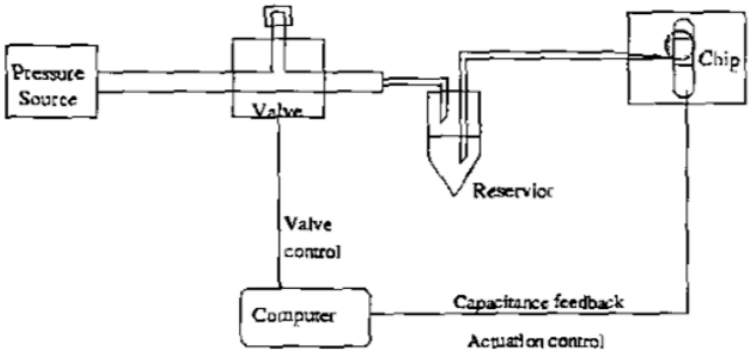

Figure 3.3 Schematic of the drop dispensing system by capacitive metering (Ren et al 2002 [39]).

They reported volume consistency of 1.2 % for repeatable drop generations. Further, they demonstrated drop generation at a speed of 120 droplets per minutes. Moreover, they tested droplet volumes in the range of 60 *nl* - 1900 *nl* with volume consistency of 10 % for repeatable drop generations.

However, the externally connected testing setup to the EWOD device is much more complicated. This complicated devise assembly reduces the simplicity of the EWOD system. As mentioned in the introduction, the main advantage of the EWOD system is dispensing droplets without externally connected pumps or valve. Therefore our attempt should be implementing methodologies to improve the volume precision of the droplets with a simple EWOD device consisting of only the microfluidic chip with the electrical wiring [37, 40].

Next, Cho et al reported a precise drop dispensing method by introducing side electrodes [17]. They patterned two side electrodes next to the main electrode array. These side

electrodes actively draw the liquid with EWOD force laterally from the main fluid path enhancing the pinch-off of the liquid column. With these side electrodes, they sequentially dispensed two droplets at the same place. These droplets were approximately equal in size with 270 *nl* in volume (Figure 3.4).

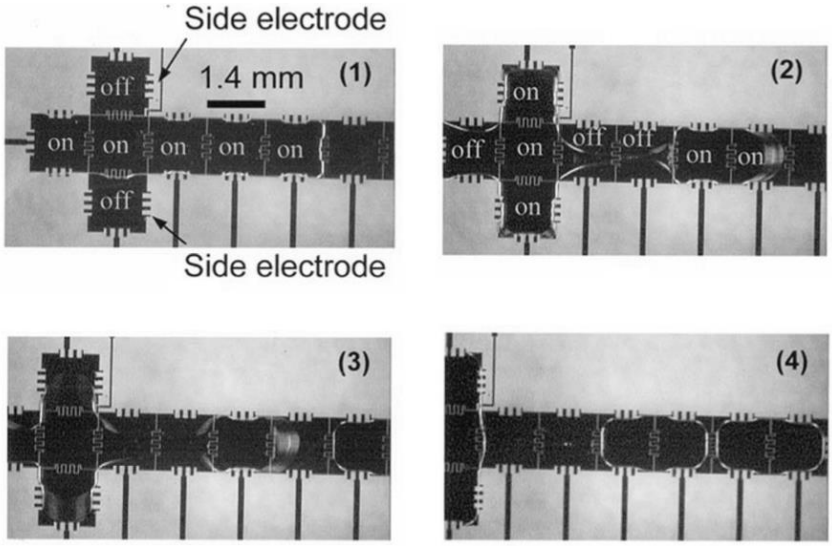

Figure 3.4 Dispensing droplets with consistent volume using side electrodes (volume of the each drop 270 *nl*) [Cho et al, 2003 [17]].

However, several weaknesses are associated with the use of side electrodes to dispense droplets in consistent volume. Specially, enhancing pinch-off of the liquid column using side electrodes does not satisfy the requirements for the volume consistency of the dispensed droplets. To improve the volume precision and consistency of droplets, scientifically designed reservoir should satisfy two requirements; 1) the reservoir should be able to minimize the tail formation of the dispensed droplet, and 2) the location of pinch-off should be consistent for repeatable drop generation. Above reservoir with side electrodes does not satisfy any of these requirements. So this design is not suitable to improve either volume precision or consistency of the droplets.

Wang et al studied the volume variation of the dispensed droplets over a range of operational parameters such as applied voltage, cutting length and the geometry of the drop

generating site [34]. They observed a larger tail at higher voltage and larger volume of the dispensed droplet as a result. Fair showed that the location of cutting depends on the EWOD force which is directly related to the applied voltage [36]. They further reported that the shape of the liquid tail depends on the location of cutting.

Gong et al mentioned that the volume of the generated droplet depends not only the above operational parameters but also by many arbitrary parameters such as surface roughness of the EWOD substrate, properties of the dielectric layer and its thickness and environmental humidity [37]. Finally, in the EWOD devices fabricated in a single electrode layer, the conducting lines running from the actuating electrodes or patterned right next to the actuating electrodes may affect to the drop volume accuracy at higher actuating voltages [37]

Gong et al presented a method to improve the volume precision of the droplets on a multilayer PCB based EWOD device [41]. Instead of side conducting lines patterned in the single conductive layer, in the multilayer PCB, individual electrode is directly and independently access from the bottom through vias drilled at the middle of each electrode. They reported acceptable volume precision of 5 % under well controlled testing conditions [42]. However, complicated post processes have to be implemented to reduce the surface topography and improve the EWOD performance on the PCB substrate. Table 3.1 summarizes all the methods mentioned above.

This chapter introduces a novel reservoir to improve the droplet volume precision and consistency. Based on the geometry of the electrodes, this reservoir is named as TCC reservoir. This TCC reservoir dispenses droplets with highly precise and consistent volumes exclusively based on the geometry and dimensions of the reservoir electrodes and the drop generating site. By observing the liquid behavior in the EWOD microfluidic device, the geometry and dimensions of the reservoir electrodes and the drop generating site were layout in such a way that the location of pinch-off is consistent with a minimum tail formation. Based on the geometry of the drop generating site, we introduce two types of TCC reservoirs; 1) TCC

reservoir with rectangular drop generating site, and 2) TCC reservoir with circular and angular drop generating site. In the second TCC reservoir, the tail formation is completely eliminated and very high volume precision was obtained. Glass based EWOD devise with DI water was used in these tests. All the experimental results agreed with the numerically simulated results at the same test conditions.

Table 3.1 Different techniques of dispensing droplets in uniform volume

Method	Mechanism	Results	Reference	Comments
Capacitance Metering	Measured the built-in capacitance of the electrode to determine the droplet volume	Rate of reproducibility: 120 droplets/min with vol. error 1.2 %	Ren et al., 2002 [39]	Both precision and consistency data
Active cutting	Introduced two side electrodes besides the main fluid path and actively pull the liquid sideways	Generated two droplets at a fixed location in equal size (~ 270 nl)	Cho et al., 2003 [17]	Only consistency, no precision data
Multilayer PCB with through substrate electrical wiring to eliminate the side connecting lines	(a)simple electrical signal switching (b) by changing the driving voltage, the droplet volume is adjusted	(a) volume precision +/-5% (b) volume precision +/- 10 %	Gong et al., 2006 [42]	Only precision, no consistency data
Real-time feedback control	Fast capacitive sensing of the droplet volume and precise control of driving signals	Precise volume control <+/-1 %, generating required droplet's volume according to pre-defined electrode pattern	Gong et al., 2006 [43]	Both precision and consistency data
Studied response of cutting electrode on droplet volume and reproducibility	Higher reproducibility for equal length cutting electrode and standard electrode	Volume variation: 3.0 %	Wang et al., 2010 [34]	Only precision, no consistency data

3.3 New Electrodes Designs: TCC Electrodes

3.3.1 TCC Reservoir

The TCC reservoir consists of one T-shaped electrode (T) and two C- shaped electrodes (C_1 and C_2). One half of the rectangular drop generating site is inside the T to reduce the cutting length and the tail formation. All the electrodes are symmetric over the X-axis. These electrodes overlap each other to allow the reservoir drop to spread to the neighboring electrode and enhance the EWOD performance (Figure 3.5). the C_2 has a larger area to supply a higher EWOD force on the reservoir drop and pull the reservoir drop into the reservoir. If the area of this TCC reservoir needs to be increased, either dimensions of C_2 can be increased or additional third C-electrode (C_3) can be added behind the C_2. Dimensions of the generating site together with the T and C_1 can be proportionally increased or decreased according to the requirements of the user.

In this present work, rectangular drop generating site with dimensions $2 \times 2\ mm^2$ was chosen for dispensing droplets. Dimensions of the other reservoir electrodes are shown in the Figure 3.5.

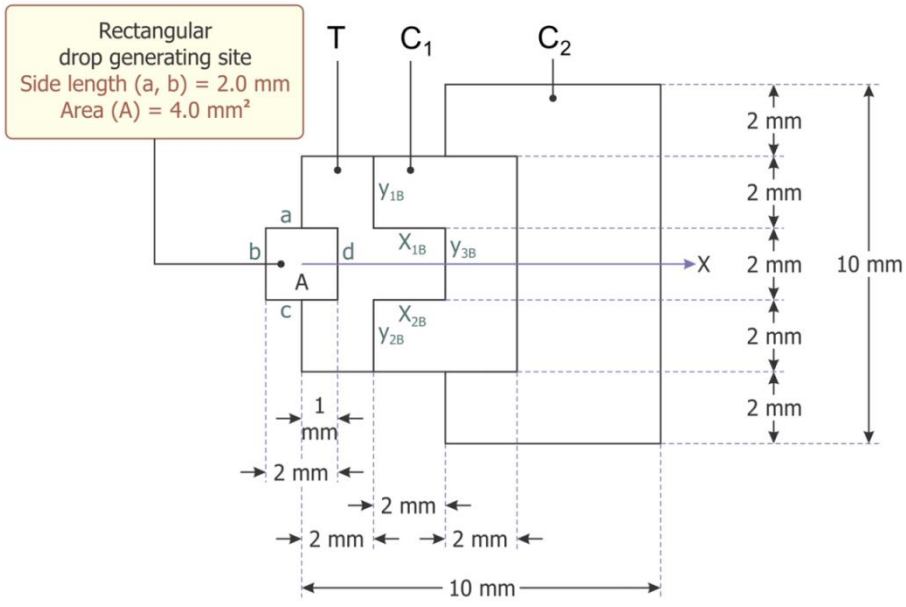

Figure 3.5 Layout of the TCC reservoir with rectangular drop generating site

3.3.2 How TCC Reservoir Works

To dispense a liquid drop from this TCC reservoir, a liquid drop is dispensed onto the reservoir by a pipette. The testing setup is assembled as described in the Chapter 2. Initially, the drop generating site and all the reservoir electrodes are grounded. To take the reservoir drop to forward towards the drop generating site, firstly, the C_1 is activated (Figure 3.6.2). Activation of the C_1 makes a reduction in contact angle of the liquid portion residing on the C_1. This reduction in contact angle induces unbalance EWOD force on the reservoir drop towards the drop generating site. This EWOD force drives the reservoir drop forward until the entire C_1 is filled with the liquid. The advantage of the electrode overlapping arrangement is that, even though the T is not activated, some part of the reservoir drop is already on some portion of the T. Since C_2 is grounded, the portion of the reservoir drop existing on the C_2 is free of EWOD force.

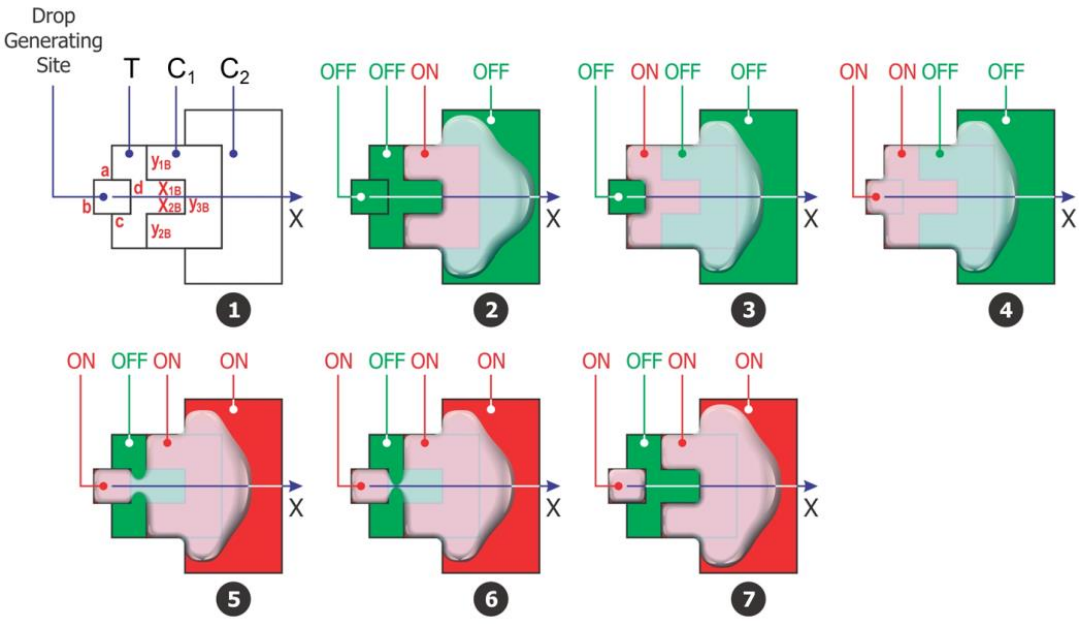

Figure 3.6 The sequence of drop dispensing from the TCC reservoir with rectangular drop generating site, OFF electrode is shown in Green, ON electrode is shown in Red.

Next, the T is activated while deactivating the C_1. As a result of that, the reservoir drop moves forward until the entire T was filled with the liquid (Figure 3.6.3). Even though the drop generating site is not activated, liquid at the front region of the reservoir drop has already spread on to the drop generating site. After that, the drop generating site is activated while keeping the T activated. This activation pulls the front meniscus of the reservoir drop forward until the barely filled drop generating site is completely filled with the liquid (Figure 3.6.4).

After that, both C_1 and C_2 and the drop generating site are activated keeping the T deactivated (Figure 3.6.4). This actuation makes both C_1 and C_2, and the drop generating site wetting while the T non-wetting. At this time, pulling EWOD force is generated backward by the C_2 on the reservoir drop. This pulling force is much higher since the area of the C_2 is much larger and entire back meniscus of the reservoir drop exists on the C_2. This pulling force is large enough to move the liquid on the de-wetting T towards the C_1. In this pulling process, firstly, the liquid amount resided on the T in front of edges y_{1B} and y_{2B} is moved onto the C_1.

The reservoir drop is still being pulled by the C_2 backward with a higher EWOD force. This EWOD force is large enough to move the left liquid amount on the de-wetting T further towards the symmetry axis (Figure 3.6.5). In this pulling process, the left liquid amount have to undergo certain constrain. Firstly, since the C_1 is activated throughout this pulling process, the front meniscus of the reservoir drop is aligned along the front edges y_{1B} and y_{2B} of the C_1. Secondly, since the drop generating site is activated throughout this pulling process, boundary of the dispensing drop is aligned along the edges *a, b* and *c* of the drop generating site. Under these two constrains, only possible motion of the liquid left on the de-wetting T is the motion perpendicular to the symmetry axis in between the edge *d* of the drop generating site and front edges y_{1B} and y_{2B} of the C_1 (Figure 3.6.6). When these perpendicularly moving two menisci meet each other, pinch-off happens and a liquid drop is dispensed. After pinching-off, the liquid portion of the reservoir drop left on the de-wetting T is pulled back into the reservoir (Figure 3.6.7).

The C_1 as well as the T plays important role in this drop dispensing process. The C_1 makes constrain to the liquid directing it to move perpendicular to the symmetric axis. The T acts as a de-wetting electrode and enhances the perpendicular motion of the liquid. Throughout the pinch-off process, the front meniscus of the reservoir drop is remained fixed along the edges y_{1B} and y_{2B} of the C_1. The shape of this fixed meniscus does not depend on the volume of the reservoir drop. As a result of that, the location of pinch-off is consistent for repeatable drop dispensing from the reservoir. Further, the cutting length, which is the horizontal gap in between the vertical edges *d* and y_{1B}, is very short. Therefore, the tail formation which is approximately half of the cutting length is much shorter. As a result of that, the volume precision of the dispensed droplet is higher. Therefore, this TCC reservoir with rectangular drop generating site can dispense droplets with highly precise and consistent volumes.

3.3.3 Comparison of TCC Reservoir with Conventional Reservoir Design

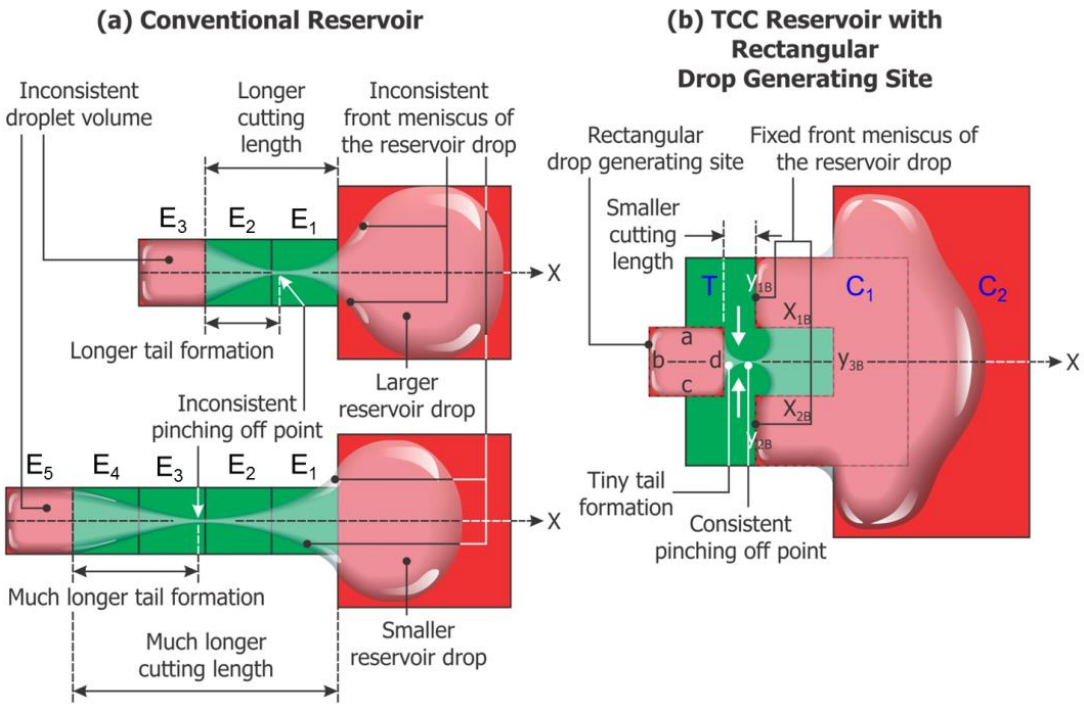

Figure 3.7 Comparing design and operational differences of the conventional and the TCC reservoirs affecting for the volume precision and consistancy of the dispensing droplets, OFF electrode is shown in Green, ON electrode is shown in Red.

To dispense a liquid droplet from the conventional reservoir, a liquid column has to be pulled outward from the reservoir and moved along an array of electrodes (Figure 3.7.a). To complete the droplet dispensing process, liquid needs to be pulled out over many electrodes. Therefore the conventional reservoir has a higher cutting length. In this pulling process, a larger liquid tail is formed behind the dispensing droplet.

After separation, this liquid tail adds some additional liquid amount to the already dispensed liquid drop. Therefore, the volume of the dispensed droplet is larger than the volume that can be occupied by the square electrode. In another word, the volume precision of the dispensed droplet is very low. Further, the location of pinch-off also moves towards the dispensing droplet. Therefore, the conventional reservoir has an inconsistent pinch-off point. Moreover, the front boundary of the reservoir also moves outward from the reservoir with the point of pinch-off. Therefore, the front boundary of the reservoir drop is inconsistent. The shape of this front boundary depends on the amount of liquid left on the reservoir. Therefore, the volume of the dispensed droplet and the location of pinch-off depend on the volume of the reservoir drop.

In the TCC reservoir, the rectangular drop generating site is placed very closer to the C_1. Therefore, the cutting length of the TCC reservoir is shorter (1 mm). Hence, the tail formation is much shorter (~ 0.5 mm). After separation, the amount of liquid added to the already formed droplet by the tiny liquid tail is very small. Therefore, the volume variation of the dispensed droplet is very small. Further, the front boundary of the reservoir drop is consistent throughout the pinch-off process. As a result of that, the location of pinch-off is consistent. Moreover, the shape of the front boundary of the reservoir drop is consistent with reproducibility of the reservoir. As a result of that, the location of pinch-off and the volume of the droplet do not depend on the volume variation of the reservoir drop.

3.4 Enhanced TCC Reservoir Design

3.4.1 TCC Reservoir with Angular Generating Site

The function of the T and the C_1 and C_2 are similar to those in the TCC reservoir with rectangular drop generating site. The only difference of the present TCC reservoir is the geometry of the drop generating site and its position. The front boundary of the present drop generating site is circular with a radius 1.1 mm. The back boundary is angular with a right angle. This drop generating site is placed completely inside the T such that the tip of the angular back boundary is aligned with the front edges of the C_1. This arrangement eliminates the cutting length and the tail formation of drop dispensing. The area of the current drop generating site (4.00 mm^2) is the same as the previous rectangular drop generating site. All the electrodes are symmetric over the X-axis. As in the previous TCC reservoir, these electrodes overlap each other to allow the reservoir drop to spread to the neighboring electrode and enhance the EWOD performance (Figure 3.8).

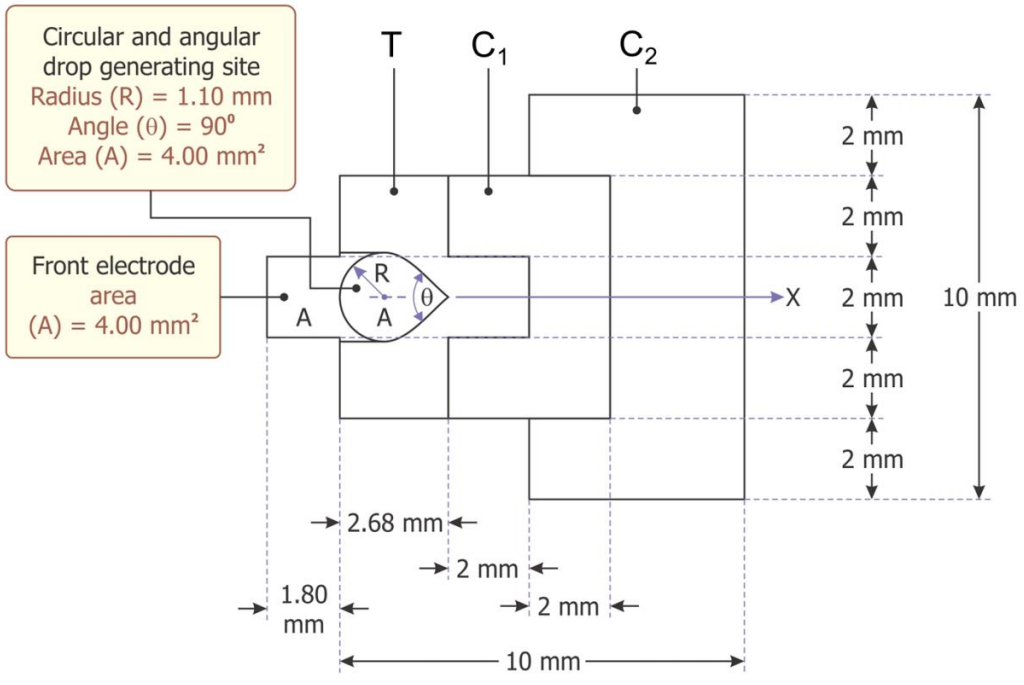

Figure 3.8 Layout of the TCC reservoir with circular and angular drop generating site

Drop dispensing procedure from this reservoir is similar to that with rectangular drop generating site as described in the section 3.3.2. To take the reservoir drop towards the drop generating site, firstly, the C_1 is activated (Figure 3.9.2). This activation drives the reservoir drop forward until the entire C_1 is filled with liquid. Next, both the T and the drop generating site are activated while deactivating the C_1. As a result of that, the reservoir drop moves forward until both T and the drop generating site are filled with the liquid (Figure 3.9.3).

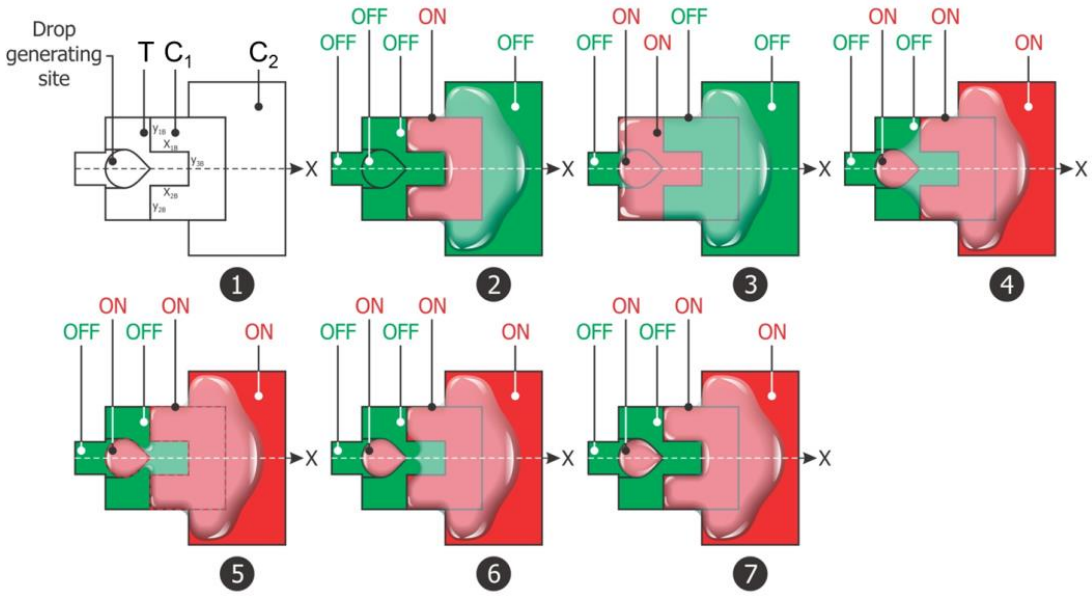

Figure 3.9 The sequence of drop dispensing from the TCC reservoir with circular and angular drop generating site, OFF electrode is shown in Green, ON electrode is shown in Red.

After that, both C_1 and C_2, and the drop generating site are activated while deactivating the (Figure 3.9.4). This actuation makes both C_1 and C_2, and the drop generating site wetting while the T-electrode non-wetting. At this time, strong pulling EWOD force is generated backward by the C_2 on the reservoir drop.

This pulling force is sufficient to move the liquid on the de-wetting T towards the C_1. In this pulling process, firstly, the liquid amount resided on the T in front of edges y_{1B} and y_{2B} is moved towards the C_1. The reservoir drop is still being pulled by the C_2 backward with strong

EWOD force. This EWOD force is sufficient to move the remaining liquid amount on the de-wetting T towards the symmetry axis (Figure 3.9.5).

In this pulling process, the left liquid amount have to undergo certain constrain. Firstly, since the C_1 is activated throughout this pulling process, the front meniscus of the reservoir drop is aligned along the front edges y_{1B} and y_{2B} of the C_1. Secondly, since the drop generating site is activated throughout this pulling process, boundary of the dispensing drop is aligned along the edge of the drop generating site.

Under these two constrains, only possible motion of the liquid amount remaining on the de-wetting T is the motion in between the angular edge of the drop generating site and the front edge of the C_1 (Figure 3.9.6). Pinch-off happens at the tip of the angular section when the two menisci meet each other. After pinching-off, the liquid portion of the reservoir drop left on the de-wetting T is pulled back into the reservoir (Figure 3.9.7)

The electrode located in front of the drop generating site is deactivated throughout the drop dispensing process. After dispensing the liquid droplet, this front electrode is used to move the dispensed liquid droplet out from the drop generating site. The area of the drop generating site and the front electrode is the same (4.00 mm^2)

3.5 Performance Tests

This section describes the detailed experimental procedure followed for computing the volume precision and consistency of the droplet dispensed from the above reservoirs.

3.5.1 Device Preparation

EWOD devices of different reservoir designs were fabricated on glass substrates as described in Chapter 2. Test setup is described in Chapter 2 as well.

The side lengths of the rectangular drop generating site (*a, b*) is 2.0 mm with area (*A*) 4.0 mm^2. The area of the rectangular reservoir ($20 \times 20\, mm^2$) is hundred times larger than the area of the drop generating site. This reservoir consists of ten rectangular stripped electrodes (E_1-E_{10}). The area of each stripped electrode (A') is $2 \times 20\, mm^2$.

These stripped electrodes are useful to take the reservoir droplet towards the drop generating site. In the current experiment, the method followed to dispense a liquid droplet is somewhat different that the previous method described in the above. In the previous method, a liquid column was pulled out from the reservoir and moved along the electrode path until a droplet is created.

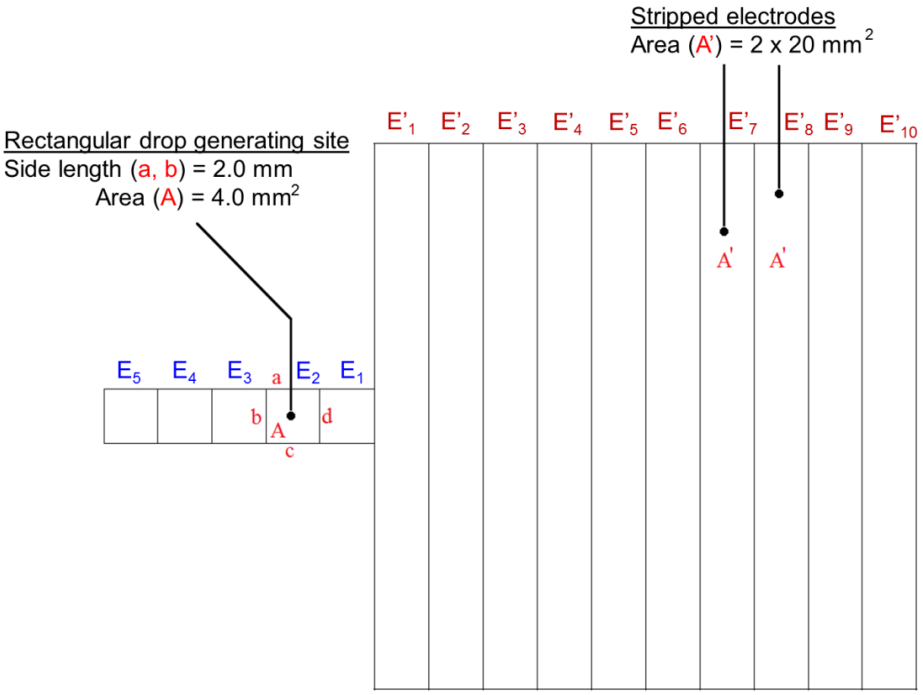

Figure 3.10 Geometry and dimensions of the conventional reservoir used in the experiment for computing volume precision of the dispensing droplet

In the present method, the liquid column was pulled out from the reservoir and moved only up to the second control electrode (E_2) in the electrode path. Liquid droplet was dispensed by activating the E_2 and all the stripped electrodes (E'_1-E'_{10}) in the reservoir while deactivating the E_1. According to the arrangement of stripped electrodes, reservoir drops with two different shapes can be formed; 1) reservoir drop in circular shape and, 2) reservoir drop in rectangular shape.

The side lengths of the rectangular drop generating site (*a, b*) is 2.0 mm with area (*A*) 4.0 mm^2. To dispense many droplets, the TCC reservoir was modified by adding two additional

C-electrodes (C_3 and C_4) behind the C_2. Total area of this modified TCC reservoir is the same as the conventional reservoir ($20 \times 20\, mm^2$) described in the previous section. All the C electrodes are positioned one behind the other in such a way that the top and bottom edges of the reservoir take a staircase arrangement. This arrangement helps to pull the reservoir drop backward into the reservoir by EWOD activation. This backward motion of the reservoir drop helps to keep the pinch-off point consistent.

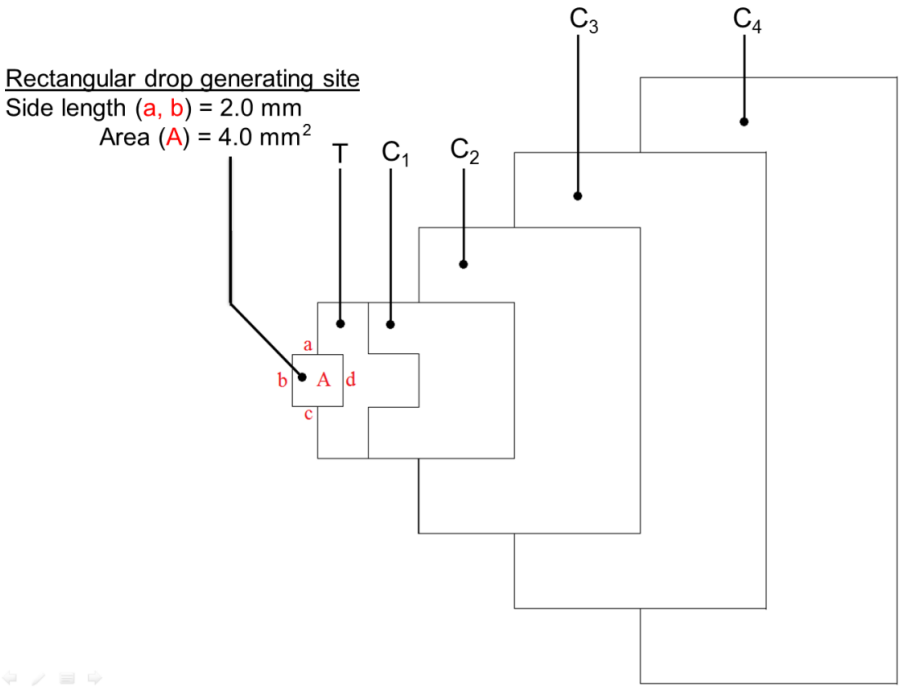

Figure 3.11 Geometry and useful dimensions of the modified TCC reservoir with rectangular drop generating site

The area of the circular and angular drop generating site is 4.0 mm^2. The radius of the front circular boundary is 1.10 mm while the angle of the back angular boundary is acute. The area of the electrode located in front of the drop generating site is the same as that of the drop generating site.

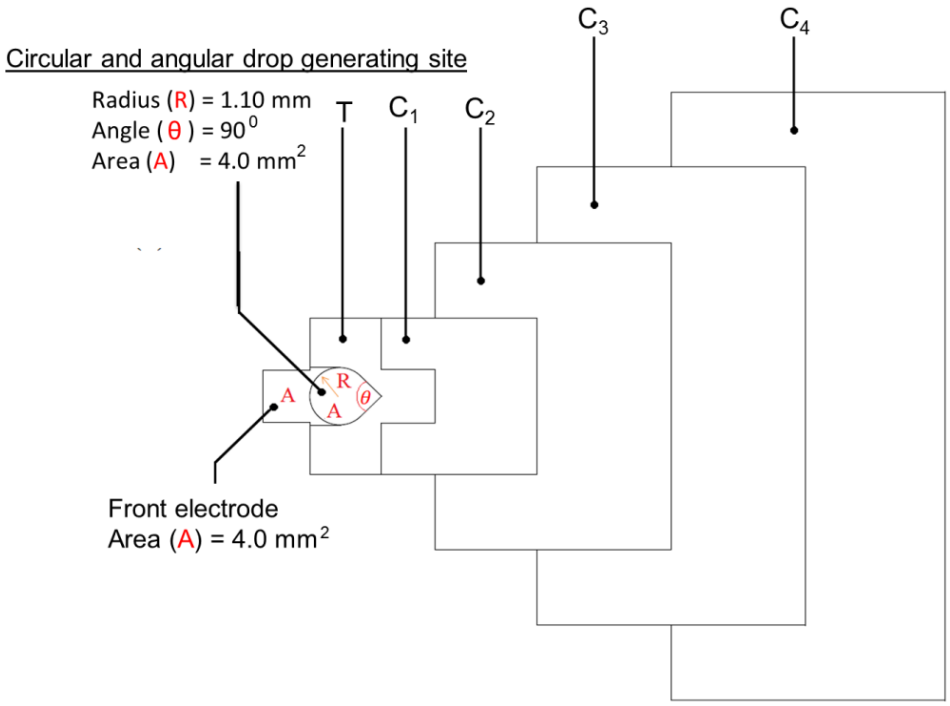

Figure 3.12 Geometry and useful dimensions of the modified TCC reservoir with circular and angular drop generating site

3.5.2 Testing Procedure

In the first case, a drop of DI water which is approximately eighty times bigger than the volume occupied by the drop generating site was dispensed onto the reservoir by a pipette. This drop was sandwiched by the cover plate with a uniform space gap (~ 100 µm). This sandwiched drop is approximately circular in shape. This circular reservoir drop was placed in contact with the first control electrode in the electrode path. To dispense a liquid droplet from this reservoir drop, a liquid column was pulled out from the reservoir and moved up to the E_2 in the electrode path. After that, a droplet was dispensed by activating the E_2 and all the stripped electrodes in the reservoir while deactivating the E_1.

In the second case, a drop of DI water with the same volume as above was dispensed onto the reservoir by a pipette. This reservoir drop was moved towards the E_2 in the electrode

path by activating stripped electrodes in the reservoir. This activation changed the shape of the reservoir drop into a rectangular shape. To dispense a liquid droplet from this reservoir drop, a liquid column was pulled out from the reservoir and moved up to the E_2 in the electrode path. After that, a droplet was dispensed by activating the E_2 and all the stripped electrodes in the reservoir while deactivating the E_1.

In each case, fifty droplets were sequentially dispensed from the reservoir. Images of these dispensed droplets were captured using optical system (Hirox-USA,Inc, RiverEdge, new Jersey) consisting of a zoom lens, a white light semi-flexible fiber optical source and a USB CCD camera. These images were image-processed in MATLAB to compute the footprint of the dispensed droplets. Same experiments were performed in Numerical Simulations for the same geometry and test conditions by Alex Yin Guan studying at the University of Texas at Arlington under the supervision of Professor Albert Y. Experimentally obtained results were compared with his numerically simulated results.

3.6 Results and Discusion

This section presents experimental volume precision results associated with the above reservoirs and compares them with the numerically simulated results.

3.6.1 Volume Precision Associated with the Conventional Reservoir: Circular Reservoir Drop

The area of the initial reservoir drop is $346\ mm^2$. The area of the reservoir is $20 \times 20\ mm^2 = 400\ mm^2$. Therefore, the initial reservoir drop occupies $86.5\ \%$ within the reservoir. When the reservoir drop is squeezed between the bottom plate and the cover plate without any confined sidewalls, the reservoir drop takes the shape of a circle (Figure 3.19).This circular shape is determined by the surface tension, which is produced by the cohesive forces of the liquid surface. At this state, the reservoir drop has the minimum possible surface area with the lowest energy.

The essential methodology to extrude a liquid column from the reservoir is to create internal pressure difference between the liquid in the reservoir and the front of the liquid column

[36]. To induce a pressure difference, we apply a voltage to the control electrodes in the electrode path [36]. If the pressure in the reservoir is larger than the pressure in the front of the liquid column, a liquid column will be extruded from the reservoir [36] (Figure 3.13).

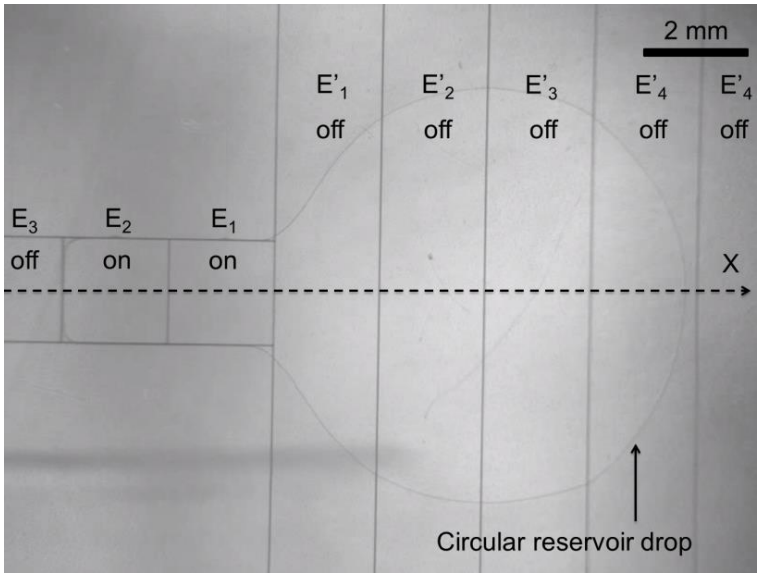

Figure 3.13 Video frame image of the circular reservoir drop

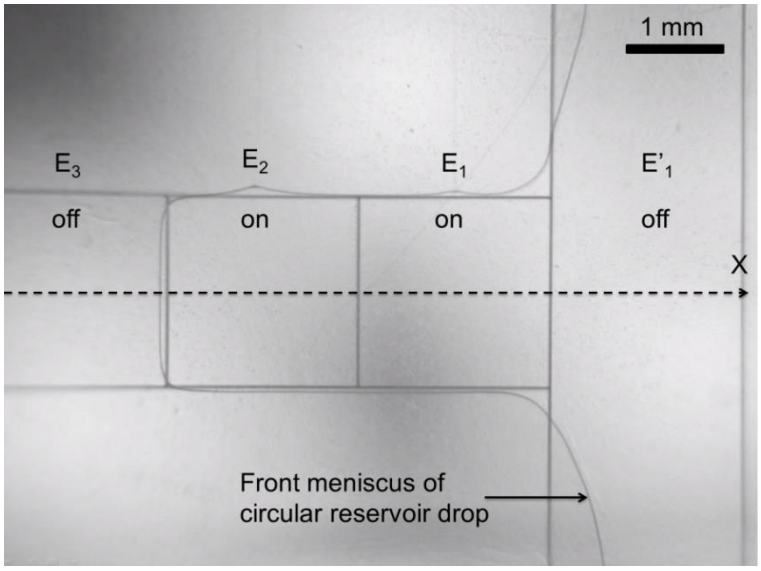

Figure 3.14 Video frame image of the extruded liquid column from the reservoir

In this pinching-off process, liquid in the reservoir and the drop generating site is stable while the liquid in the neck is unstable [36].

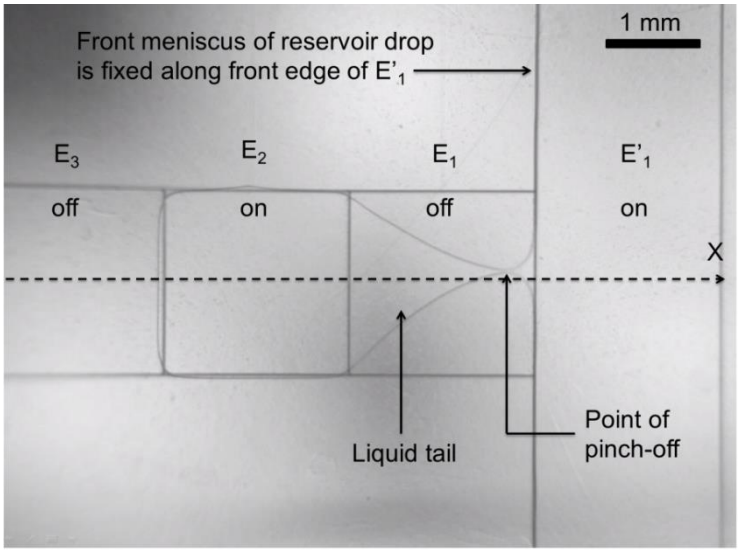

Figure 3.15 Video frame image of the liquid column which is subjected to the neck formation and pinch-off. A larger tail has formed behined the already formed liquid droplet.

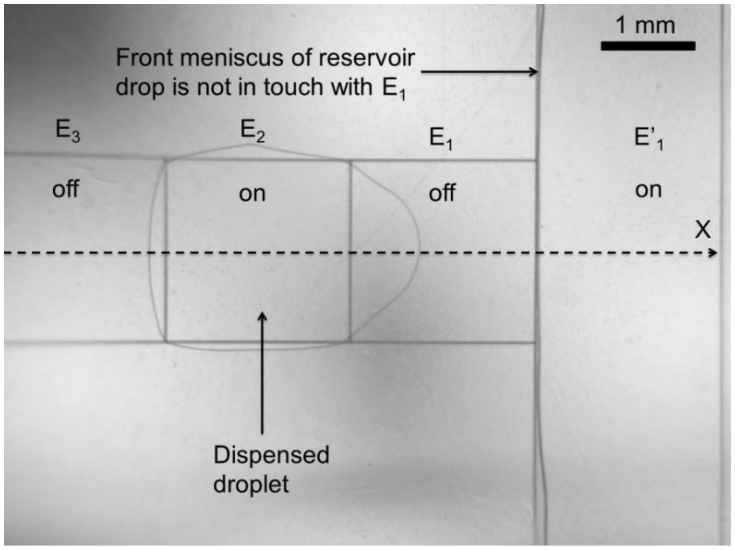

Figure 3.16 Video frame image of the dispensed droplet. The size of the dispensed droplet is bigger than the size of the electrode

After pinchin-off, some of the liquid is drawn back to the reservoir while the left amount is drawn into the already dispenesed droplet [36]. A maximu presure is generated at the location of pinch-off [36]. This pressure relationship depends on the droplet size, the space gap between the bottom pate and the cover plate and the EWOD actuating volateg [36].

This method of dropet dispensing is lack of reproducibility. After pinch-off, the reservoir drop is pulled backward into the reservoir so that the front boundary of the reservoir is not in touch with the E_1 (Figure 3.16). Since the entire reservoir is a single electrode, the reservoir drop cannot be moved forward until it is in touch with the first control electrode. Therefore, this method is capable of dispensing only one droplet. That is the main disadvantage of this droplet dispensing method.

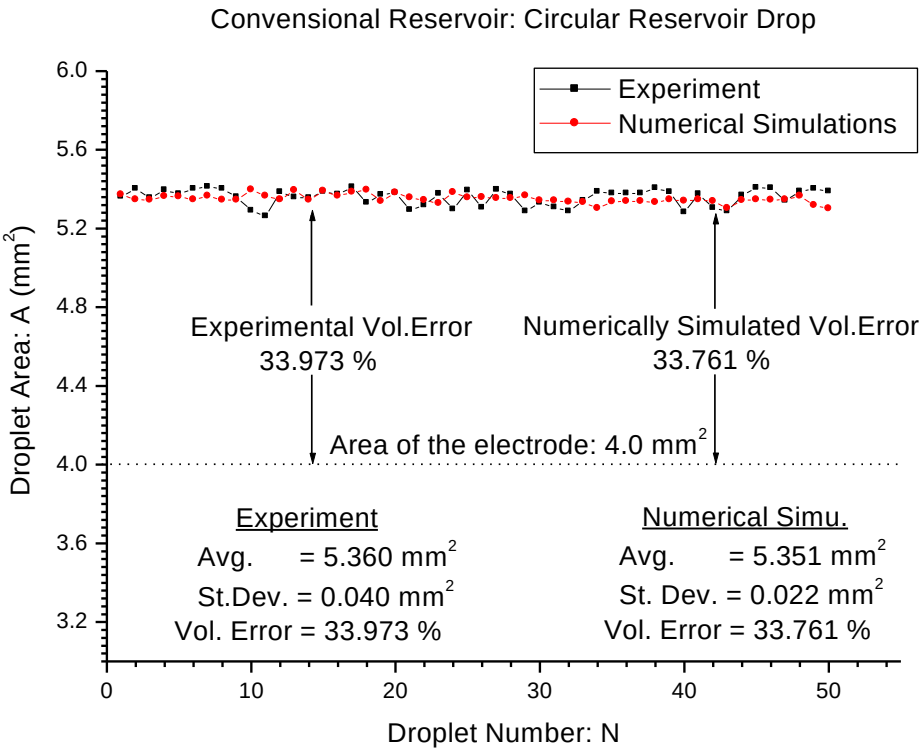

Figure 3.17 Volume precision and consistency of the droplets dispensed from the conventional reservoir with a circular reservoir drop. Black curve represents the experimentally obtained results. Red curve represents the numerically simulated results

To study the reproducibility, the reservoir drop was artificially moved forward by activating stripped electrodes in the reservoir. Therefore, this reproducibility is called artificial reproducibility. As shown in the Figure 3.17, the volume of the dispensed droplets was maintained approximately in a steady value even though droplets continued to be dispensed without replenishing the reservoir. According to the above Figure, experimentally obtained average volume error was 33.973 % while the numerically simulated average volume error was 33.761 %. Thus, there is a very good agreement between the experimental and numerically simulated results.

3.6.2 Volume Precision Associated with the Conventional Reservoir: Rectangular Reservoir Drop

The area of the initial reservoir drop is $327\ mm^2$. It occupies $81.75\ \%$ within the reservoir. To move the reservoir drop forward and backward, a set of stripped electrodes are activated. Therefore, in this droplet dispensing process, the reservoir drop takes the shape of a rectangle (Figure 3.18).

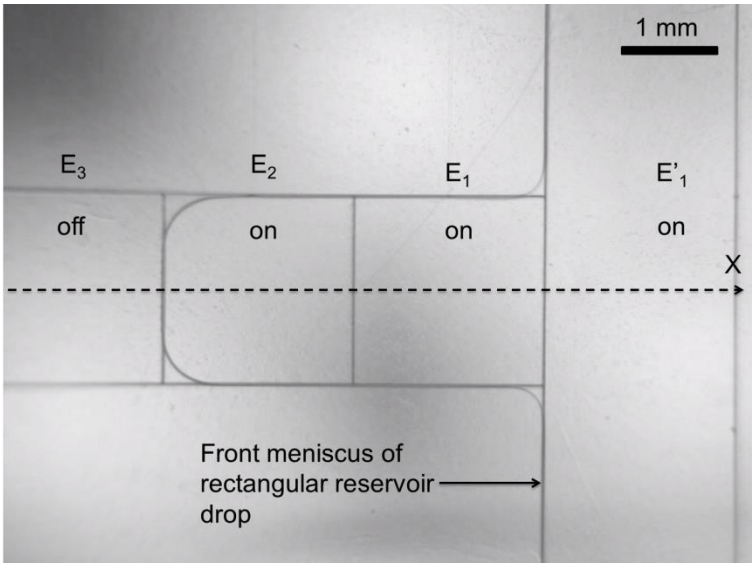

Figure 3.18 Video frame image of the reservoir drop and the extruded liquid column from the reservoir drop

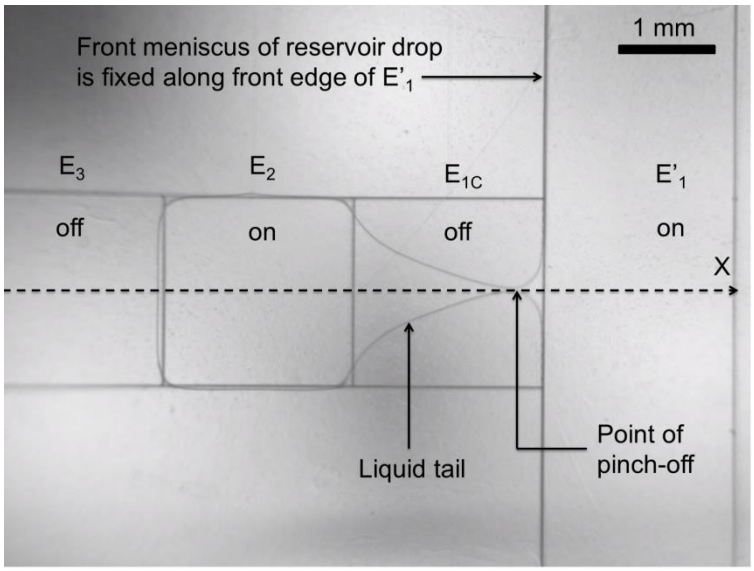

Figure 3.19 Video frame image of the liquid column which is subjected to the neck formation and pinch-off. A larger tail is formed behined the already formed liquid droplet

As shown in the Figure 3.29, as droplets continued to be generated without replenishing the reservoir, the volume of the dispensed droplet was gradually increased. According to the experiments, the volume of the dispensed droplet was increased by 3.3% when the reservoir dispensed 50 droplets. According to the numerical simulations, the volume of the dispensed droplet was increased by 2.4 % when the reservoir dispensed 50 droplets. This is because the pinch-off point is more likely to be affected by the long liquid-gas interface along the left boundary of the first stripped electrode, while the long interface doesn't exist in the circular reservoir drop in the first case.

According to the Figure 3.29, experimentally obtained average volume error was 30.652 % while the numerically simulated average volume error was 29.965 %. Thus, there is a very good agreement between the experimental and numerically simulated results.

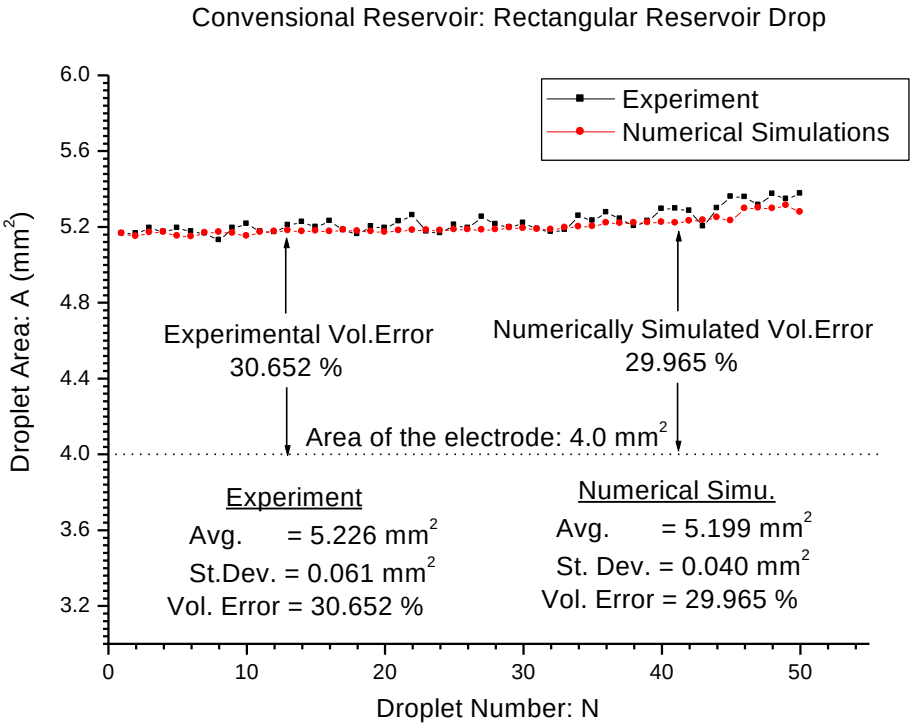

Figure 3.20 Volume precision and consistency of the droplets dispensed from the conventional reservoir with a rectangular reservoir drop. Black curve represents the experimentally obtained results. Red curve represents the numerically simulated results

3.6.3 Volume Precision Associated with the TCC Reservoir with Rectangular Drop generating Site

The size of the initial reservoir drop was $342\ mm^2$. It occupied $85.5\ \%$ of the reservoir.

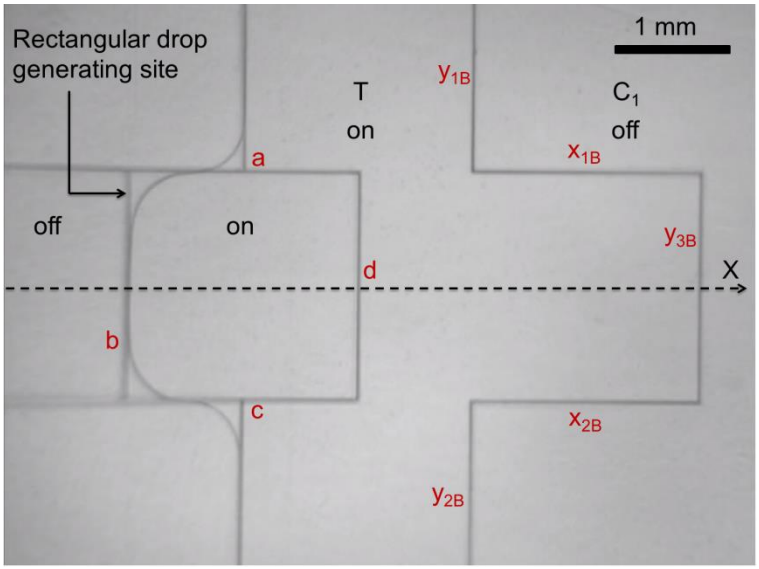

Figure 3.21 Video frame image of the initial reservoir drop. Both T-electrode and the drop generating site are wetting

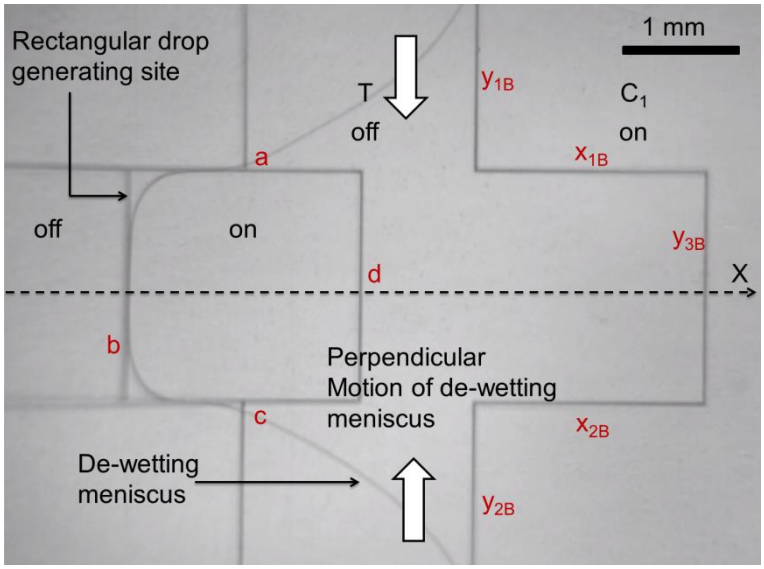

Figure 3.22 Video frame image showing the motion of the menisci on the de-wetting T-electrode at the beginning of droplet dispensing

The menisci on the de-wetting T-electrode is moving towards the reservoir until they meet the edges y_{1B} and y_{2B}. As the reservoir drop continued to be pulled, the menisci align over the edges *a,b* and *c* of the drop generating site and the edges y_{1B} and y_{2B} of the first C-electrode.

The edges *a, b* and *c* of the drop generating site and the edges y_{1B} and y_{2B} of the first C-electrode act as constrain for the menisci moving on the de-wetting T-electrode. At these wetting edges, the menisci stop their motion as shown in the Figure 3.23.

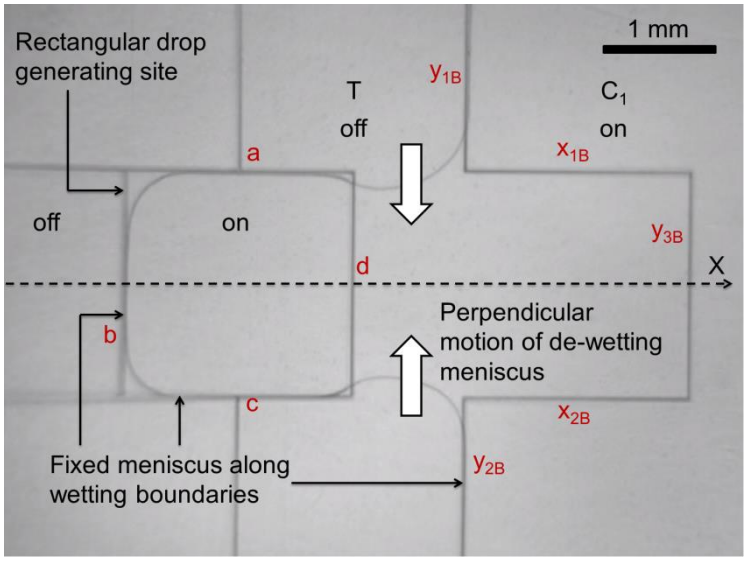

Figure 3.23 Video frame image of the dispensing droplet. Menisci align along the edges *a,b* and *c* of the drop generating site and the front edges y_{1B} and y_{2B} of the first C-electrode and stop their motion

Hence, this constrain changes the moving direction of the liquid on the de-wetting T-electrode. Therefore, under these constrain conditions, the only possible direction of menisci motion is in between the drop generating site and the first C-electrodes towards each other.

As the liquid on the de-wetting T-electrode is continued to be pulled towards the reservoir, first, the menisci start to align along the vertical back edge *d* of the drop generating site as shown in the Figure 3.34. This positioning produces a perpendicular motion. At the meantime, the menisci start to align along the horizontal front edges x_{1B} and x_{2B} of the first C-electrode. This positioning produces axial motion.

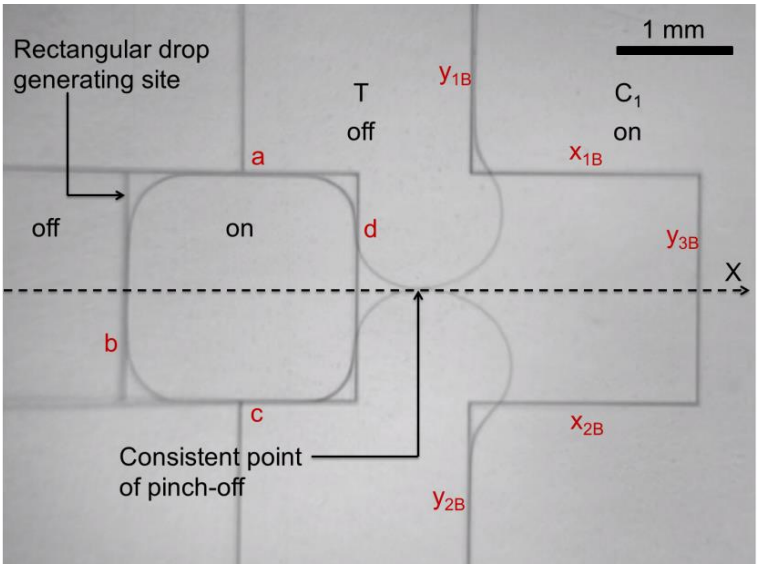

Figure 3.24 Video frame image of the dispensing droplet. Pinch-off happens at the point the two menisci meet each other

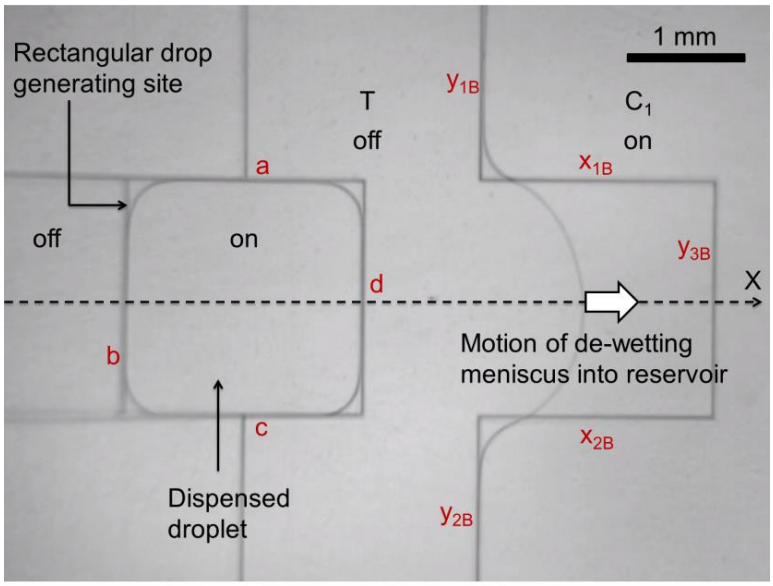

Figure 3.25 Video frame image of the dispensing droplet. De-wetting meniscus of the reservoir drop is moving back to the reservoir.

After pinch-off, the reservoir drop is separated from the dispensed droplet and pulled backward into the reservoir. In this pulling motion, liquid on the de-wetting T-electrode moves in between the edges x_{1B} and x_{2B} of the first C-electrode, which is the second constrain for the droplet dispensing (Figure 3.25). When the moving meniscus meets the edge y_{3B} of the first C-electrode, reservoir drop comes to the rest and becomes stable (Figure 3.26).

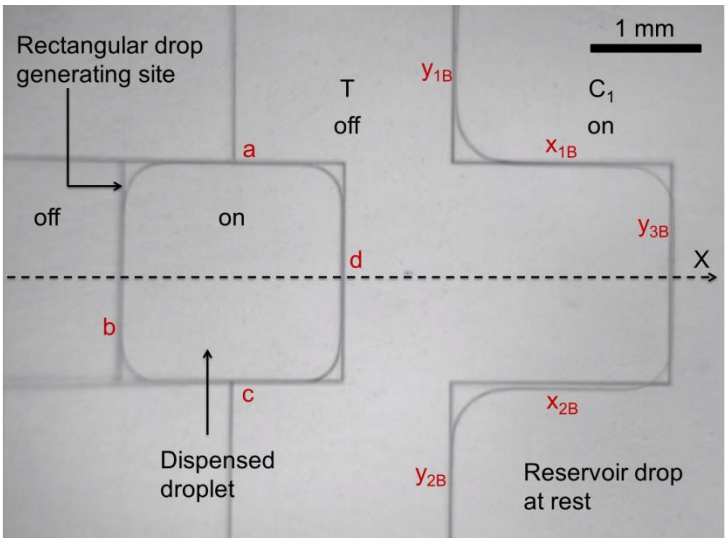

Figure 3.26 Video frame image of the dispensed droplet. Volume of the dispensed droplet is almost equal to the volume occupied by the drop generating site. Front boundary of the reservoir drop is aligned over the front edge of the first C-electrode

According to the Figure 3.27, experimentally obtained average volume error was 3.700 % while the numerically simulated average volume error was 4.093 %. Thus, there is a very good agreement between the experimental and numerically simulated results. When compared with the conventional reservoir, the droplet's volume accuracy dispensed from the TCC reservoir with a rectangular drop generating site is much higher. This very small volume error occurs as a result of the tiny tail formation behind the dispensing droplet.

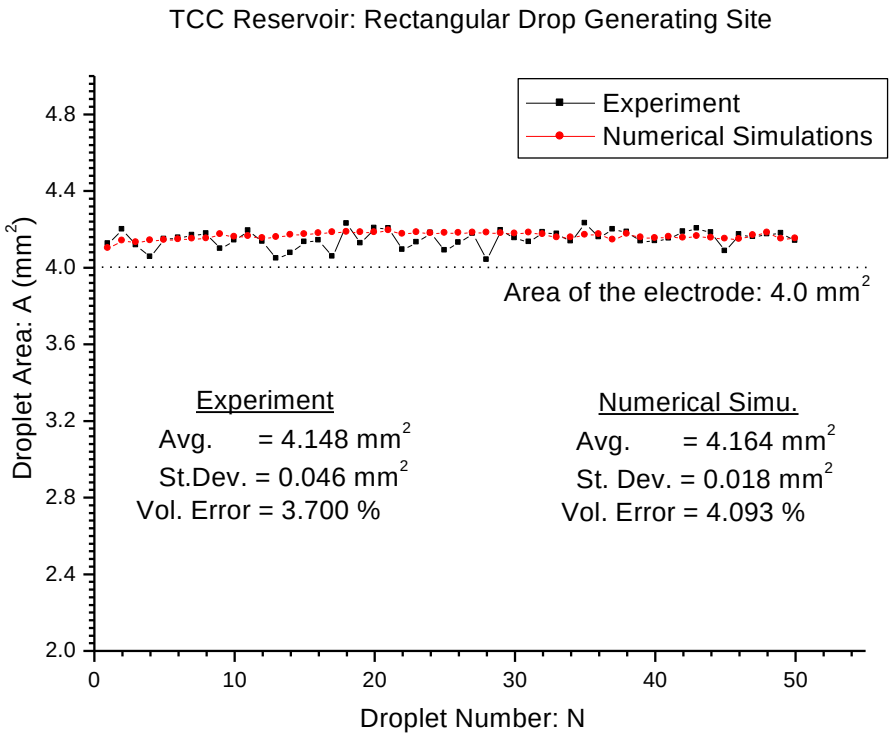

Figure 3.27 Volume precision and consistency of the droplets dispensed from the conventional reservoir with a rectangular reservoir drop. Black curve represents the experimentally obtained results. Red curve represents the numerically simulated results

3.6.4 Volume Precision Associated with the TCC Reservoir with Circular and Angular Drop generating Site

The size of the initial reservoir drop is $280\ mm^2$. It occupies $70.0\ \%$ of the reservoir. The front boundary of the reservoir drop is aligned over the front edge of both the T-electrode and the drop generating site.

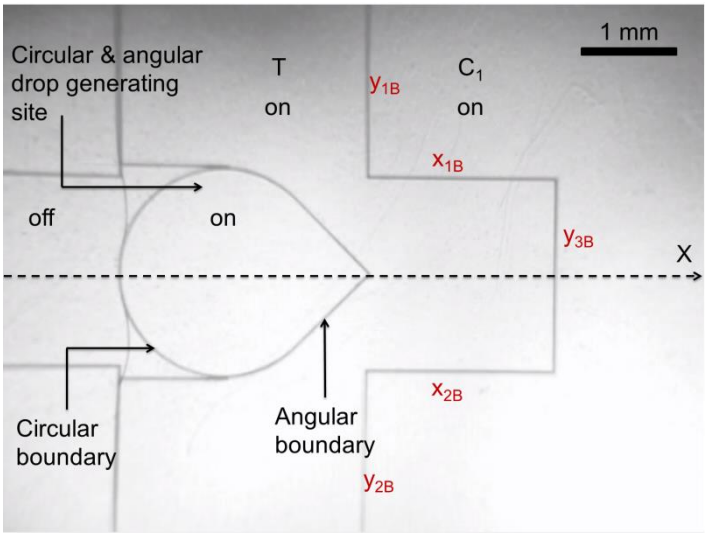

Figure 3.28 Video frame image of the initial reservoir drop. Both T-electrode and the drop generating site are wetting

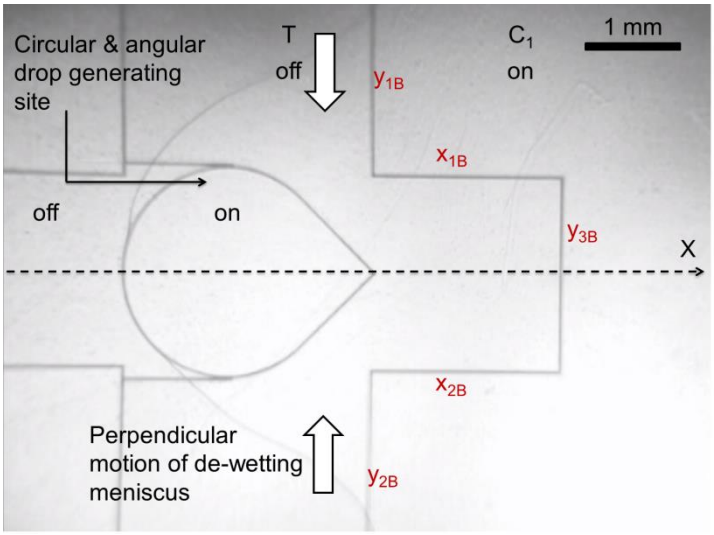

Figure 3.29 Video frame image showing the motion of the meniscus on the de-wetting T-electrode at the beginning of droplet dispensing. The meniscus starts to align over the front circular edge of the drop generating site and the front edges y_{1B} and y_{2B} of the first C-electrode

At these edges, the menisci stop their motion as shown in the Figure 3.30. Liquid meniscus perfectly aligns along the front circular front boundary without any area mismatch (Figure 3.30). This identical alignment helps to dispense a droplet whose footprint is equal to the area of the electrode.

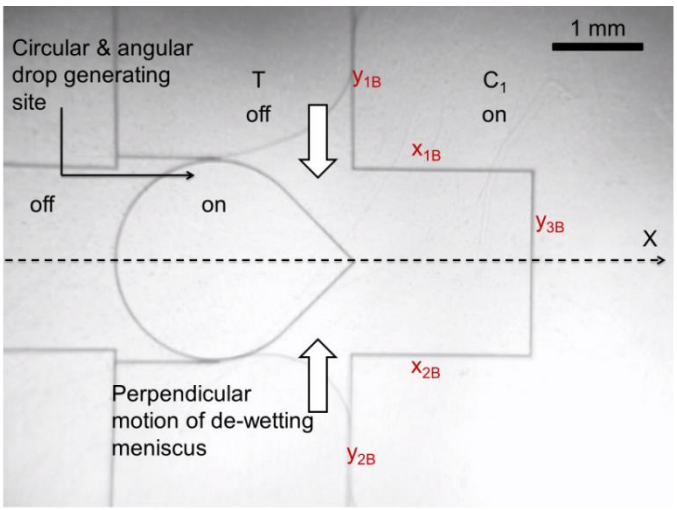

Figure 3.30 Video frame image of the dispensing droplet. Liquid meniscus has perfectly aligned along the front circular edge of the drop generating site. Liquid meniscus is still aligning along the front edge of the first C-electrode.

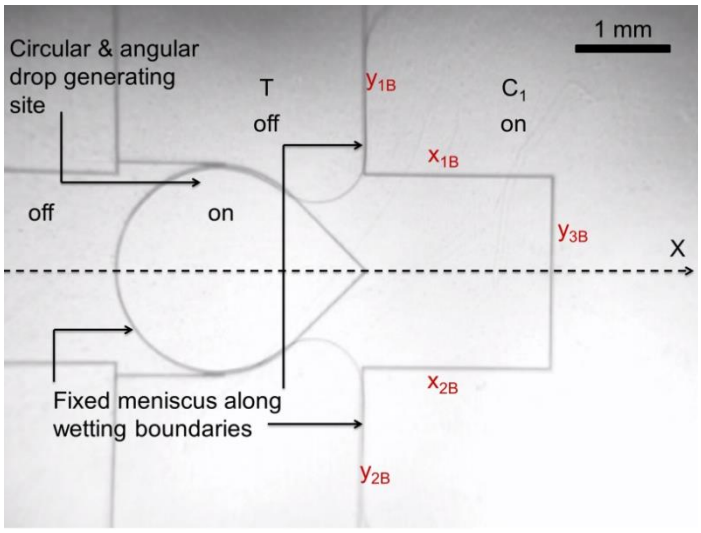

Figure 3.31 Video frame image of the dispensing droplet. At the reservoir side, liquid moves parallel along the vertical edge of the first C-electrode. At the drop generating site, liquid follows the angular edge of the drop generating site

The liquid on the de-wetting T-electrode is free to move into the reservoir in between the horizontal edges x_{1B} and x_{2B} of the first C-electrode. At this constrain, at the reservoir side, liquid moves parallel along the horizontal edges x_{1B} and x_{2B} of the first C-electrode. At the drop generating site, liquid follows the remaining halfway of the angular edge towards the tip of the angle (Figure 3.32).

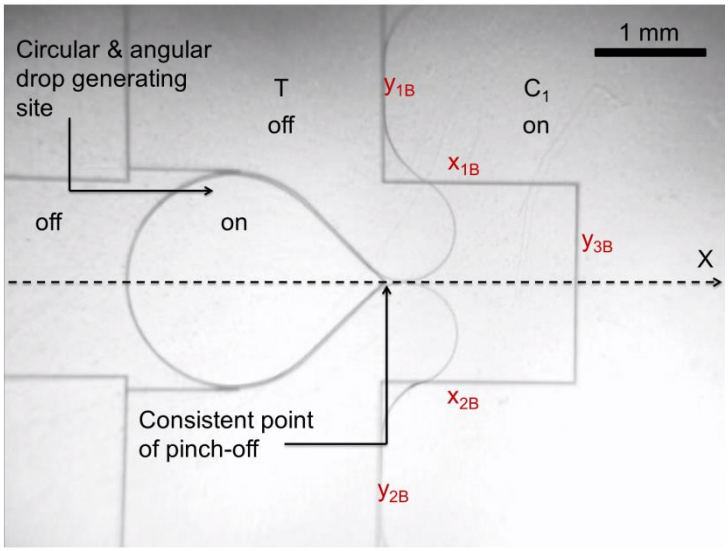

Figure 3.32 Video frame image of the dispensing droplet**.** At the reservoir side, liquid moves parallel along the horizontal edges x_{1B} and x_{2B} of the first C-electrode. At the drop generating site, liquid follows the remaining halfway of the angular edge towards the tip of the angle

With this horizontal and angular motion of the liquid, the two menisci from the top and bottom get closer to each other. At a certain point, these moving menisci meet each other at which the pinch-off occurs (Figure 3.32). According to the Figure 3.32, menisci formation is symmetric over the middle x-axis. The pinch-off occurs at the tip of the angular region of the drop generating site. Therefore, the point of pinch of is consistent and it can be exactly located. The shape of the already formed droplet takes the shape of the drop generating site. Therefore, there is no any area mismatch between the footprint of the dispensed droplet and the drop generating site. The cutting length is zero. There is no any tail formation behind the droplet.

Therefore, the volume of the dispensed droplet is exactly equal to the volume occupied by the drop generating site. After pinch-off, the liquid portion of the reservoir drop which is on the de-wetting T-electrode moves in between the edges x_{1B} and x_{2B} of the first C-electrode towards the reservoir (Figure 3.33). When the moving meniscus meets the edge y_{3B} of the first C-electrode, reservoir drop comes to the rest and becomes stable.

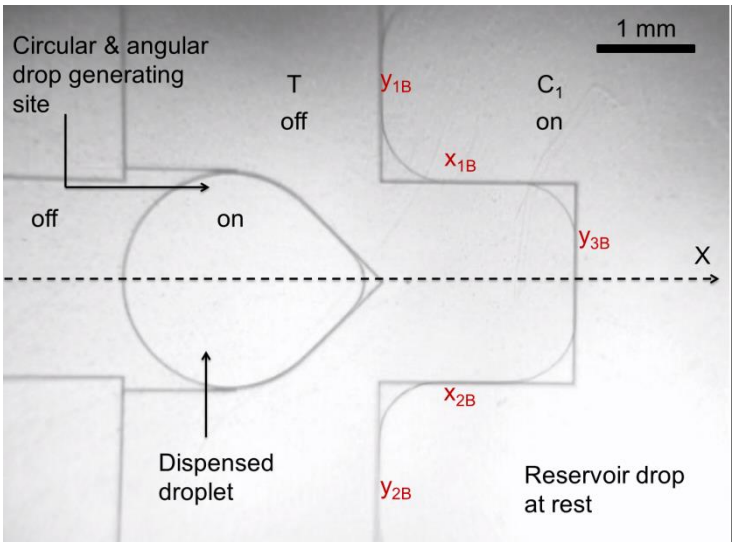

Figure 3.33 Video frame image of the dispensed droplet. Volume of the dispensed droplet is equal to the volume occupied by the drop generating site. Front boundary of the reservoir drop is aligned over the front edge of the first C-electrode

For this experiment, a very smaller spacer gap has to be maintained in between the bottom plate and the cover plate (~ 100 µm). For higher space gaps, separation is difficult due to zero cutting length and the very narrow gap in between the drop generating site and the first C-electrode. Instead of separating, entire droplet on the drop generating site can be pulled back into the reservoir. Further, the separation capability depends on the concentration of the hydrophobic coating. Droplets can be easily dispensed from the reservoir for the hydrophobic coatings of higher concentration.

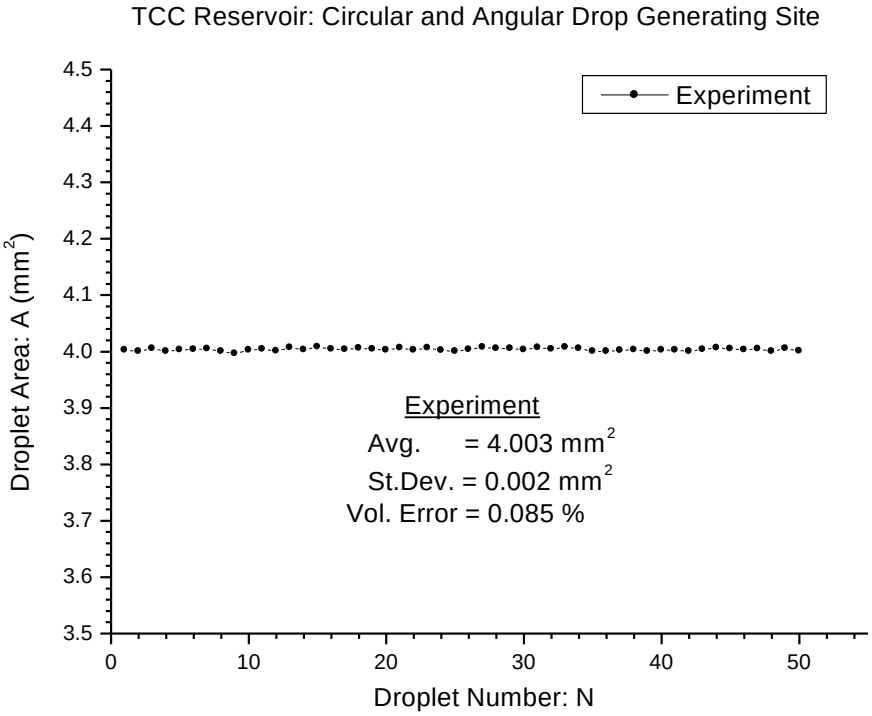

Figure 3.34 Volume precision and consistency of the droplets dispensed from the TCC reservoir with circular and angular drop generating site

According to the Figure 3.34, experimentally obtained average volume error was 0.085 %. When compared this result with the volume accuracy for the TCC reservoir with rectangular drop generating site, this volume accuracy is 50 times higher. Further, this result is 360 times accurate than the result obtained for the conventional reservoir with rectangular reservoir drop and 400 times accurate than the result obtained for the conventional reservoir with circular reservoir drop. This much higher volume precision was achieved solely on the geometrical design factors of the reservoir; 1) zero cutting length, 2) eliminating the tail formation, 3) eliminating the area mismatch between the droplet and the drop generating site.

Figure 3.35 summarizes the results of droplet's volume dispensed from different reservoirs. According to the Figure 3.35, the area of the droplet dispensed from the TCC reservoir with circular and angular drop generating site is almost equal to the area of the drop generating site. The droplet area corresponding to the TCC reservoir with rectangular drop generating site is somewhat larger than the area of the drop generating site. The droplet area dispensed from the conventional reservoirs is significantly larger than the area of the drop generating site.

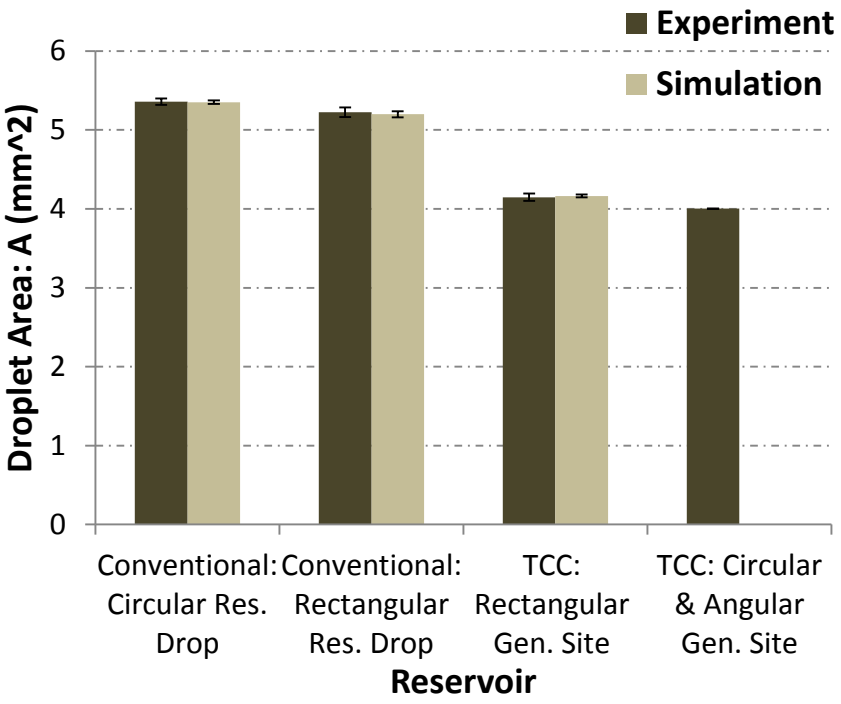

Figure 3.35 Volume of the droplets dispensed from the different reservoirs: The area of the drop generating site is the same (4.00 mm^2)

According to the experiments, the area of the droplet obtained from the TCC reservoir with circular and angular drop generating site was 4.003 mm^2. For the TCC reservoir with rectangular drop generating site, experiments showed a value of 4.148 mm^2 while simulations demonstrated a value of 4.164 mm^2. Experimentally obtained area for the droplet by the

conventional reservoir with rectangular reservoir drop was 5.226 mm^2 while numerically simulated result was 5.199 mm^2. Using the conventional reservoir with circular reservoir drop, droplet areas of 5.360 mm^2 and 5.351 mm^2 were obtained respectively.

Figure 3.36 summarizes the results of percentage volume error of the droplet dispensed from different reservoirs. According to the Figure 3.36, the TCC reservoir with circular and angular drop generating site demonstrates the highest volume precision with negligible volume error of the droplet. Next, the TCC reservoir with rectangular drop generating shows higher volume precision with a very small volume error which is less than 5%. However, droplets dispensed from the conventional reservoirs have very high volume errors above 30%.

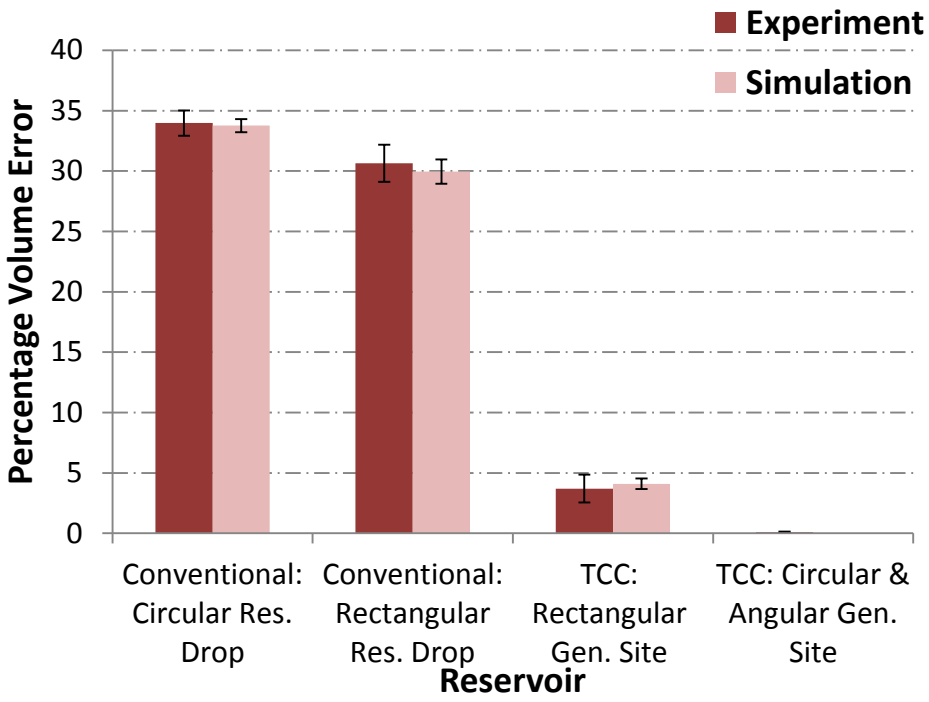

Figure 3.36 Percentage volume precision of the droplets dispensed from the different reservoirs: The area of the drop generating site is the same (4.00 mm^2)

According to the experiments, the TCC reservoir with circular and angular drop generating site demonstrated a volume precision of 0.083 %. For the TCC reservoir with

rectangular drop generating site, experiments showed a volume accuracy of 3.700 % while simulations demonstrated a value of 4.093 %. Experimentally obtained volume error for the droplet for the conventional reservoir with rectangular reservoir drop was 30.952 % while numerically simulated result was 29.965 %. Using the conventional reservoir with circular reservoir drop, volume error of 33.973 % and 33.761 % were obtained respectively.

3.7 Conclusion

In this chapter, we report a novel method of dispensing droplets with higher volume precision and consistency: drop dispensing by TCC reservoir. First, the challenges associated with dispensing droplets by the conventional reservoir by pulling a liquid column out from the reservoir are discussed. The major factors affecting for the droplet's volume variation are identified; 1) higher cutting length, 2) larger tail formation, 3) inconsistent location of cutting, and 4) inconsistent drop boundaries at the pinch-off. Next, to resolve the above challenges, TCC reservoir with rectangular drop generating site was designed. By arranging the positioning of the electrodes, a tiny tail formation with very shorter cutting length was achieved. By constructing the geometry of the electrodes to control the menisci formation under constrains, a consistent pinch-off point with fixed boundaries was achieved.

To further improve the volume precision, the drop generating site of the TCC reservoir was modified: the rectangular drop generating site was replaced by circular and angular drop generating site. By arranging the positioning of this drop generating site, the cutting length and the tail formation were completely eliminated. The point of pinch-off was properly controlled and exactly located. All the experimental results were compared with the numerically simulated results and verified. All the experiments were performed in air environment under atmospheric pressure.

CHAPTER 4

STUDYING MAJOR PARAMETERS THAT AFFECT THE SPEED OF DROP MOTION

This chapter presents experimental study of major parameters that affect the speed of drop motion in an EWOD device. Among many parameters, three were selected from our previous experiences; 1) surface roughness, 2) electrode size, and 3) electrode geometry. The first section of the chapter describes the study of surface roughness towards enhancing speed of drop motion. Two EWOD substrates were tested for surface roughness measurement; 1) PCB based EWOD substrate, and 2) glass based EWOD substrate. Experimentally obtained surface roughness values and corresponding maximum speed of drop motion are presented in each case. The second section demonstrates the study of electrode size towards enhancing speed of drop motion. Two electrode sizes were tested (2×2 mm^2 and 3×3 mm^2). The last section explains the study of electrode geometry towards enhancing speed of drop motion. Two electrode geometries, solid electrode and modified stripped electrodes were tested. Both glass based EWOD device and Silicon (Si) based EWOD device were used in this study.

4.1 Parameter 1: Surface Roughness

It has been observed that the roughness of the surface where a drop contacts in EWOD device significantly vary the speed of drop motion. Therefore, for systematic study of this parameter, at least two roughness of the EWOD device surface were created and the speed of drop motion for each surface were measured. To obtain enough contrast of two different surfaces yet put minimum effort, we selected two different substrates on which EWOD devices are fabricated. First surface is provided with a glass wafer (soda-lime, polished). The other

surface is prepared with printed circuit board (PCB). Glass surface is supposed to have a negligible surface roughness while PCB is expected to have a significantly rough surface. Unexpectedly, other hindrances than surface roughness against drop motion were found in PCB EWOD devices. First, trenches located in between two electrodes exert a resistive force on the moving droplet in opposite direction [48]. The boundary of the trench is decided by the height (43 μm) of solder pads and the gap (150 μm) between solder pads. To relocate the droplet from one electrode to the adjacent one, the droplet should fill the trench first with liquid and then move over the trench to meet the adjacent electrode. In this manner, after spreading liquid onto the neighboring electrode, droplet can be pulled by EWOD actuation by the neighboring one. During this pulling process, the tail of the liquid droplet has to move over the former trench. This motion created a resistive force on the droplet to pull the droplet backward. To overcome this resistive force and initialize the drop motion, much higher actuating voltage is required [48].

Next, via holes drilled at the middle of the electrode generate a resistive force for the drop motion [48]. As the droplet moves over a via hole, it is likely to attach to the via hole creating a drag force on the moving droplet. Further, the diameter of a via hole (356 μm) is comparably larger than the space gap (100 μm) between the bottom and the cover plates. Since the droplet squeezed between the two plates has a higher internal pressure [47], liquid is forced to enter into a via hole [48]. This will create problems for the motion of the droplet on the PCB surface. Moreover, the PCB based EWOD substrate has higher surface irregularities than the glass based EWOD substrate [48].

To eliminate the problem caused by trenches and via holes, we developed several steps to treat PCB surfaces. First, to reduce the surface irregularities on the PCB surface, trench was filled by dielectric materials (SU-8). After that, a via holes were filled by lead. To further improve the surface flatness, PCB surface was polished by Chemical Mechanical Polishing (CMP). The well-polishes PCB surface was coated with layers of dielectric (SU-8-5) and hydrophobic (Teflon).

Surface roughness of this PCB substrate was measured by Profilometer (AlphaStep-IQ, Nanofabrication facility, The University of Texas at Arlington). After that, PCB based EWOD device was tested to find the maximum droplet motion speed. In the same way, surface roughness of the glass based EWOD substrate was measured. Finally, the glass based EWOD substrate was tested to find the maximum speed of drop motion.

4.2 Parameter 2: Electrode Size of Square Electrodes

To study the effect of electrode size, square electrodes with two different sizes were tested (2×2 mm^2 and 3×3 mm^2). Corresponding to each electrode size, three sets of electrode arrays were patterned as shown in the Figure 4.1. Each electrode array consists of ten electrodes. The gap between each electrode is 10 μm. In addition to the size of electrode, arrangements of two adjacent electrodes have variations. Interdigitating arrangement of fingers attached to an electrode may increase the chance of a drop to contact the adjacent electrode. In each electrode array, arrangements between two adjacent electrodes are different; 1st row: square electrodes only without any interdigitating fingers as a reference, 2nd row: many interdigitating fingers, and 3rd row: a few fingers (Figure 4.2). TCC reservoirs are added to each set of electrode array to generate liquid droplets. In each case, size of the drop generating site of the TCC reservoir is equal to the size of the electrode of the electrode array.

In the experiment, three droplets dispensed from the reservoir were accelerated over the electrode arrays by reducing the switching time of actuation. Drop motions over the each electrode array were recorded by the high-speed camera (FASTEC. TS3, frame rate: 1250 fps). These videos were analyzed to determine the maximum speed of drop motion.

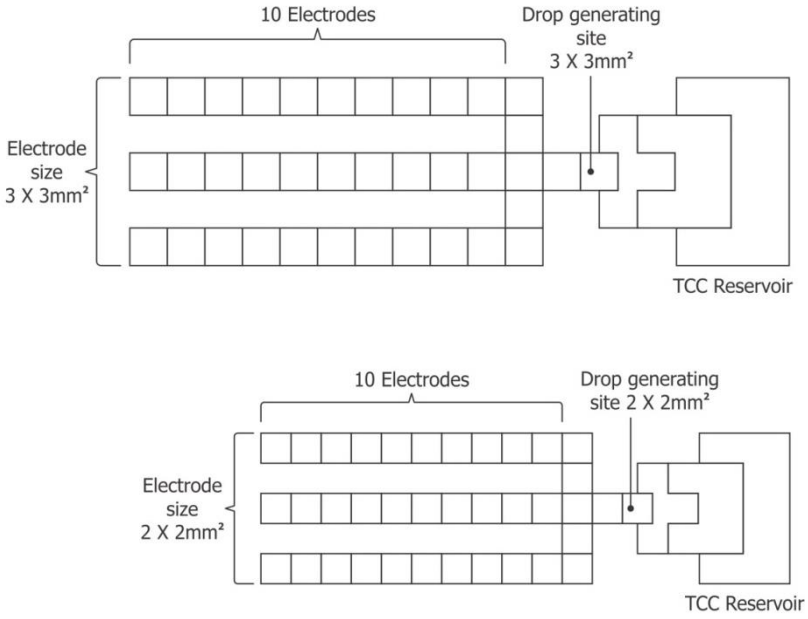

Figure 4.1 Electrode arrays with two different electrode sizes to study effect of electrode size on the speed of drop motion.

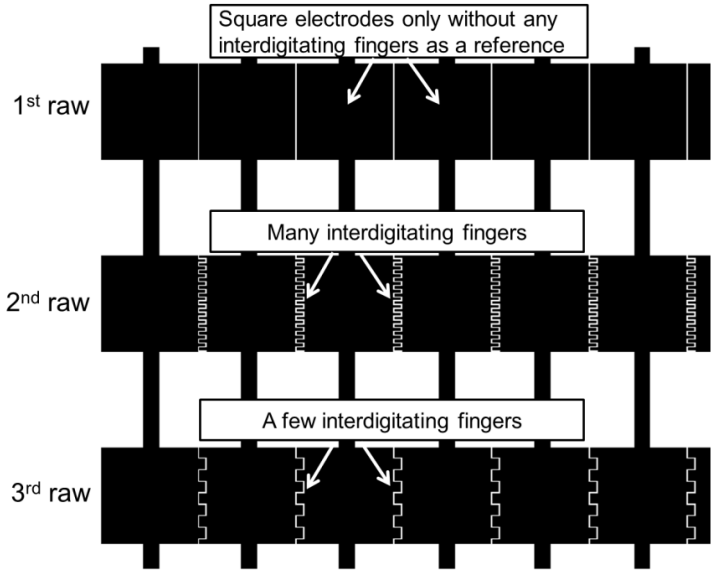

Figure 4.2 In each electrode array, arrangements between two adjacent electrodes are different; 1st row: square electrodes only without any interdigitating fingers as a reference, 2nd row: many interdigitating fingers, and 3rd row: a few fingers.

4.3 Parameter 3: Electrode Geometry

Two different electrode geometries were studied towards enhancing speed of drop motion. One is solid square shape of electrodes that typically have been used in EWOD devices. By careful examination of the drop motion over solid square electrodes, major factors affecting the drop motion at high speed were identified; 1) smaller EWOD force, 2) higher inertia resisting the motion, 3) longer tail formation, and 4) larger deformation of the droplet. To alleviate these adverse effects, we introduce the second geometry of electrodes, a set of five rectangular strips of electrodes. These modified stripped electrodes and operation sequences could generate higher EWOD force on the droplet and reduce the resistances against the drop motion.

4.3.1 Solid Electrodes (Square Electrodes)

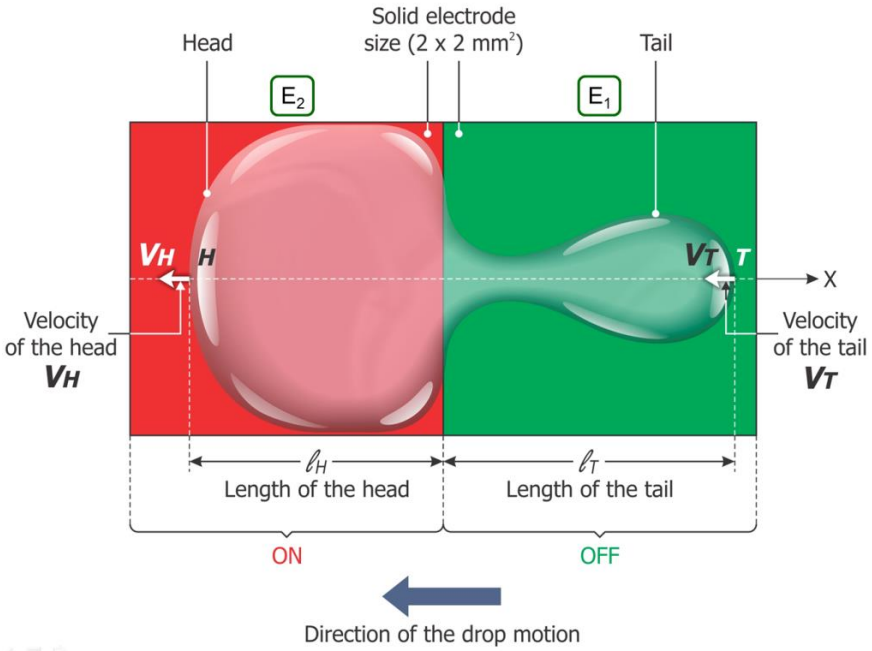

Figure 4.3 Motion of a droplet over the solid electrodes

The size of the tested solid electrode is 2 × 2 mm^2. After careful examination, we found that the motion of the liquid portion on the wetting electrode (head of the droplet) is different

from the motion of the liquid portion on the de-wetting electrode (tail of the droplet). Correspondingly, the head and tail possess two different speed profiles (velocity-time graphs) during the transition from one electrode to the next (Figure 4.3).

As shown in the Figure 4.3, the droplet is moving from electrode 1 on the right to electrode 2 on the left (E_1 to E_2). Initially, as liquid enters into the E_2, it is pulled by the EWOD force towards the E_2. This pulling force forms a circular meniscus formation on the E_2. This meniscus formation deforms the droplet separating it into two regions as head and tail. During the transition, liquid tail follows the liquid head behind and shape of both head and tail are varied with time. This creates two different velocity profiles for head and tail (V_H and V_T). To study the behavior of the head and tail motion, both V_H and V_T were plotted with respect to time.

4.3.2 Stripped Electrodes (Rectangular Electrodes)

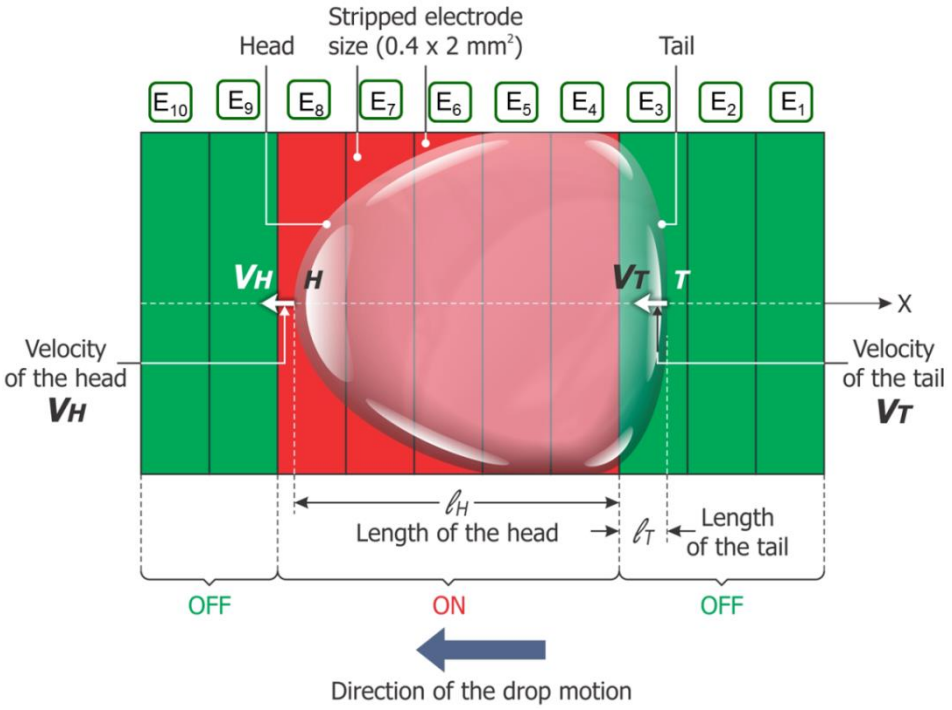

Figure 4.4 Motion of a droplet over the stripped electrodes

Stripped electrodes are designed by dividing a square electrode into five equal rectangular parts. The size of the resulted stripped electrode is 0.4 × 2 mm^2 (Figure 4.3). For

the drop motion, a set of five adjacent stripped electrodes should be actuated simultaneously. As shown in the Figure 4.4, the droplet is moving from electrode 1 on the right to electrode 10 on the left (E_1 to E_{10}).

Since five stripped electrodes are activated simultaneously, the head of the droplet is much larger than the tail formation. Therefore, liquid head experience much higher EWOD force from the wetting electrodes (Figure 4.5). The tail formation behind the head is shorter. Therefore, the inertia of the tail that resists the drop motion is lower. During the transition of the droplet from one set of stripped electrodes to the next set, deformation of the droplet is very little compared to the solid electrodes. As a result of these improvements, much higher speed of drop motion can be achieved on the stripped electrodes.

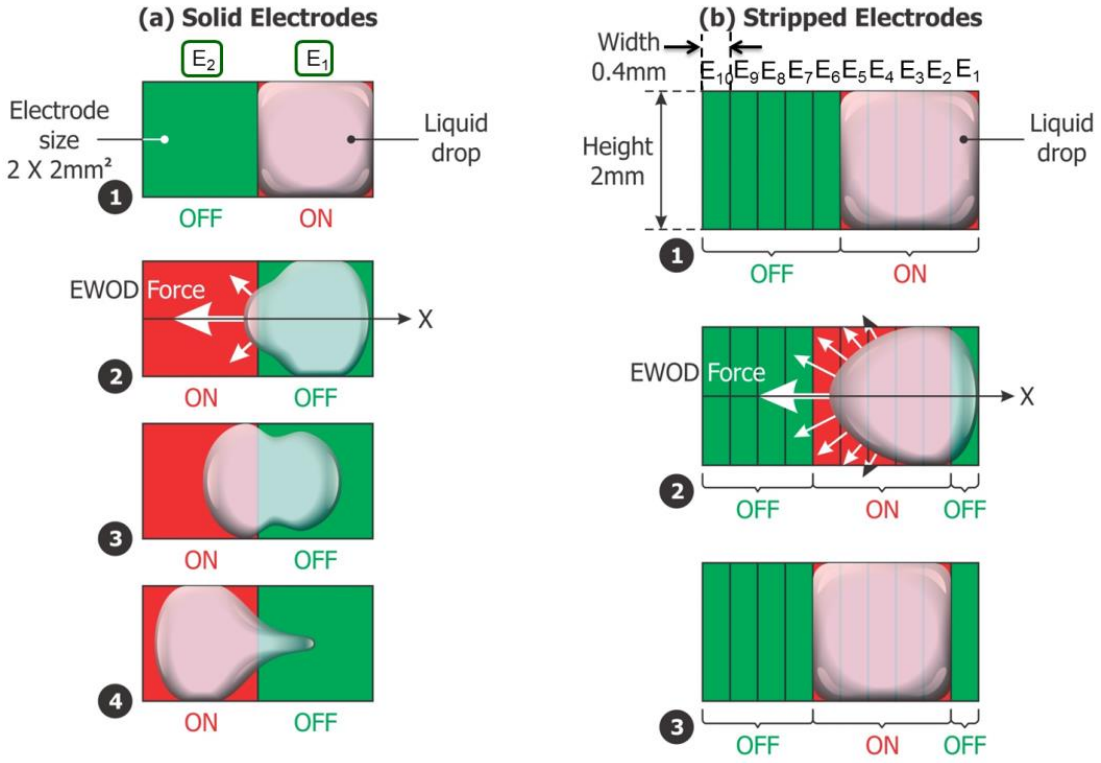

Figure 4.5 Comparison of drop motion on solid and stripped electrodes

4.4 Results and Discussion

4.4.1 Surface Roughness of the PCB-Based and Glass-Based EWOD Substrates

Roughness measurements of PCB surface and glass surface are presented in Figure 4.6 through 4.8

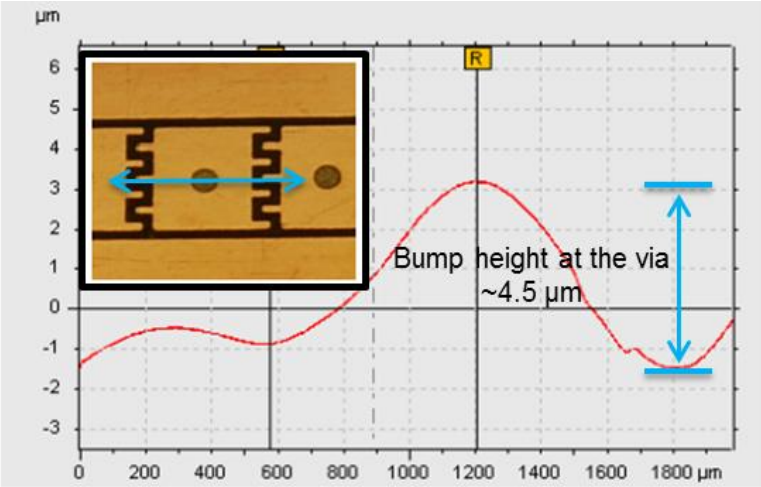

Figure 4.6 Surface irregularities on the surface of the PCB substrate over the filled via hole

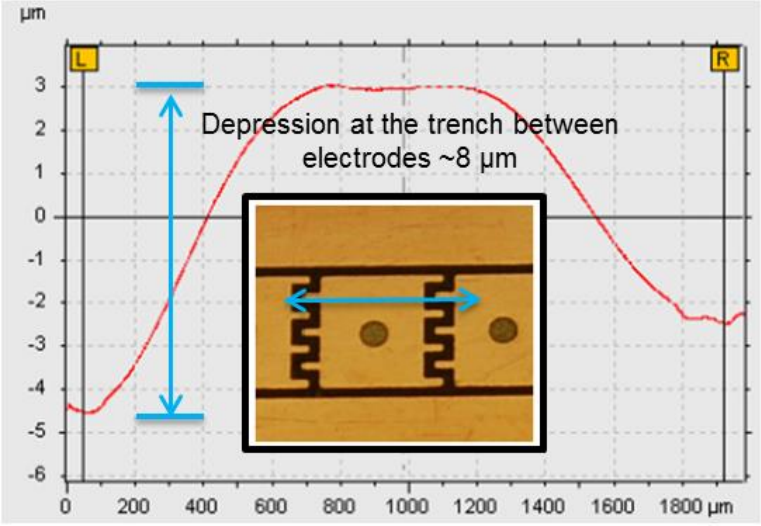

Figure 4.7 Surface irregularities on the surface of the PCB substrate besides the via hole

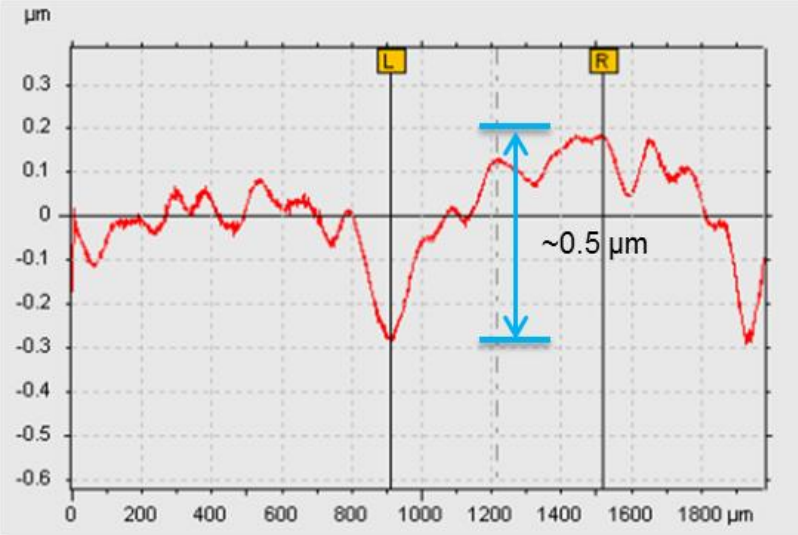

Figure 4.8 Surface roughness of the glass substrate

4.4.2 Electrode Size of the Solid Electrodes

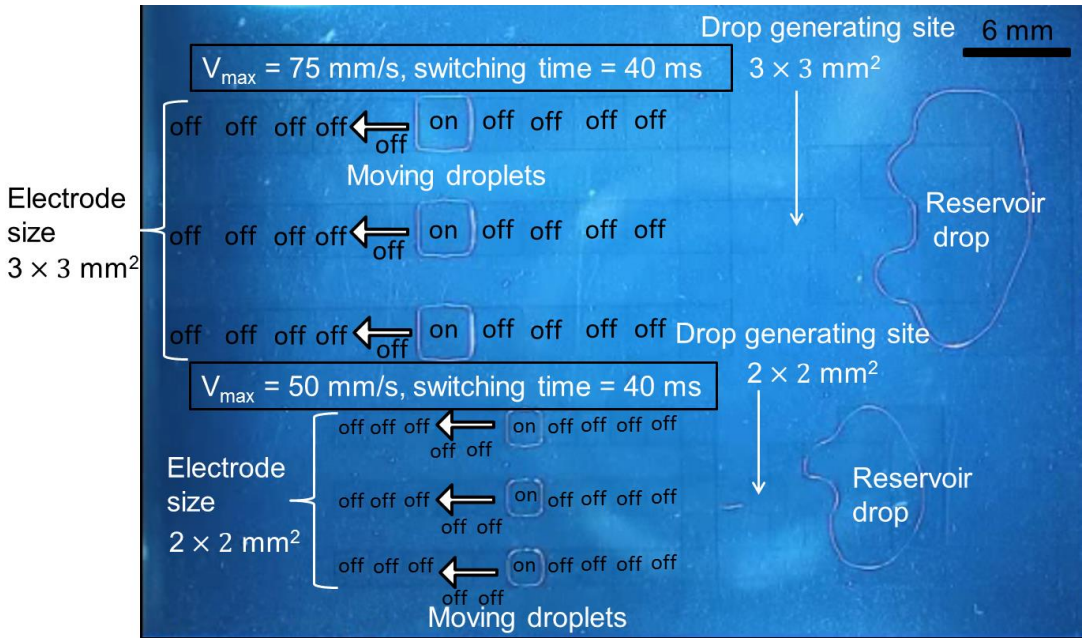

Figure 4.9 Studying the effect of electrode size for the speed of drop motion on the glass-baes EWOD device. Video frame image shows higher speed of drop motion for larger electrodes

The minimum switching time corresponding to the maximum speed of drop motion was 40 ms. Corresponding to this switching time, maximum speed of 75 mm/s was achieved for larger electrodes ($3 \times 3\ mm^2$) while maximum speed of 50 mm/s was achieved for smaller electrodes ($2 \times 2\ mm^2$). These results are explained in more details in the next section.

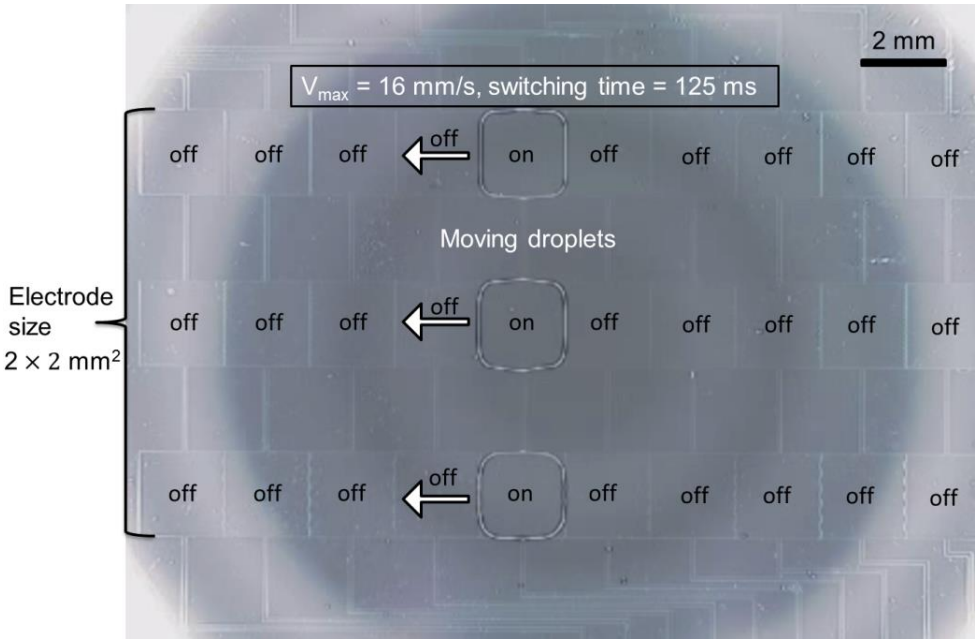

Figure 4.10 Studying the effect of electrode size for the speed of drop motion on the Si-based EWOD device. Video frame image shows higher speed of drop motion for larger electrodes

The minimum switching time corresponding to the maximum speed of drop motion was 125 ms. Corresponding to this switching time, maximum speed of 24 mm/s was achieved for larger electrodes 3 × 3 mm^2 while maximum speed of 16 mm/s was achieved for smaller electrodes 2 × 2 mm^2. According to these results, the maximum speed of drop motion on Si is lower than that of the glass surface. In future, we will investigate the reason for this difference.

4.4.3 Electrode Geometry: Solid Electrodes (Square Electrodes)

Figures 4.11-20 show video frame images of a moving droplet at 100 ms interval (frame rate 1250 fps with a resolution 800×600). The applied actuation voltage is 125 V with electrode ON time of 100 ms ($V_{average} = 20\ mm/s$). Solid electrode size is $2 \times 2\ mm^2$. Droplet is moving from right electrode to the left.

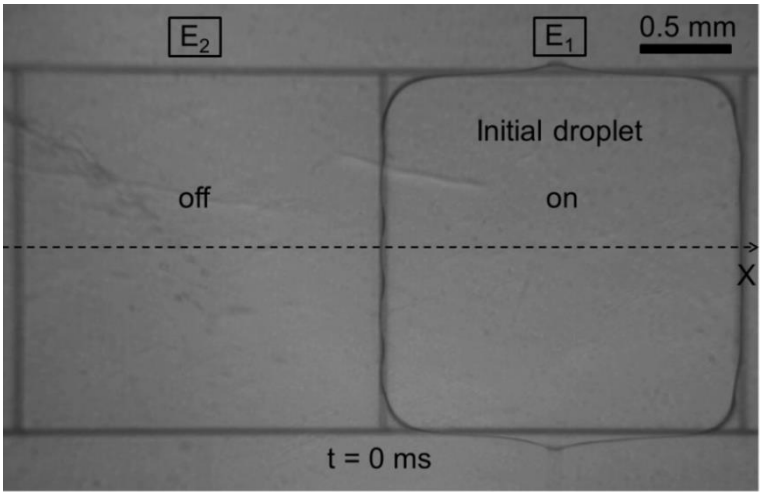

Figure 4.11 Video frame image of the droplet siting on the right electrode (E_1) just before it starts the motion (time: t = 0).

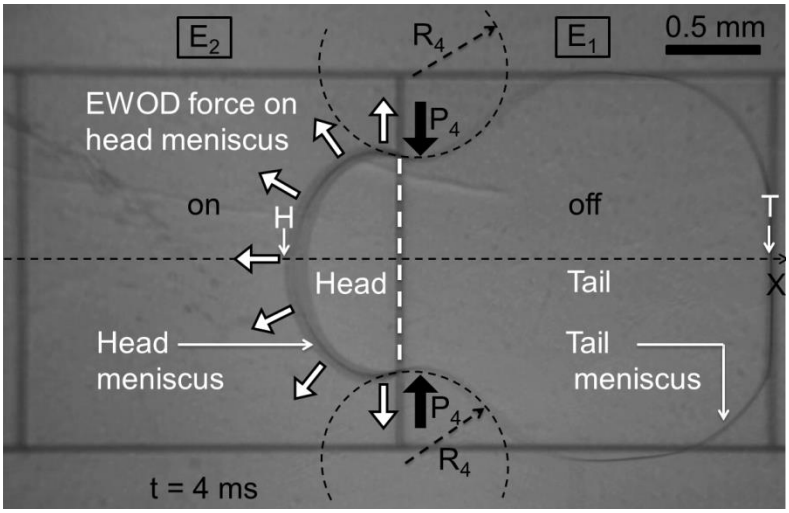

Figure 4.12 Video frame image of the moving droplet (time: t = 4 ms).

E_1 is deactivated. E_2 is activated. While liquid enters into the E_2, it is pulled by the EWOD force towards the E_2. Velocity of the head and tail is measured with respect to the point H and T respectively.

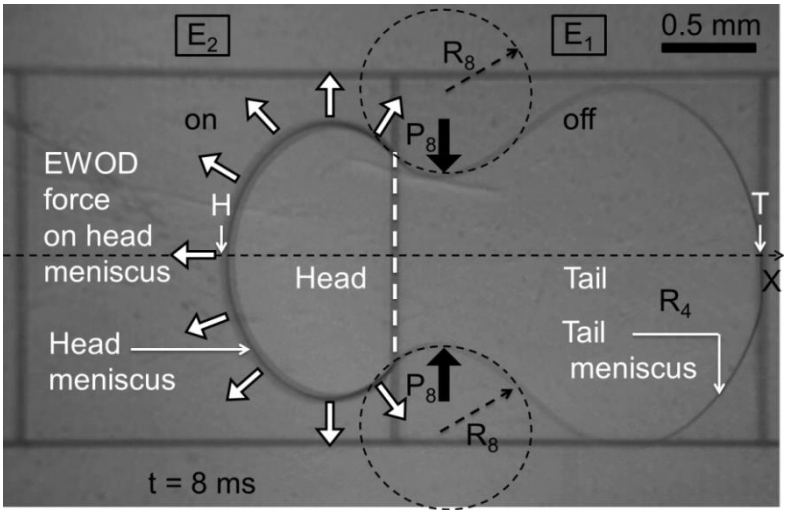

Figure 4.13 Video frame image of the moving droplet (time:t = 8 ms).

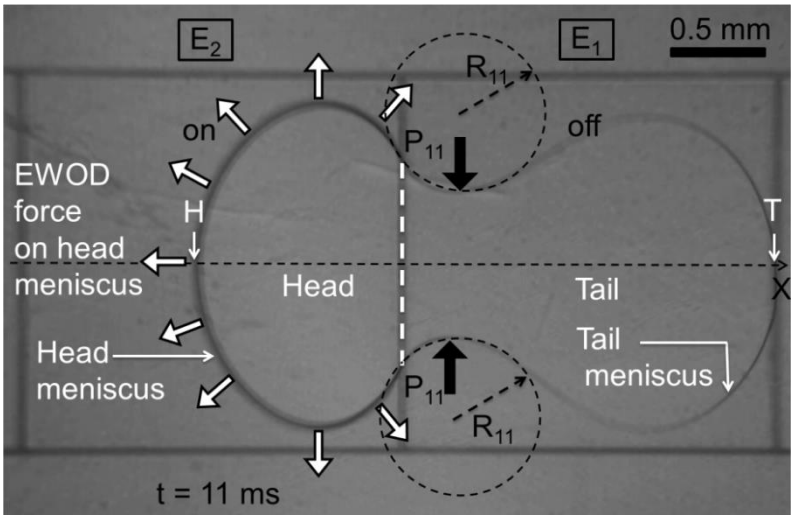

Figure 4.14 Video frame image of the moving droplet (time: t = 11 ms).

EWOD force acting on the head forms a circular head meniscus on the E_2. Back side of the head meniscus is forced to align along the wetting edge of E_2 developing a pressure squeezing the droplet at the middle along the orthogonal direction to the x-axis.

While more liquid enters into E_2, principle radius of curvature at the middle of the droplet decreases. According to the Laplace equation, which is $P \propto \gamma(1/R)$, For decreasing R, P is increasing. That is droplet is narrow down at the middle. Therefore, during the transition, droplet deforms.

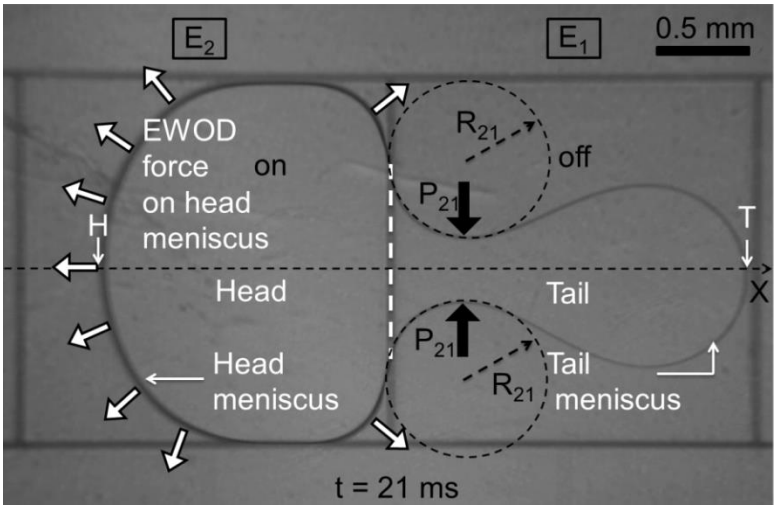

Figure 4.15 Video frame image of the moving droplet (time: t = 21 ms).

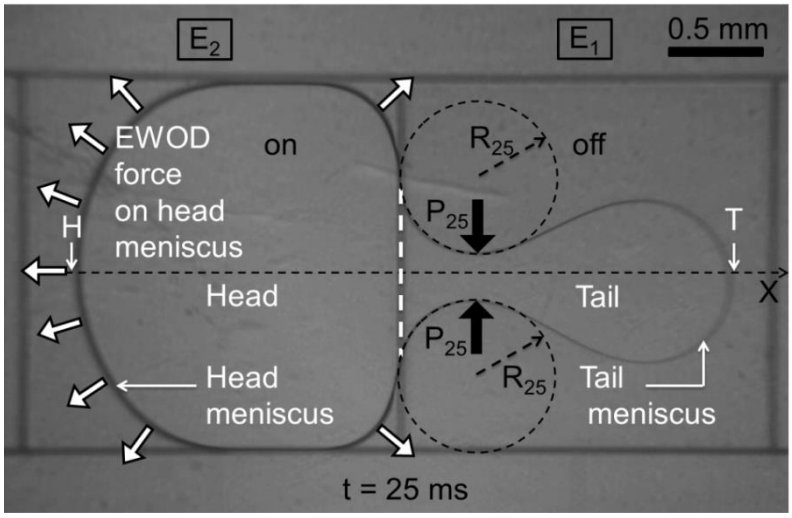

Figure 4.16 Video frame image of the moving droplet (time: t = 25 ms).

The head meniscus is decelerating. The neck of the tail is still narrow down. Point T is moving towards E_2 with increasing acceleration.

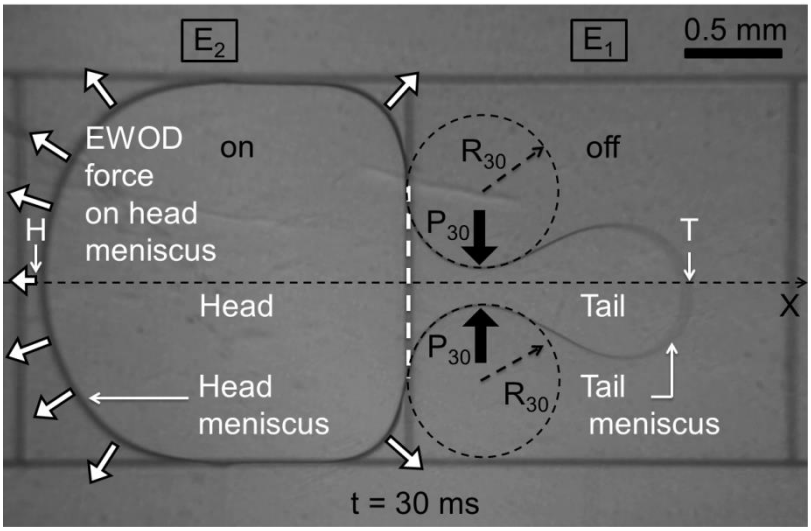

Figure 4.17 Video frame image of the moving droplet (time: t = 30 ms).

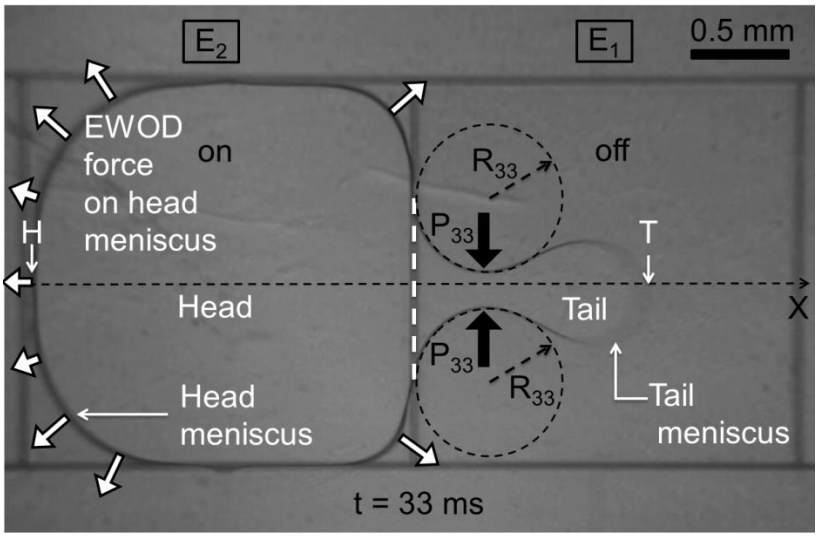

Figure 4.18 Video frame image of the moving droplet (time: t = 33 ms).

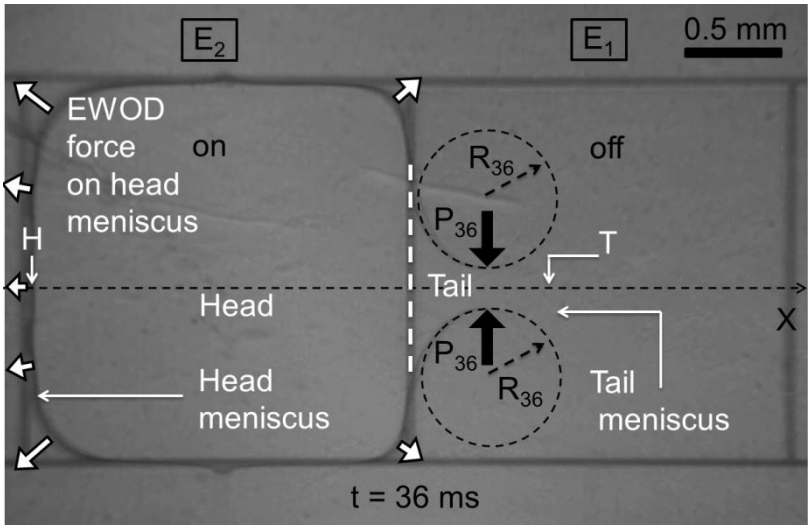

Figure 4.19 Video frame image of the moving droplet (time: t = 36 ms).

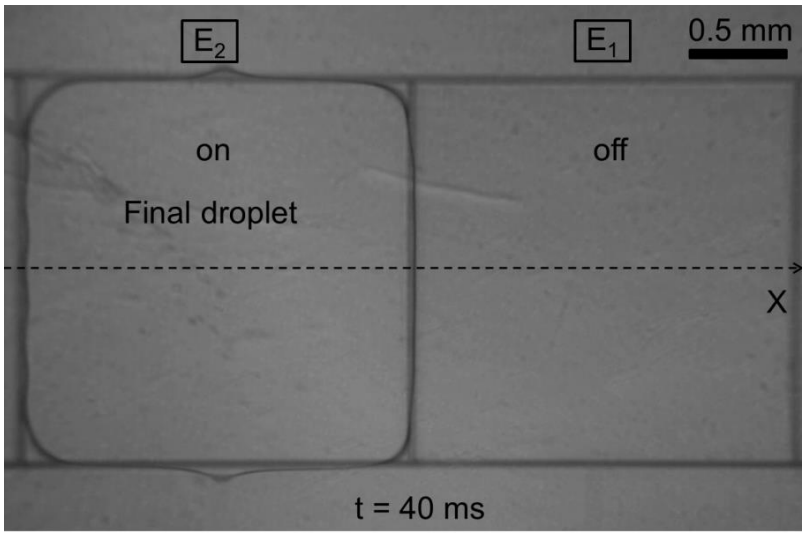

Figure 4.20 Video frame image of the moving droplet (time: t = 40 ms).

The head has come to the rest. The neck of the tail is still narrow down. Point T is moving towards E_2 with increasing acceleration.

To determine the velocity profile of the moving droplet, let's consider a droplet with volume *V* sandwiched in between the bottom plate and the cover plate with a radius *r*. The droplet's velocity in the parallel plate device $U_{parallel-plate}$, is computed based on the argument surface tension force (F_{ST}) due to wettability change is equal to the viscous shear force (F_{shear}) on the droplet. Other resistive forces such as contact line friction or drag force are neglected.

$$F_{shear} = \Gamma \pi r^2 = \frac{\mu U_{parallel-plate}}{d} \pi r^2 \tag{4.1}$$

Where, Γ is the shear stress, πr^2 is the foot print area of the droplet, *d* is the spacer gap between the bottom plate and the cover plate and μ is the viscosity of the liquid.

The surface tension force is given by,

$$F_{ST} = \frac{2\gamma_{LG}}{d}(cos\theta_L - cos\theta_R) \tag{4.2}$$

Where, γ_{LG} is the interfacial tension between liquid-air interface, θ_L and θ_R are the contact angles at left and right menisci of the liquid droplet. Balancing these two forces, $U_{parallel-plate}$ is given by,

$$U_{parallel-plate} = \frac{2\gamma_{LG}}{\mu \pi r^2}(cos\theta_L - cos\theta_R) \tag{4.3}$$

For a specific liquid, μ and γ_{LG} remains constant. Under constant applied electric potential, θ_L and θ_R remains constant. Therefore,

$$U_{parallel-plate} \propto \frac{1}{r^2} \tag{4.4}$$

During the transition of the droplet from one electrode to the next, the droplet is deformed non-uniformly along the direction of drop motion. With this deformation, the radius of curvature of the leading meniscus (head) undergoes a certain time dependent variation ($r_{head} = f_1(t)$) while the radius of curvature of the trailing meniscus (tail) undergoes a different time dependent variation ($r_{tail} = f_2(t)$) as shown in the Figures 4.11-4.20. By observing the behavior of curvature of head and tail, we can predict the $V - t$ trajectory of head and tail by using equation (4.4).

Figure 4.22 represents the velocity-time graph (V-t) for the above droplet motion. Red curve represents the motion of the head while black curve represents the motion of the tail. The velocity of the head is calculated with respect to the leading meniscus of the droplet (at the point H) while the velocity of the tail is calculated with respect to the trailing meniscus of the droplet (at the point T) (see Figure 4.3). According to these curves, the instantaneous velocity of both head and tail are non-uniform.

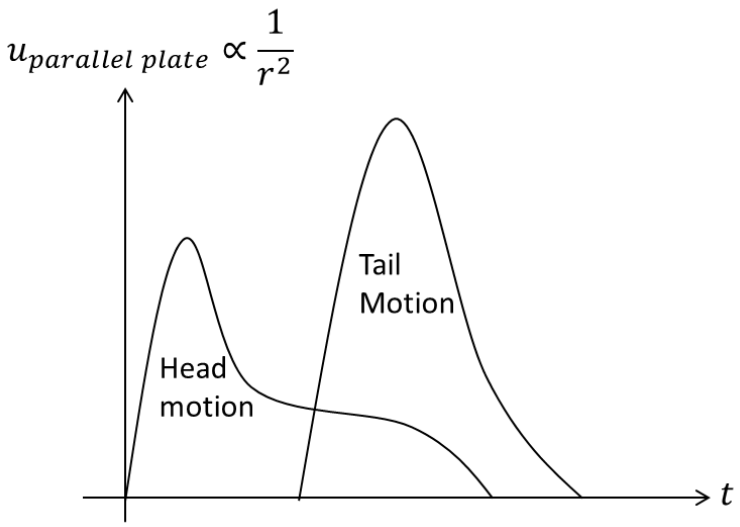

Figure 4.21 Predicted $V - t$ trajectory of head and tail by using equation [4.4].

During the transition, first, H stats the motion while T is at rest on E_1. Velocity of H increases rapidly. Since the larger amount of liquid in the tail exerts a drag force on the moving head, H reaches to the maximum velocity (~ 155 mm/s) and then decelerates. At the meantime, liquid in the tail follows the head and starts the motion. After majority amount of liquid in the tail starts the motion, it reduces the inertia for the droplet motion. As a result of that, deceleration of H is reduced and the velocity of H reaches to a steady value (~ 50 mm/s). Later, T starts the motion and H starts to accelerate again with reduced inertia for the droplet motion. As H reaches to the end of E_2, H decelerates to zero velocity.

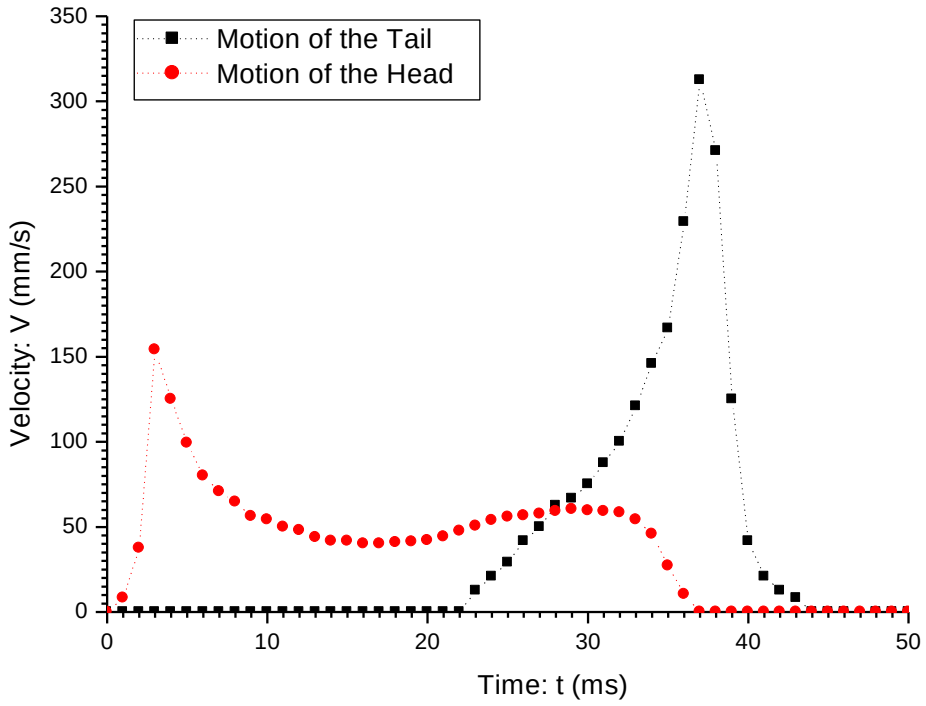

Figure 4.22 Instantaneous velocity of the droplet motion. Red curve represents the head motion. Black curve represents the tail motion. Electrode size: $2 \times 2\ mm^2$, applied voltage: 125 V, switching time 100 ms.

When T starts the motion, majority amount of liquid has already entered into E_2. Due to higher EWOD force acting on the head meniscus and the increasing pressure developing at the neck of the tail, T is moved towards E_2 with increasing acceleration. During the motion, T reaches to a maximum velocity (~ 330 mm/s) and then decelerates to zero velocity.

According to the Figure 4.21, T starts the motion after long time delay than H starts the motion (~ 22 ms). Further, the velocity profiles corresponding to Ha and T are different from each other. These differences reflect that the droplet is largely deformed during the transition from E_1 to E_2. H stops its motion around $t = \sim 37\ ms$. Since the switching time of the motion is 100 ms, H remains at rest during the left period of time from 37 ms to 100 ms. T stops its motion around $t = \sim 44\ ms$. After that it remains at rest from 44 ms to 100 ms. Next, the distance

traveled by both H and T is the same (the length of the square electrode: 2 mm). Therefore, the area under the trajectories of both H and T should be the same (2 mm).

4.4.4 Electrode Geometry: Stripped Electrodes (Rectangular Electrodes)

Figures 4.23-30 show video frame images of a moving droplet at 20 ms interval (frame rate 1250 fps with a resolution 800×600). The applied actuation voltage is 125 V with electrode ON time of 20 ms. Stripped electrode size is $0.4 \times 2\, mm^2$. These images show only one transition of the droplet from stripped electrodes E_3-E_7 to E_4-E_8. Similar motion is repeated in subsequent transitions.

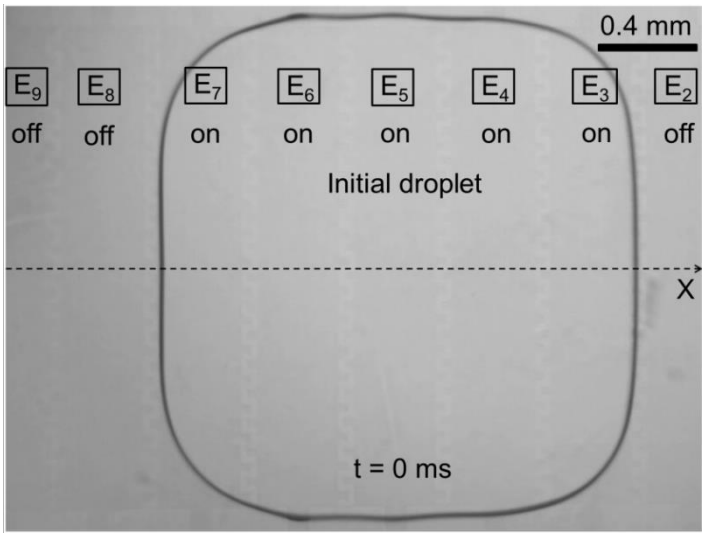

Figure 4.23 Video frame image of the droplet siting on the electrodes E_3-E_7 just before it starts the motion (time: t = 0 ms).

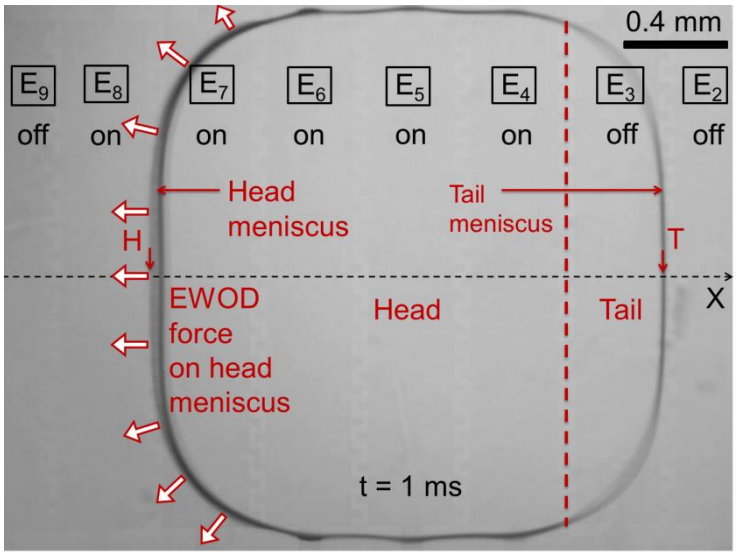

Figure 4.24 Video frame image of the moving droplet (time t = 1 ms).

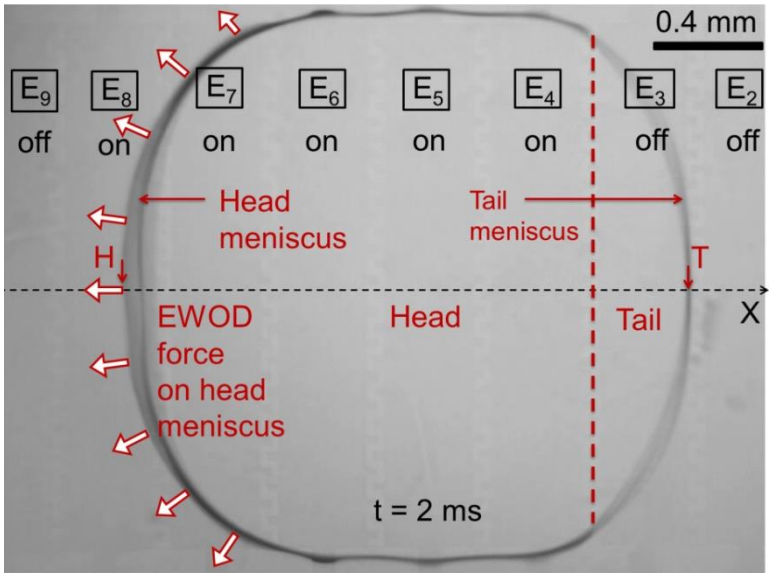

Figure 4.25 Video frame image of the moving droplet (time: t = 2 ms).

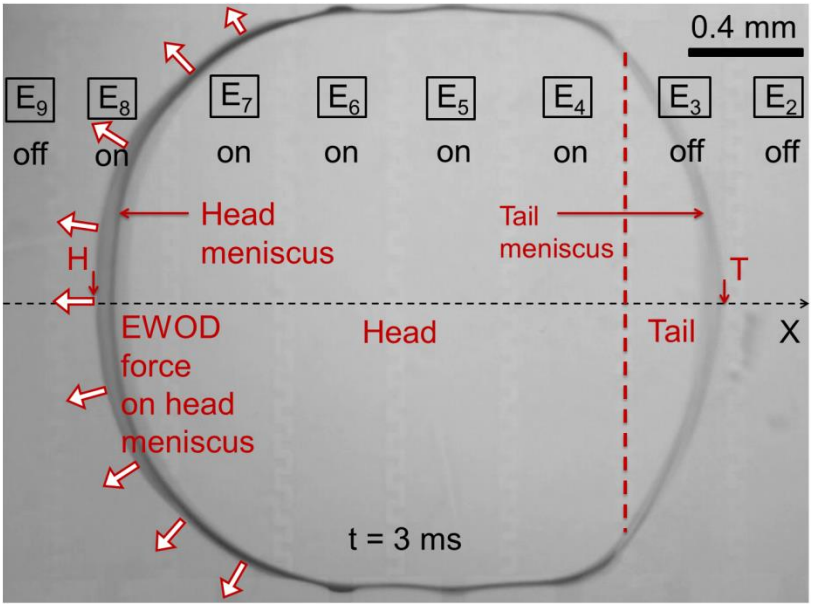

Figure 4.26 Video frame image of the moving droplet (time: t = 3 ms).

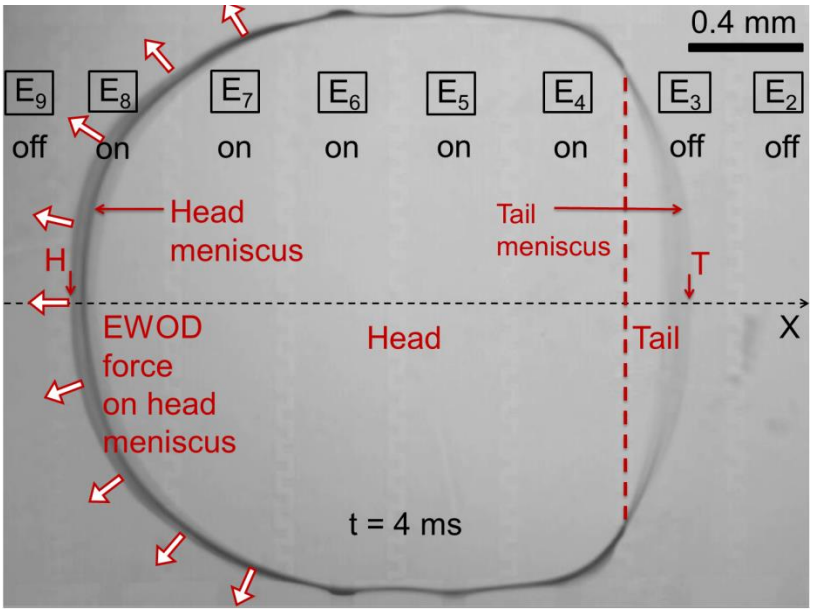

Figure 4.27 Video frame image of the moving droplet (time: t = 4 ms).

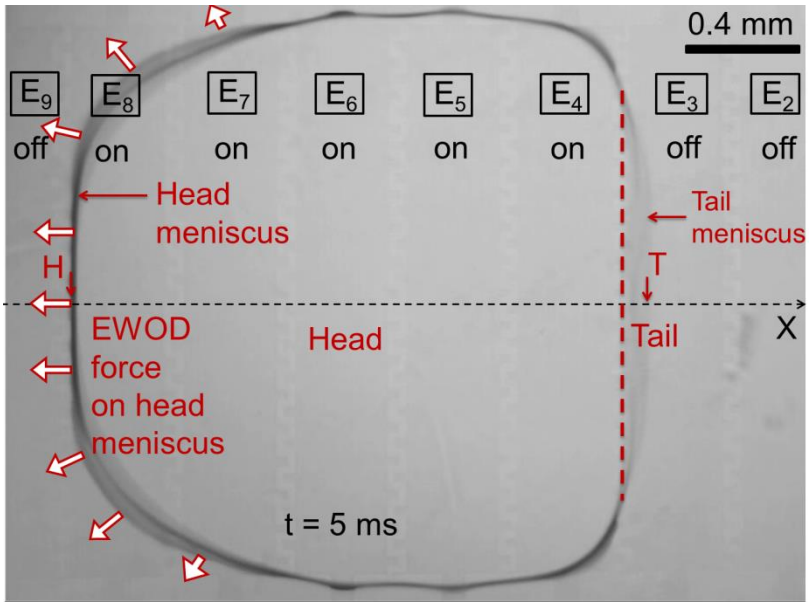

Figure 4.28 Video frame image of the moving droplet (time: t = 5 ms).

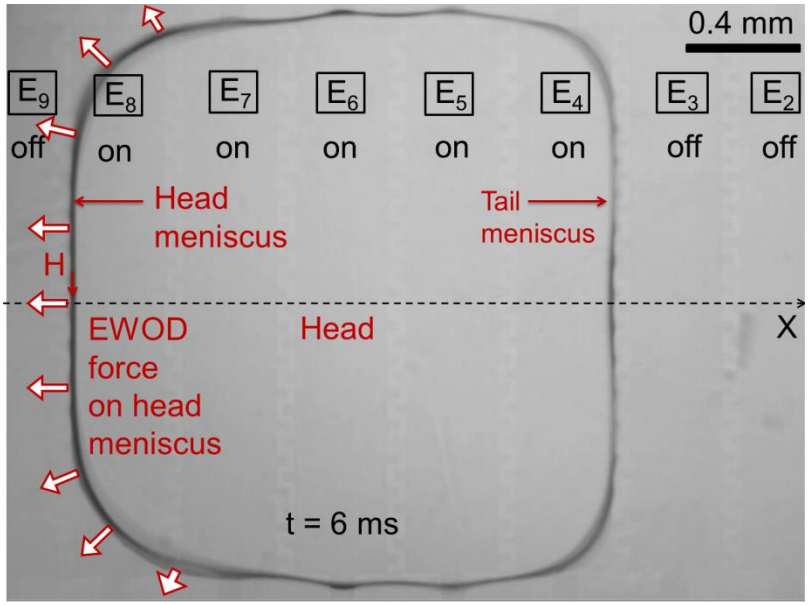

Figure 4.29 Video frame image of the moving droplet (time: t = 6 ms)

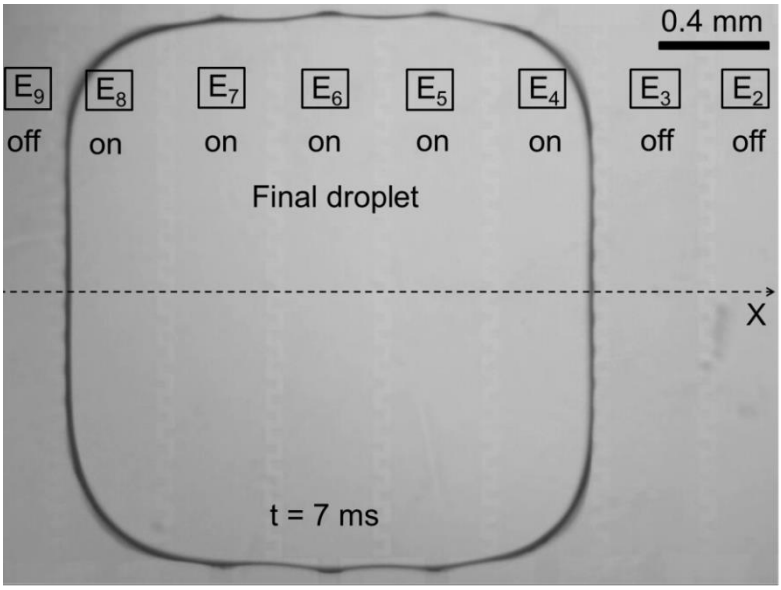

Figure 4.30. Video frame image of the moving droplet (time; t = 7 ms).

Figure 4. 31 represents the velocity-time graph (V-t) for the above droplet motion. Red curve represents the motion of H while black curve represents the motion of T. The trajectories for both H and T are almost identical. Further time delay between the motions of H and T is very little. This is because the deformation of the droplet is very little and the tail formation is very short. This shorter liquid tail follows the same head motion right behind the head. Since the EWOD force acting on the head is much higher, the head complete its motion within very short time (~7 ms) and stays at rest during the remaining time (7-20 ms) until the next voltage pulse is coming at $t = 20\ ms$. Since the area under the V-t trajectory is equal to the distance traveled by the droplet, the area under each transit curve should be equal to the length of the strip electrode (0.4 mm).

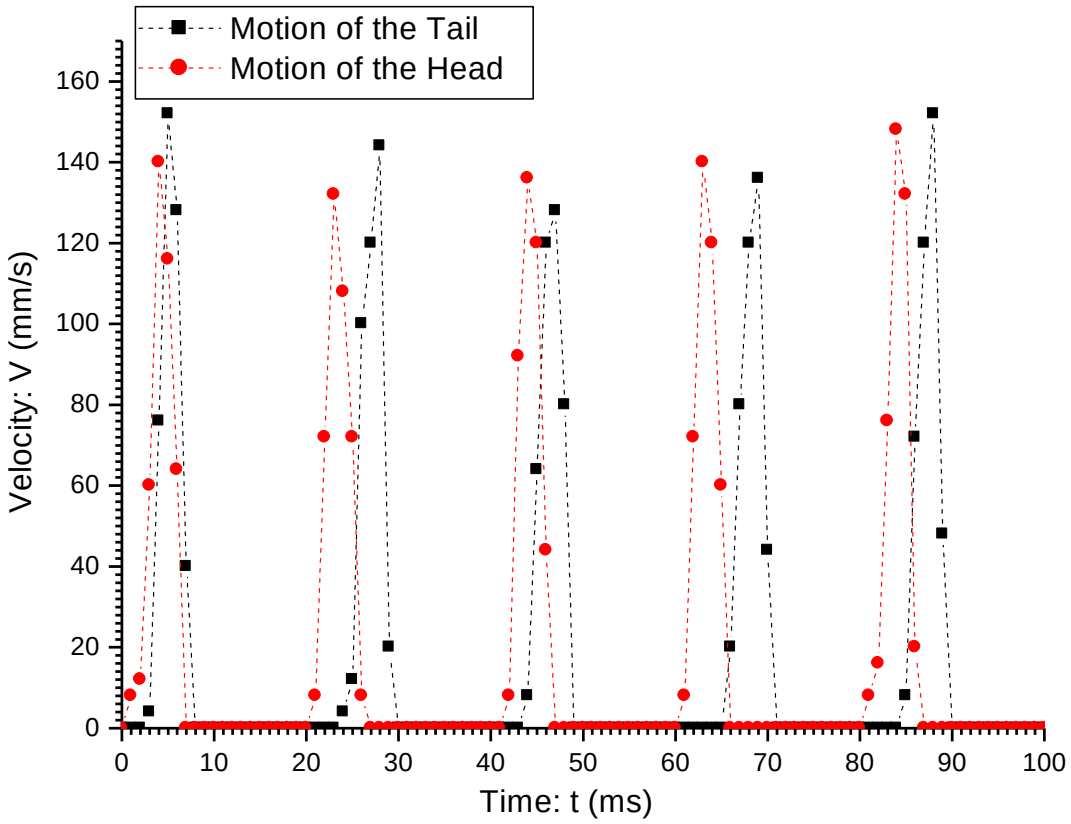

Figure 4.31 Instantaneous velocity of the droplet motion. Red curve represents the motion of H. Black curve represents the motion of T. Electrode size: $0.4 \times 2\ mm^2$, applied voltage: 125 V, switching time 20 ms. Both H and T reach to a maximum velocity (~ 140 mm/s) and then decelerates.

The trajectories for both H and T are almost identical. Further time delay between the motions of H and T is very little. This is because the deformation of the droplet is very little and the tail formation is very short. This shorter liquid tail follows the same head motion right behind the head. Since the EWOD force acting on the head is much higher, the head complete its motion within very short time (~7 ms) and stays at rest during the remaining time (7-20 ms) until the next voltage pulse is coming at $t = 20\ ms$. Since the area under the V-t trajectory is equal to

the distance traveled by the droplet, the area under each transit curve should be equal to the length of the strip electrode (0.4 mm).

4.4.5 Speed Enhancement: Solid electrodes

To increase the speed of drop motion on solid electrodes further, drop motion was studied by reducing the switching time to 66 ms ($V_{average} = 30\, mm/s$). Figure 4.32 shows the V-t trajectory for the motion of H corresponding to switching times of 66 ms (Red curve). The V-t trajectory for the motion of H corresponding to the switching times of both 100 ms (Black curve) is also shown in the same graph as reference.

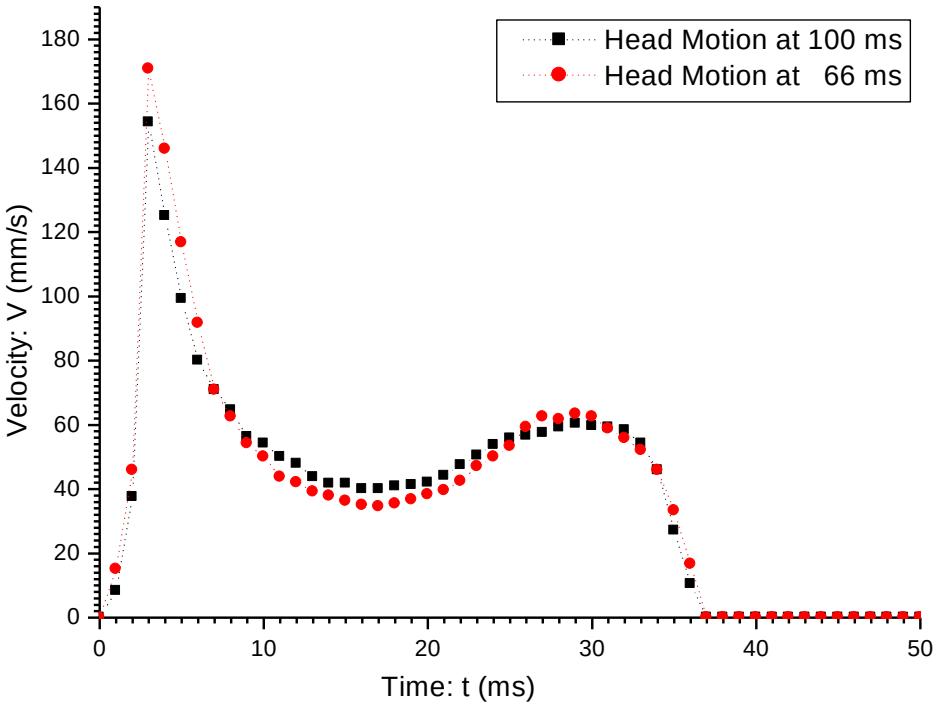

Figure 4.32 Instantaneous velocity of the motion of H on solid electrodes corresponding to two different switching times. Red curve represents the motion of H at 66 ms. Black curve represents the motion of H at 100 ms. Electrode size: $2 \times 2\, mm^2$, applied voltage: 125 V

According to Figure 30, both trajectories are almost identical except the ending time (66 ms and 100 ms). In both cases, H decelerates to zero velocity approximately at $t = 37\ ms$. Beyond that time, H stays at rest until the switching time is over. The time at which H decelerates to zero velocity does not depend on the switching time. To increase the speed of the droplet, we can reduce the switching time further up to this value ($t = 37\ ms$). For smaller switching times beyond this limit, H does not reach the next electrode to keep on the continuous motion. Therefore, the motion of droplet stops on the way. Corresponding to this minimum switching time, we can predict the maximum speed of droplet motion on solid electrodes ($V_{max} = 54\ mm/s$).

4.4.6 Speed Enhancement: Stripped Electrodes

To increase the speed of drop motion on stripped electrodes further, drop motion was studied by reducing the switching time to 10 ms ($V_{average} = 40\ mm/s$), 8 ms ($V_{average} = 50\ mm/s$) and 5 ($V_{average} = 80\ mm/s$) ms. Figure 4. 33 shows the V-t trajectory for the motion of H corresponding to the switching times of 10 ms (Black curve). The V-t trajectory for the head motion corresponding to the switching times of 20 ms (Red curve) is also shown in the same graph as reference.

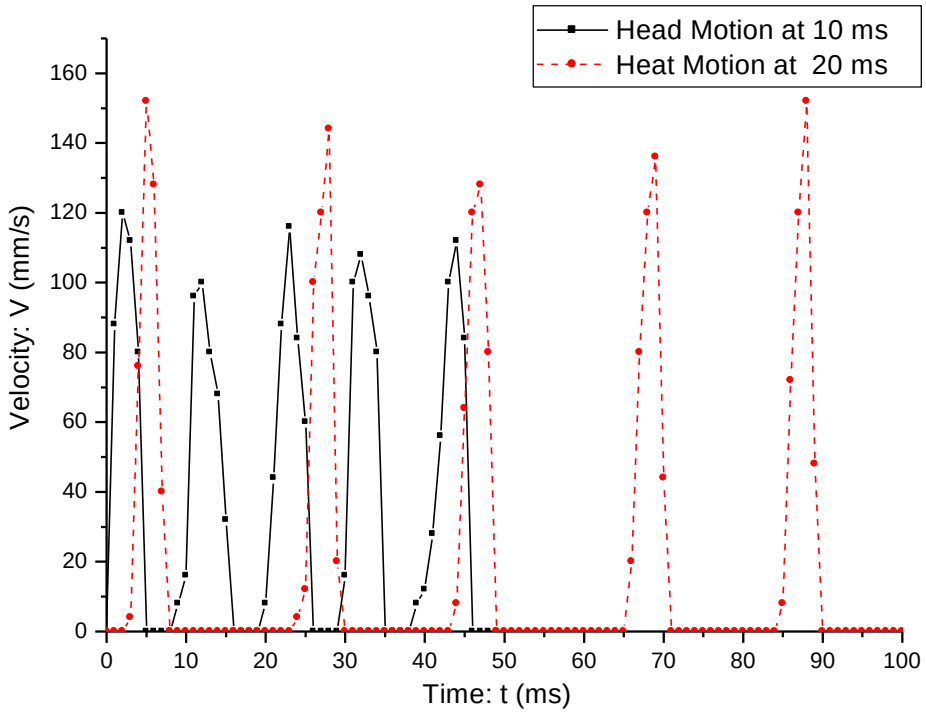

Figure 4.33 Instantaneous velocity of the motion of H on stripped electrodes corresponding to two different switching times. Black curve represents the motion of H at 10 ms. Red curve represents the motion of H at 20 ms. Electrode size: $2 \times 2\ mm^2$, applied voltage: 125 V

The interesting feature of the drop motion over the stripped electrodes is that the droplet remains at rest for a certain period of time in between each transition. According to the Figure 4.34, when the switching time is reduced, this time period during which the droplet remains at rest is reduced. When we consider the motion of H corresponding to the switching time of 20 ms, after decelerating to rest, liquid drop remains at rest around 13 ms before it starts the next transition. When the switching time is reduced to 10 ms, liquid drop remains at rest around 3 ms before it starts the next transition. Figure 4.34 shows the V-t trajectory for the motion of H corresponding to the switching times of 8 ms (Black curve). The V-t trajectory for the motion of H corresponding to the switching times of 10 ms (Red curve) is also shown in the same graph as reference

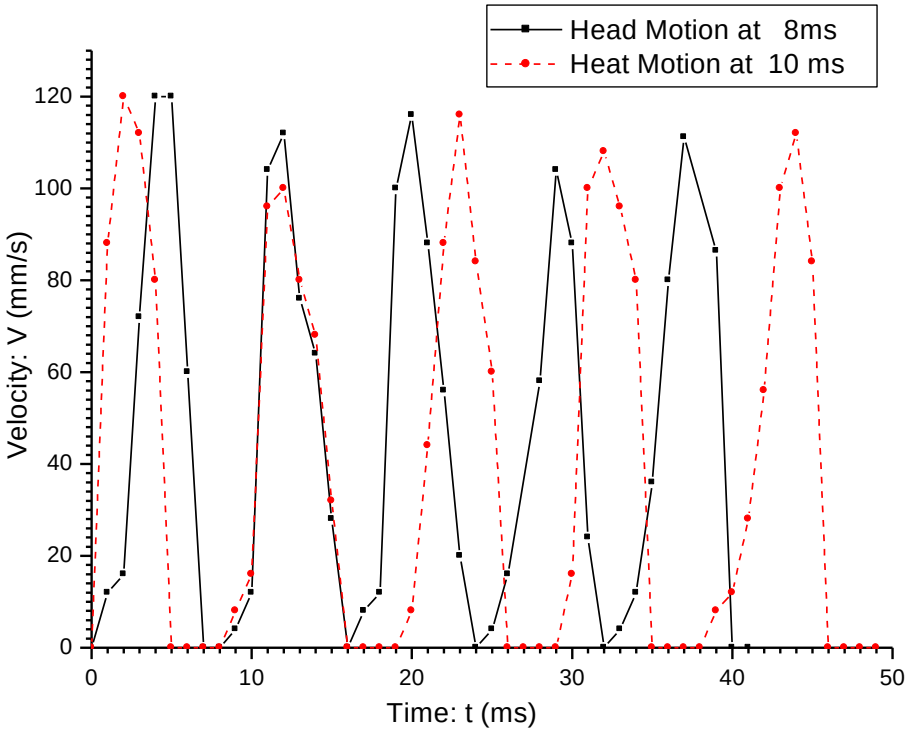

Figure 4.34 Instantaneous velocity of the motion of H on stripped electrodes corresponding to two different switching times. Black curve represents the motion of H at 8 ms. Red curve represents the motion of H at 10 ms. Electrode size: $2 \times 2\ mm^2$, applied voltage: 125 V

According to the Figure 31, when the switching time is reduced to 8 ms, the time period during which the droplet remains at rest is reduced to zero. Figure 33 shows the V-t trajectory for the motion of H corresponding to the switching times of 5 ms (Black curve). The V-t trajectory for the motion of H corresponding to the switching times of 8 ms (Red curve) is also shown in the same graph as reference.

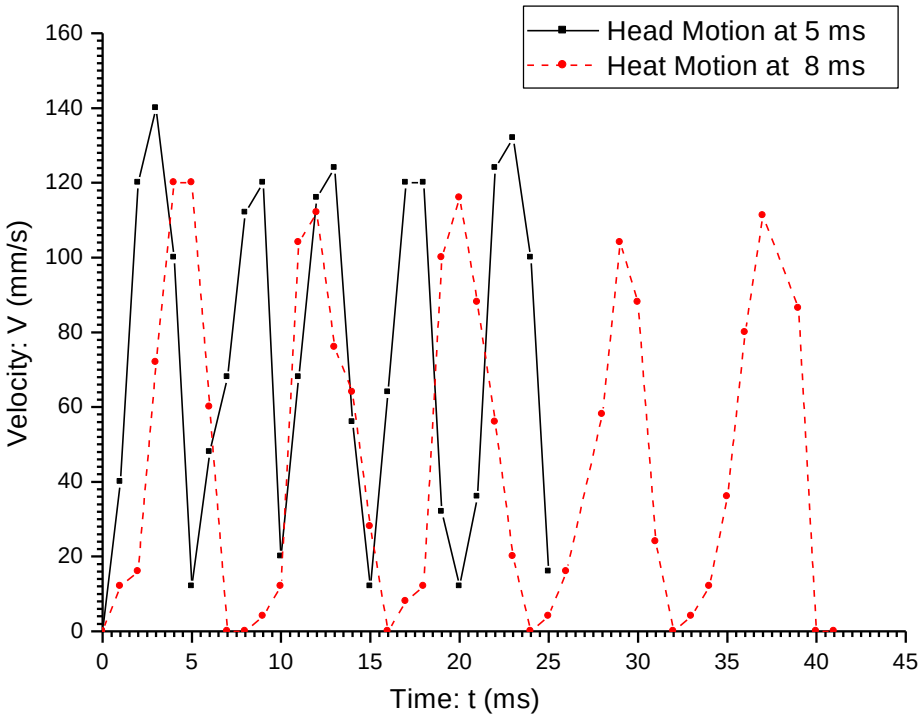

Figure 4.35 Instantaneous velocity of the motion of H on stripped electrodes corresponding to two different switching times. Black curve represents the motion of H at 5 ms. Red curve represents the motion of H at 8 ms. Electrode size: $2 \times 2\ mm^2$, applied voltage: 125 V.

The area under the entire trajectory is equal to the distance travelled by the droplet over five stripped electrodes ($0.4 \times 5 = 2\ mm$). Even though the switching time is reduced, the area under the V-t trajectory remains constant. According to the Figure 33, when the switching time is reduced further down to 5 ms, the V-t trajectory shifts from the time axis to keep constant area under the trajectory. In this manner, the speed of drop motion on the stripped electrodes can be increased by reducing the switching time further. The maximum speed we achieved is 400 mm/s for a switching time of 1 ms.

4.5 Conclusion

In this chapter, we report completion of one of the essential requirements of the EWOD DMF towards the thin-film evaporative cooling platform: the fast motion of coolant nanodrops to the hotspot to avoid dry-out. To achieve this goal, three major parameters that affect the speed of drop motion in the EWOD device were studied; 1). surface roughness, 2). electrode size, and 3). electrode geometry. First, the surface roughness of the EWOD substrate was studied for enhancing speed of drop motion.

Two EWOD substrates were tested for surface roughness measurement; i). PCB based EWOD substrate and, ii). glass based EWOD substrate. Experimental results reveal that PCB based EWOD substrate has large surface roughness and surface irregularities. As a result of that, the maximum speed achieved on the PCB based EWOD substrate is very low (17.3 mm/s). To remove the above issues, glass based EWOD substrate was suggested.

To study the effect of electrode size towards enhancing speed of drop motion, two electrode sizes were tested ($2 \times 2\ mm^2$ and $3 \times 3\ mm^2$). Higher speed of drop motion was achieved for larger electrodes. However, the minimum switching time corresponding to the maximum speed is independent from the electrode size. For the glass based EWOD deice, corresponding minimum switching time is approximately 40 ms while for the Si based EWOD device, corresponding minimum switching time is around 125 ms.

To study the effect of electrode geometry towards enhancing the speed of drop motion, two electrode geometries were tested; i).solid electrode and, ii). modified stripped electrodes. Speed of drop motion on solid electrodes is lower due to several factors; 1). smaller EWOD force, 2). larger tail formation and higher inertia associated with the liquid tail, and 3). larger deformation of the droplet during the transition. For the solid electrode size of $2 \times 2\ mm^2$, a maximum speed of around 50 mm/s was achieved.

Stripped electrodes are designed by dividing a solid electrode into five parts. Not like in the solid electrodes, five electrodes are activated simultaneously in stripped electrodes. Therefore, liquid

head experience much higher EWOD force. The tail formation behind the head is shorter. Therefore, the inertia of the tail that resists the drop motion is lower. During the transition of the droplet from one set of stripped electrodes to the next set, deformation of the droplet is very little compared to the solid electrodes. As a results of these improvements, much higher speed of drop motion is achieved on the stripped electrodes (~ 400 mm/s).

CHAPTER 5

SIMULTANEOUS ACHIVEMENT OF INCREASING FREQUENCY AND DECREASING VOLUME OF DROPLETS TO THE HEATED SECTION

In the previous chapters, the capabilities of EWOD device to create droplets with high accuracy and consistency in volume and to translate droplets with high speed were successfully demonstrated. However, as introduced in Chapter 1, those two capabilities should be achieved simultaneously toward thin-film evaporation application, i.e. small and accurate volume of coolant droplets should arrive to the hot spot with high frequency. Therefore, in this chapter, the simultaneous enhancement in frequency and volume of droplets arriving to the heated section is studied and demonstrated.

It is understood through our experiments that the true bottleneck of the high frequency of droplet supply is the time to create a droplet from a reservoir, not the droplet moving speed. Although a droplet can move 400 mm/s (1ms switching time) with stripped electrode design (stripped electrode size: $0.4 \times 2\ mm^2$) shown in Chapter 4, it usually takes 200 times longer time (200 ms switching time) to generate one droplet from a reservoir. Therefore, to tackle this problem, two distinct approaches have been taken: (1) simultaneous generation of multiple droplets, and (2) reduction of time to dispense one droplet. Both approaches have been done by designing novel electrodes geometries of EWOD devices and modifying them.

Section 5.1 discusses multiple droplets generation method. Section 5.2 presents the reduction of time to dispense one droplet. The combined method of these two approaches is introduced in section 5.3. Experimental results are followed in section 5.4.

5.1 Generation of Multiple Droplets: Droplet Splitting at C-Junction

In this method, electrodes shapes and positions are organized to make fine liquid column that is unstable under EWOD actuation resulting in two droplets with approximately equal volumes with very minimum volume error. This method is distinguished from the splitting a droplet into two, which is shown in Chapter 3. Unlike the splitting a droplet where electrowetting forces of opposite directions were applied at the each ends of a droplet, in this proposed method, long and thin liquid column is generated first and electrowetting forces in the same direction are applied to form multiple droplets. To dispense a long and thin liquid column, in the present application, a slender rectangular electrode with size $1 \times 8\ mm^2$ is designed. Two square electrodes with the same size $2 \times 2mm^2$ are patterned ahead of the slender rectangular electrode. The combination of the rectangular electrode and the two square electrodes exhibits a junction in C-shape. Hence, this junction is named *C-junction*. Both square electrodes are connected each other to dispense two droplets at the same time (Figure 5.1). The area of the slender rectangular electrode should be equal to the total area of two square electrodes. The gap between two square electrodes should be at least the side length of one square electrode (2 mm). The system of electrode is symmetric over the x-axis at the middle.

Initially, a long and thin liquid column is on the activated rectangular electrode (E_3). Both square electrodes (E_1 and E_2) are grounded (Figure 5.1(a)). To actuate the C-junction splitting, both E_1 and E_2 are activated simultaneously while E_3 is deactivated (Figure 5.1(b)). Then liquid column is pulled by EWOD force into E_1 and E_2 equally.

Liquid portion above the x-axis is pulled by E_1 while the liquid portion below the x-axis is pulled by E_2. During the pulling process, the inner boundary (blue dotted line), which belongs to the liquid portion on the wetting square electrodes (E_1 and E_2), aligns quickly along the horizontal edge *a* and *b* of E_1 and E_2, respectively. Throughout the pulling process, this inner boundary remains the same. As a result, the inner boundary of the liquid column, which is on

the de-wetting rectangular electrode (E_3), forms a circular arc meniscus with a fixed radius of curvature (R_1).

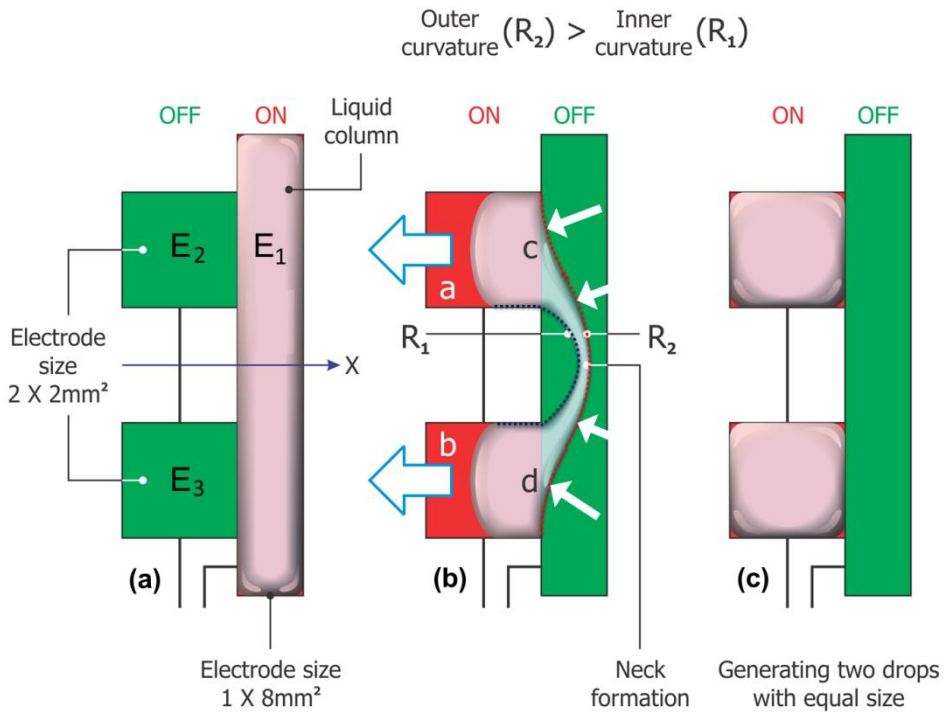

Figure 5.1 A droplet splitting sequence at C-junction. (a) Liquid column formation by activating slender rectangular electrode, (b) Liquid column undergoes a neck formation; the meniscus of the neck has a fixed radius of curvature (R_1), outer meniscus is approaching towards the inner meniscus with increasing radius of curvature (R_2), and (c) After separation, two droplets with equal volume are created.

In the meantime, the outer boundary (orange dotted line), which belongs to the liquid portion on the wetting square electrodes (E_1 and E_2) starts to align along the vertical edge *c* and *d* of E_1 and E_2, respectively. As a result, the outer boundary of the liquid column, which is on the de-wetting rectangular electrode (E_3), forms a circular arc meniscus with a varying radius of curvature (R_2). As the liquid continued to be pulled by E_1 and E_2, this alignment is growing all the way along the side *c* and *d* towards the middle x-axis. As a result of that, meniscus with R_2 is moving towards the meniscus of R_1, i.e. R_2 increases. At a certain point, this moving outer

meniscus meets the fixed inner meniscus and pinch-off happens as creating two droplets with approximately equal in volume very minimum volume error.

Another interesting feature of the C-junction splitting is that it executes two operations at the same time; 1) droplet motion in certain direction and 2) droplet splitting. Therefore, instead of generating a drop in small volume and delivering it to the heated section one by one, by using C-junction splitting, higher delivery frequency of the droplets with decreased droplet volume can be achieved.

5.1.1 Application of C-Junction to a High-Frequency Droplet Delivery System

To decrease the droplet volume further, one more C-junction is inserted in front of the each square electrode to allow droplets to experience another splitting so that droplet volume reduces to half while the number of droplet in operation doubles. Four TCC reservoirs together with C-junction splitting mechanism were designed at the four sides from the heated region so that drop delivery from each side can be controlled individually (Figure 5.2). Using this method the droplet volume that arrives to the heated section becomes 4 times smaller than the volume of droplet generated from the TCC reservoir. In addition, the droplet arrival frequency can be 16 times higher when all the electrodes are operated individually.

As shown in the Figure 5.2, the size of the drop generating site of the TCC reservoir is $2 \times 2\, mm^2$. The electrode sizes at the C-junctions are chosen in such a way that the size of the unit coolant drop that arrives to the heated region is $1 \times 1\, mm^2$. Since the TCC reservoir dispenses droplets with higher volume consistency and C-junctions split those droplets into two with highly identical volume, the unit coolant droplets that arrive to the heated region have a higher volume precision with very small volume error (see results and discussion section for more details).

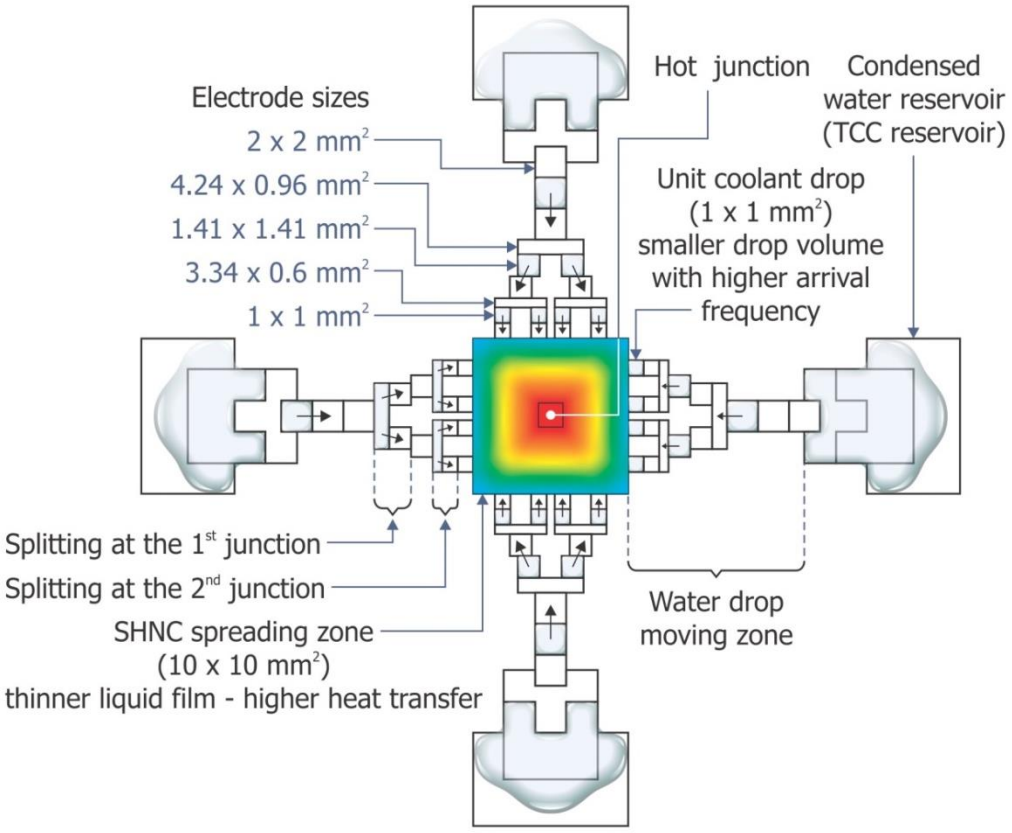

Figure 5.2 Drop delivery system with decreased droplet volume and increased delivery frequency. Electrode path starting at the TCC reservoir is branching out at the C-junction. Four TCC reservoirs together with C-junction splitting mechanism were placed at the four sides from the heated region

5.1.2 Future Work: Complete Test Vehicle for Thin-Film Evaporative Characterization

Our next goal is to assemble the testing setup to deliver coolant to the SHNC and characterizing thin-film evaporative cooling. Therefore, we plan to combine our coolant delivery system with the thin-film evaporative cooling system based on SHNC developed by Shailesh Mala, a PhD student at the University of Texat at Arlington, under the supervision of Professor Seung M. You. To characterize thin-film evaporative cooling on the SHNC, they developed a resistive heating layer on Silicon (Si) with high power limit to emulate high heat flux hot-spot.

Figure 5.3 shows the cross sectional diagram of the proposed method of coolant delivery to the SHNC to make thin-film of liquid.

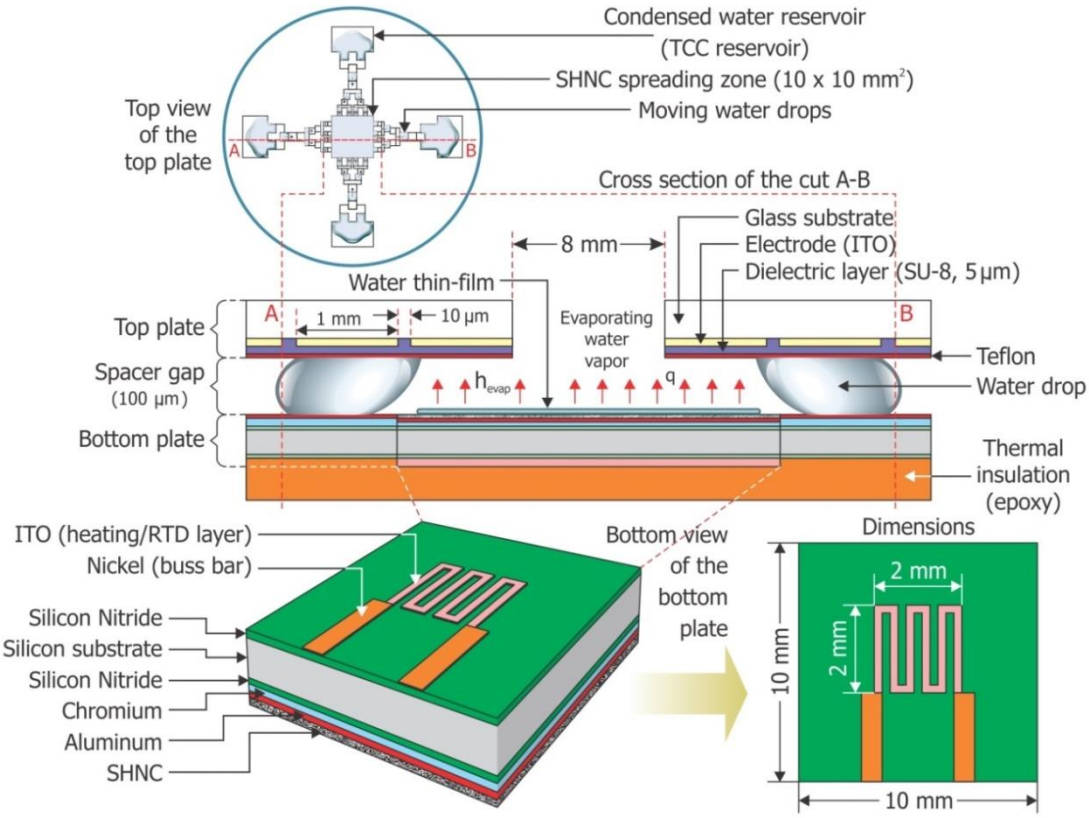

Figure 5.3 Schematic diagram of the proposed method of delivering coolant to the SHNC to make thin-film of liquid

5.2 Reduction of Time to Dispense a Droplet: Droplet Dispensing at L-Junction

This is a novel technique of drop dispensing with very high speed and higher volume precision. The layout of the junction at which droplets are dispensed takes the L-shape. Therefore, this technique of drop dispensing is named as *L-junction* drop dispensing. A L-junction consists of stripped electrodes. All the stripped electrodes have the same area. Stripped electrodes at both vertical (E_1-E_{10}) and horizontal (E_{15}-E_{24}) branches are rectangular with the size $0.56 \times 2.83\ mm^2$ (Figure 5.4). For simplicity, Figure 5.4 shows stripped electrodes

at the L-junction only. For more details of electrode layout, please refer Appendix C. Stripped electrodes at the L-junction (E_{11}-E_{14}) are angular with the angle 22.5^0. These angular electrodes help to turn the moving liquid front around the acute angle at the L-junction while maintaining the same speed of the liquid front.

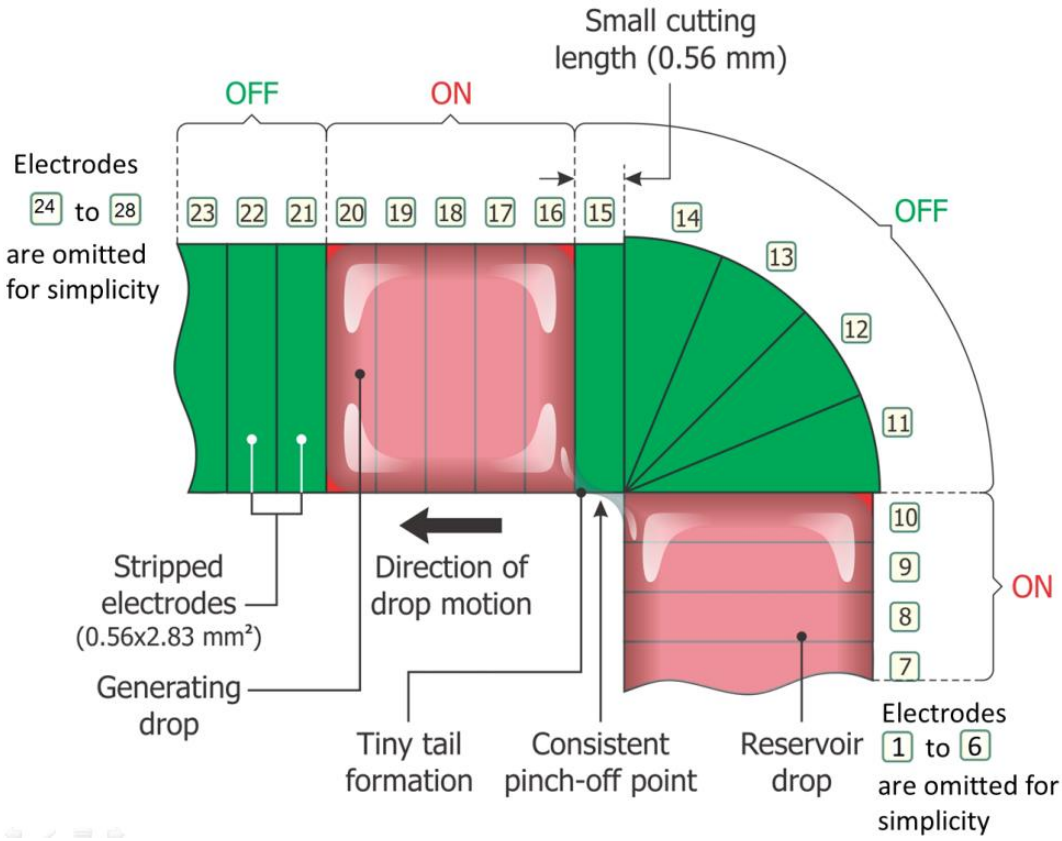

Figure 5.4 Dispensing a droplet from the L-junction reservoir. Reservoir drop does not supply any backward force to cause pinch-off

To dispense a liquid droplet at the L-junction, first, a liquid column is pulled out from the reservoir and moved over the stripped electrodes all the way from E_1 to E_{15} by sequentially activating them one by one. Next, a droplet has to be formed while the rotation of the liquid column. To start droplet formation, stripped electrode E_{12}-E_{16} were activated together with E_1-E_{10} while deactivating E_{11}. As a result of this actuation, de-wetting occurs on the E_{11} and it starts the pinch-off process. After that, stripped electrode E_{13}-E_{17} were activated together with

E_1-E_{10} while deactivating both E_{11} and E_{12}. This actuation makes higher de-wetting on the angular electrodes than the previous case enhancing the pinch-off.

In this manner, by activating a set of five stripped electrodes together, a square shaped droplet can be pulled out from the liquid column forward into the horizontal branch. Pinch-off occurs when the liquid droplet arrives onto the electrodes E_{16}-E_{20}. In this droplet dispensing, the cutting length is very small (0.56 mm); hence, the tail formation behind the already formed droplet is much smaller (~ 0.28 mm). Therefore, this droplet has a higher volume precision with very small volume error. Further, pinch off occurs at the same speed as the droplet is moving on the stripped electrodes. Since the speed of drop motion on the stripped electrodes is much higher than the solid electrodes, the speed of drop dispensing by the L-junction is much higher than that by the TCC reservoir. Further, L-junction dispenses droplets without any backward motion of the reservoir drop. Therefore, droplet dispensing from the L-junction has a higher rate of reproducibility

5.3 Combined Method: Multiple Drop Dispensing at Y-Junction

This is a novel technique of dispensing multiple drops simultaneously with very high speed and higher volume precision. This Y-junction is used to split the droplet into two at the same speed as it is dispensed by the L-junction. Entire Y-junction consists of stripped electrodes. Stripped electrodes in the left and right braches are indicated respectively by the letters *L* and *R* placed next to the corresponding electrode number (Figure 5.5). The size of these stripped electrodes is the same ($0.39 \times 2.0\ mm^2$). Corresponding stripped electrodes are connected together. For an example, *30-L* and *30-R* are connected.

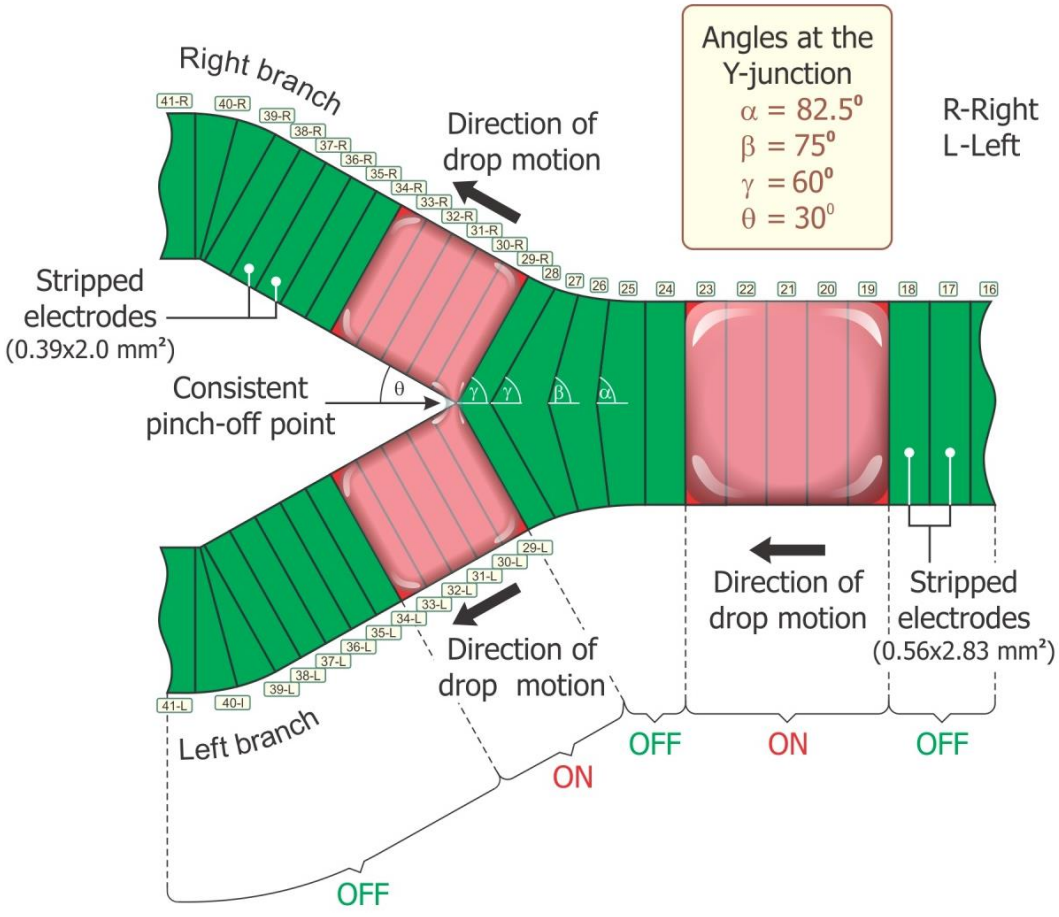

Figure 5.5 Dispensing two droplets at the Y-junction simultaneously. Droplet splitting happens at the same speed it moves on the stripped electrodes

In the present application, both *L* and *R* branches make an angle of 30^0 (θ) to the horizontal. This angle plays an important role of deciding the point of pinch-off of the droplet. If θ is too small, the droplet moves away from the Y-junction to the left over several electrodes until pinch-off occurs. For larger values of θ, pinch-off occurs right at the Y-junction. Next, the front edges of the stripped electrodes which are at the right from the Y-junction are designed in angular shape with angles α (82.5^0), β (75^0), and γ (60^0). At the pinch off process, these angular edges push the back boundary of the liquid droplet towards the tip of the Y-junction while the inner edges with angle θ of the Y-junction are holding the front boundary of the liquid droplet

generating much higher pressure at the point of pinch-off. As a result of this higher pressure, pinch-off occurs quickly and the droplet is split into two with a higher speed (see Results and Discussion for more information).

5.4 Results and Discussion

All the video frame images were captured by the FASTEC-TS3 high speed camera at a frame rate of 1000 fps with a resolution 800×600. The applied actuation voltage is 125 V. Droplet is moving from the right to the left.

5.4.1 Droplet Splitting at C-Junction

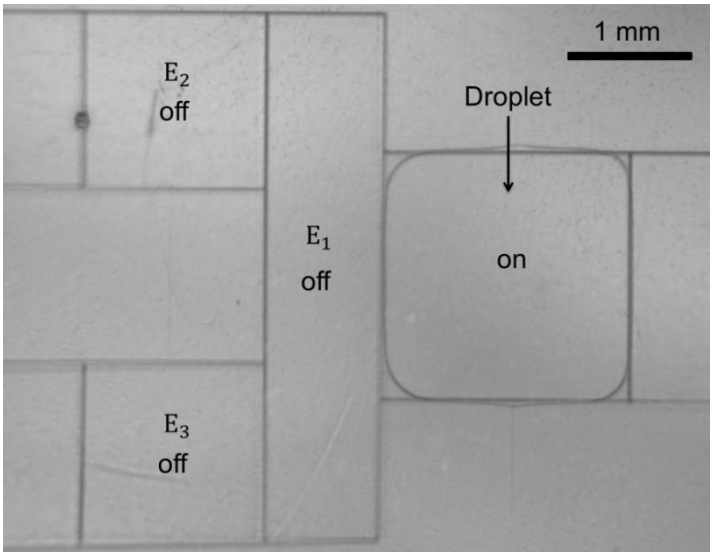

Figure 5.6 Droplet dispensed from the TCC reservoir. The size of the square electrode on which droplet occupies is $2 \times 2\ mm^2$

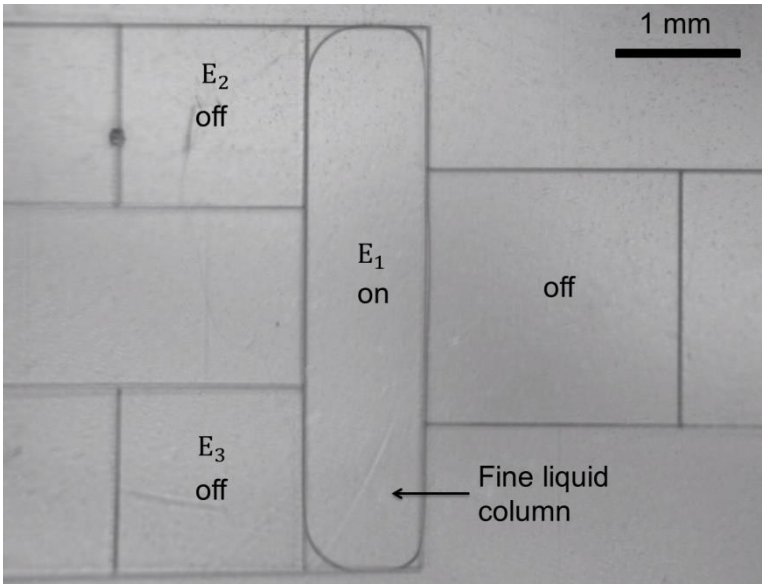

Figure 5.7 Fine liquid column on the rectangular electrode $E_1(E_1 = 0.96 \times 4.24\, mm^2)$

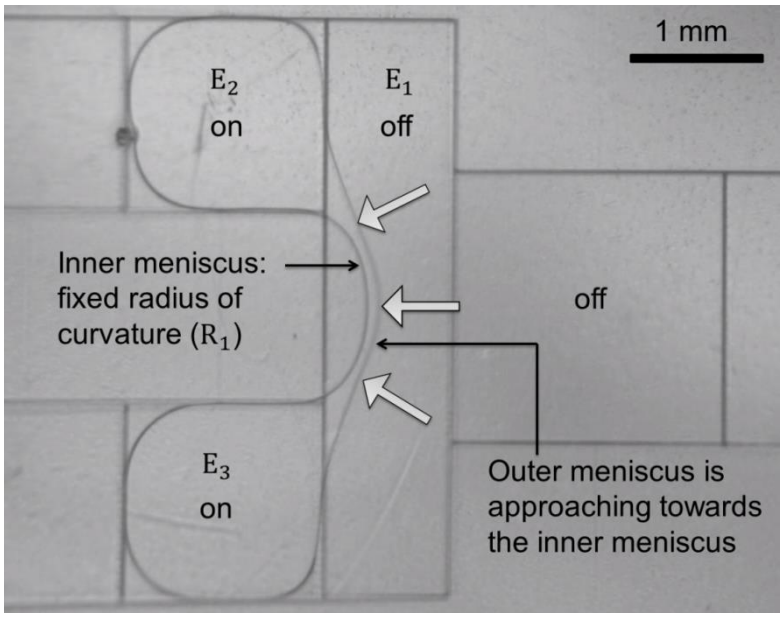

Figure 5.8 Liquid column undergoes a neck formation; inner boundary has a fixed radius of curvature, outer boundary is approaching towards the inner boundary with increasing radius of curvature

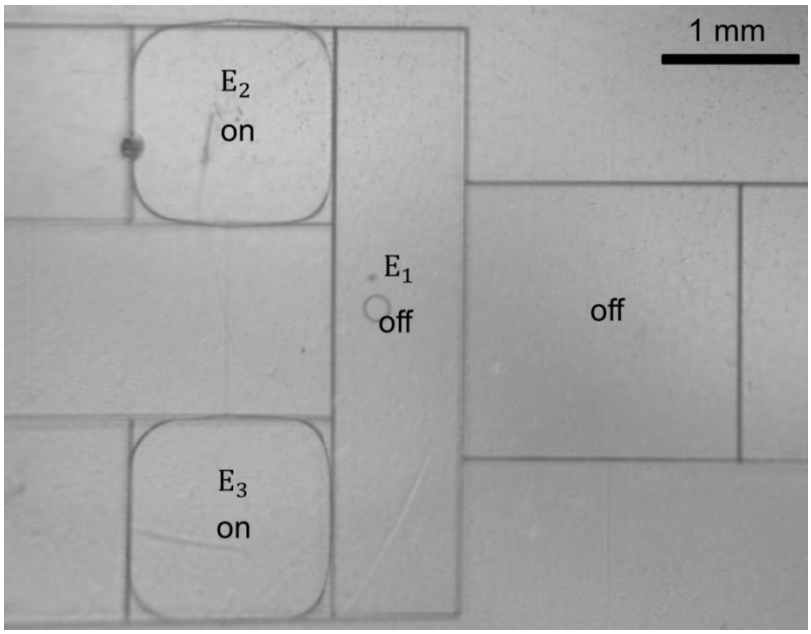

Figure 5.9 After pinch-off, two droplets with highly identical volumes are created. Electrode size: $(E_2, E_3 = 1.41 \times 1.41 mm^2)$

5.4.2 Droplet splitting and delivery using Double C-junction

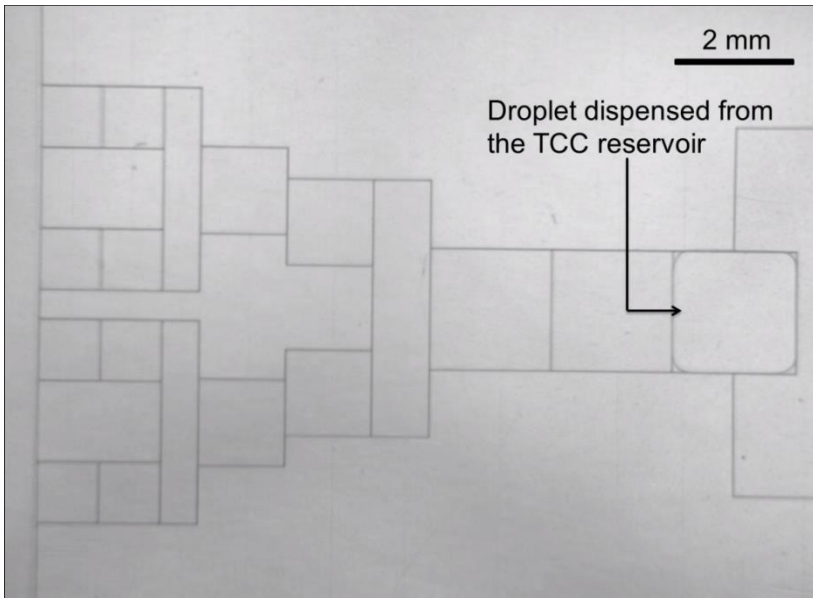

Figure 5.10 Droplet dispensed from the TCC reservoir. Electrode size on which the droplets exists is $2 \times 2\ mm^2$

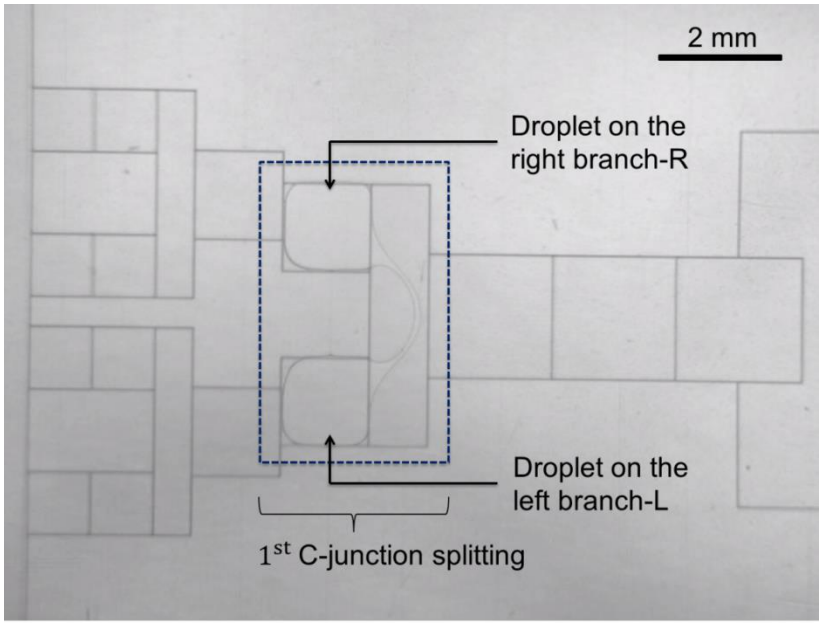

Figure 5.11 Splitting at the 1st C-junction. Electrode size: $1.41 \times 1.41 mm^2$

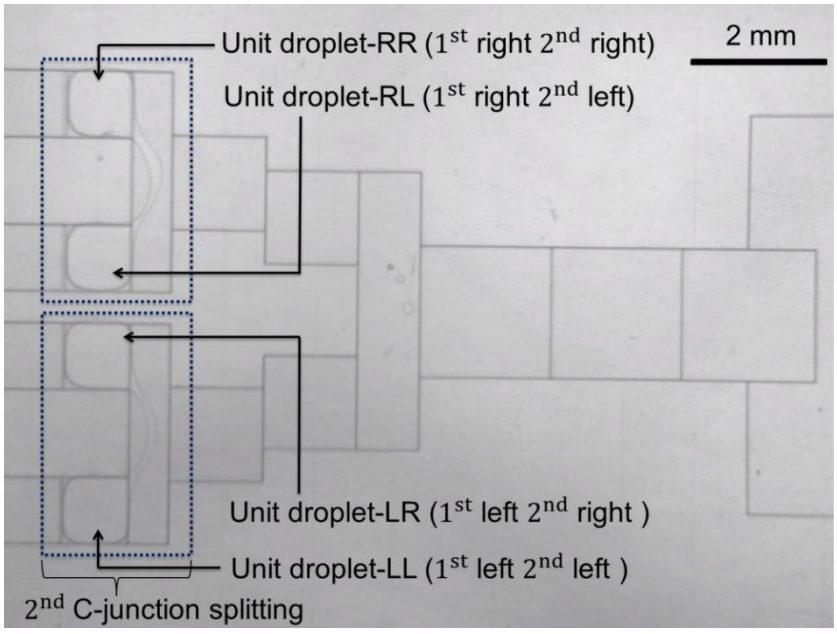

Figure 5.12 Splitting at the 2nd C-junction. Electrode size: $1.0 \times 1.0\ mm^2$

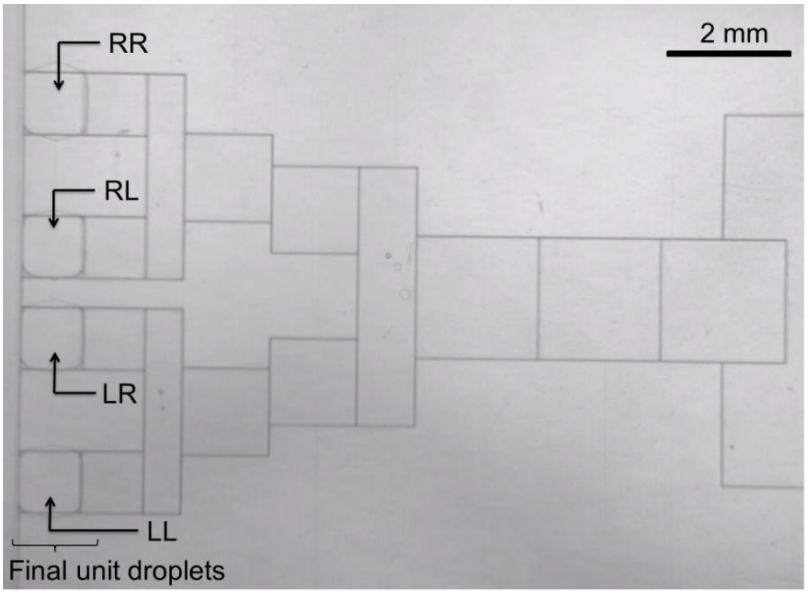

Figure 5.13 Resulted four droplets at the end of the splitting process. Electrode size: $1.0 \times 1.0\ mm^2$

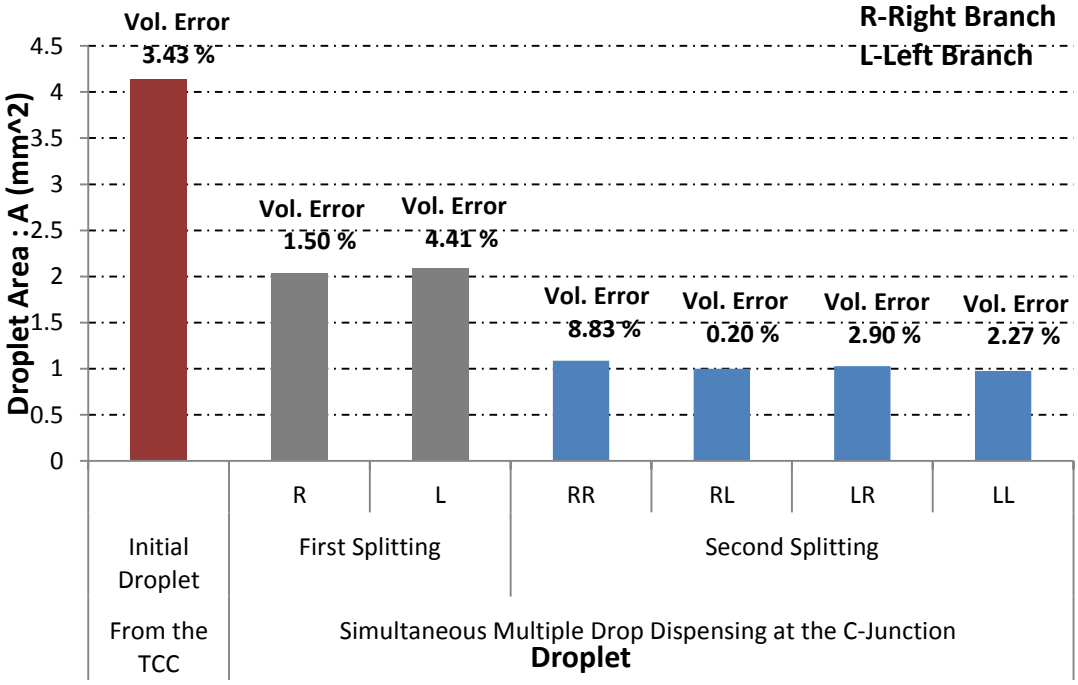

Figure 5.14 Volume precision of the liquid droplet moving from the TCC reservoir to the spreading zone in the Figure 5.16

According to the above Figure, even though we dispense droplets from the TCC reservoir with higher accuracy in volume (< 5 %), we cannot guarantee the volume precision of the unit droplet arriving to the spreading zone. Uneven hydrophobic coating, unsymmetrical C-junction splitting and non-uniform spacer gap between the bottom plate and the cover plate can be reasons for this issue.

5.4.3 Reduction of time to dispense a drop: Dispensing at L-Junction

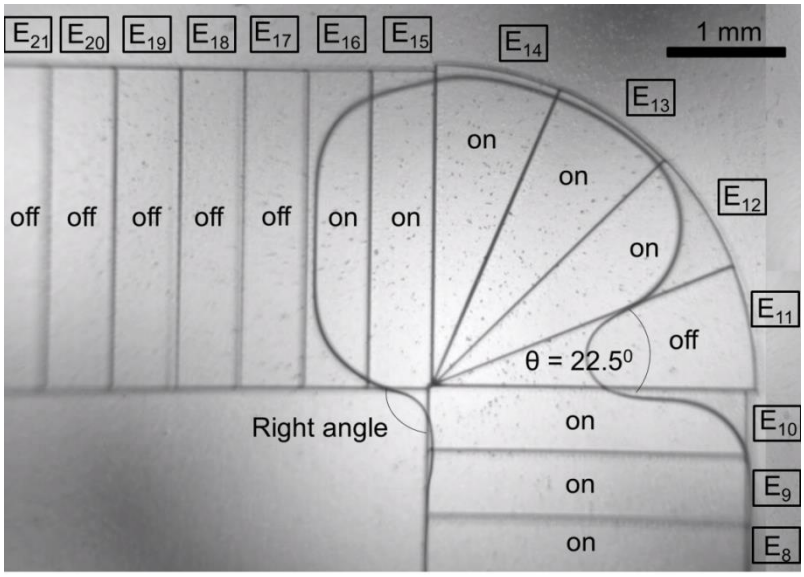

Figure 5.15 At the beginning of forming a droplet. De-wetting occurs on the stripped electrode E_{11} and pinch-off starts. Stripped electrodes $E_1 - E_{10}$: wetting, E_{11}: de-wetting, $E_{12} - E_{16}$: wetting, E_{17}, E_{18}…de-wetting.

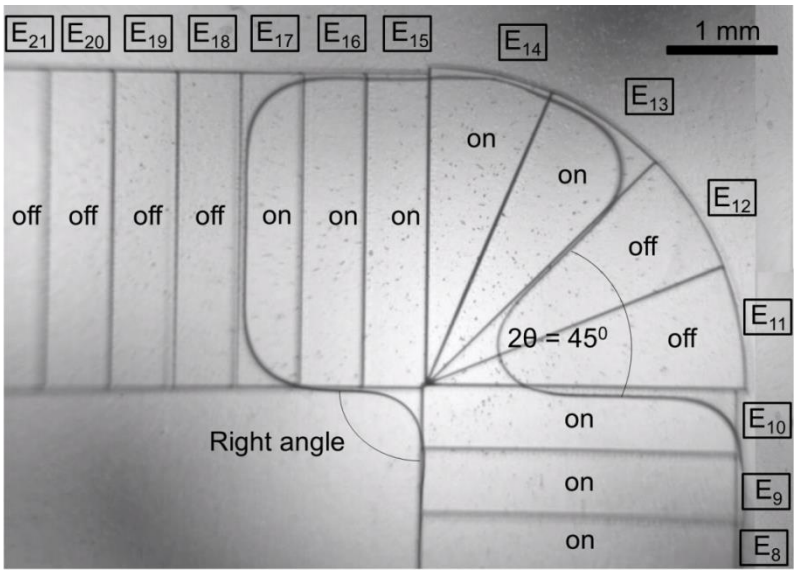

Figure 5.16 Droplet is on electrodes $E_{13} - E_{17}$. De-wetting occurs on both E_{11} and E_{12}. Neck formation is growing up

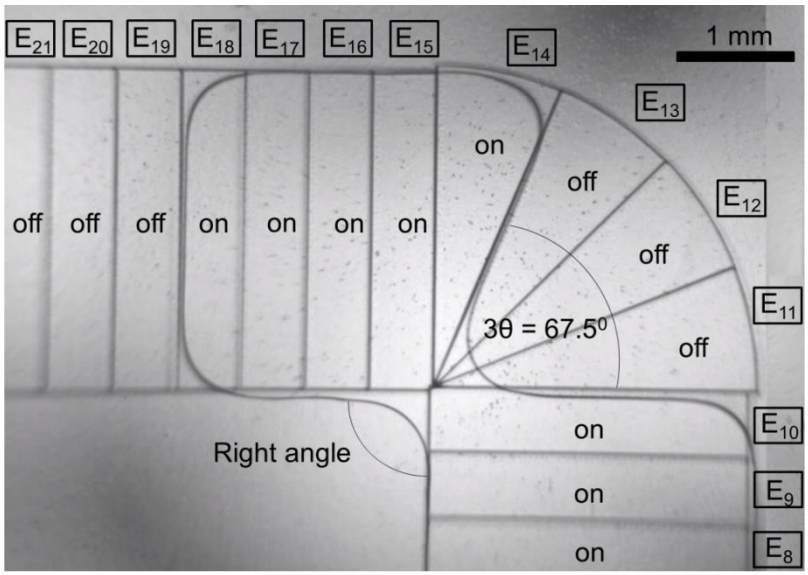

Figure 5.17 Droplet is on electrodes $E_{14} - E_{18}$. De-wetting occurs on electrodes $E_{11} - E_{13}$. Neck formation is becoming narrower

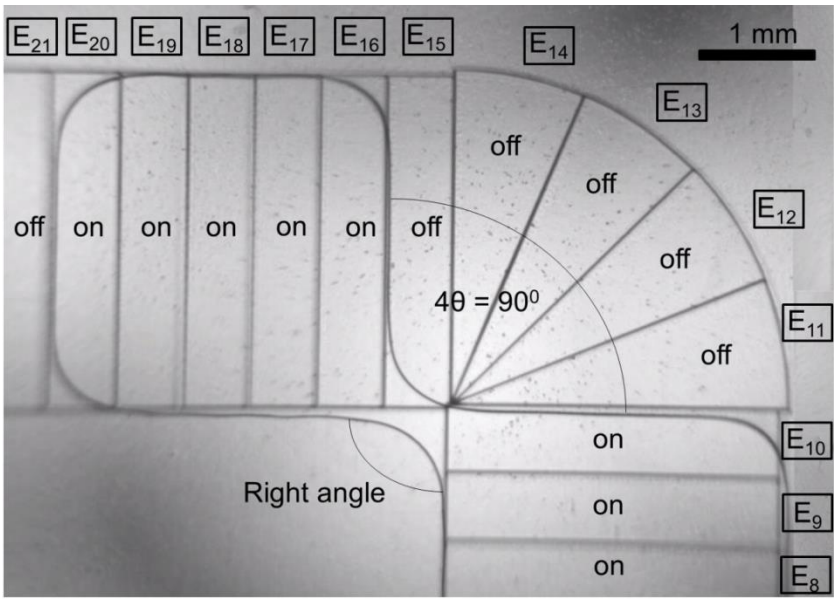

Figure 5.18 Square shaped droplet has already been formed on electrodes $\mathrm{E}_{15} - \mathrm{E}_{19}$. De-wetting occurs on electrodes $\mathrm{E}_{11} - \mathrm{E}_{14}$. Neck formation is still growing

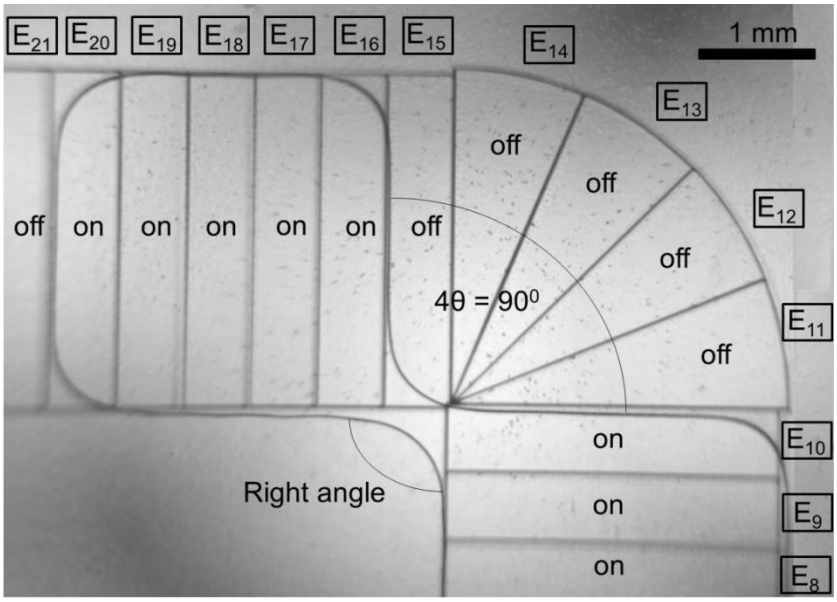

Figure 5.19 Already formed droplet before pinch-off

Droplet is on the electrodes 16-20. De-wetting occurs on electrodes 11-15. As soon as the next set of electrodes (17-21) is activated, pinch-off occurs and droplets is separated from the liquid column. The size of the set of electrodes (17-21) on which droplet occupies is $2.83 \times 2.83\ mm^2$. The boundaries of both liquid droplet and the reservoir drop are positioned in acute angular shape by the edges of the electrodes. It creates higher pressure on the liquid neck at the acute angle of the L-junction. This higher pressure enhances the pinch-off and a droplet is created as a result.

Table 5.2 Comparison of speed of drop dispensing and reproducibility of TCC reservoir and L-junction, Supplied voltage is 120 V for both cases

Drop dispensing from the TCC reservoir		Drop dispensing from the L-junction	
Maximum speed of drop dispensing (minimum drop dispensing time)	Maximum speed of reproducibility	Maximum speed of drop dispensing (Minimum drop dispensing time)	Maximum speed of reproducibility
300 ms	3 drops per second	11 ms	90 drops per second

Although TCC reservoir dispenses droplets with higher volume precession, its rate of reproducibility is much lower. Therefore, TCC reservoir is not suitable for steady state drop delivery for longer time with a higher frequency. According to the above table, the rate of reproducibility of the L-junction is much higher than the that of the TCC reservoir. Therefore, L-junction is much suitable for drop dispensing purposes.

5.4.4 Comparing L-Junction with the Conventional Design

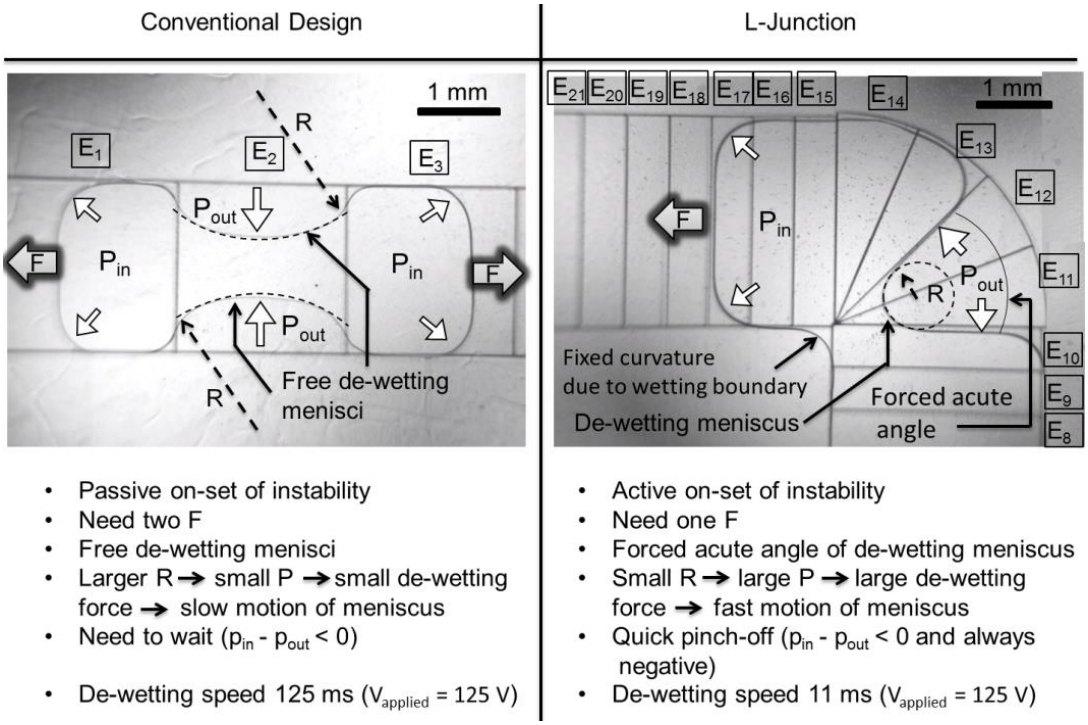

Figure 5.20 Comparison of L-junction drop dispensing with the conventional method

To dispense a droplet by either conventional reservoir or TCC reservoir, two electrodes are activated at the same time; 1) reservoir electrode and, 2) drop dispensing site. This process is comparable with conventional design of splitting a droplet into two by applying two opposite forces by two electrodes. In the conventional design, the way that the droplet is finally pinch-off is due to the hydrodynamic instability. Initially the droplet is stable. Now we apply forces in two different directions. That force creates liquid motion. Some mass is moving opposite direction while area within the droplet is being emptied. Because of that, pressure difference is developed within the droplet. This pressure difference forces two menisci to keep pushing in towards each other from two opposite directions making a neck formation. Sometimes, although we see that this neck is there, the cutting does not happen. Sometimes, necking happens and finally gets cut. This cutting process totally depends on the hydrodynamic instability and it is a major role in droplet pinch-off process.

The problem of conventional design is, it is passive on-set of instability. What it means is we are very irresponsible of cutting the droplet. That is, we do not know this instability is really happening or not. The liquid column becomes unstable if $P_{in} - P_{out} < 0$ under two opposite forces (F). If the instability happens, we have to wait until the unstable menisci are setup. Once it is set up, it is moving towards each other. This motion is called de-wetting. According to the Laplace equation, pressure is defined by $P \propto \gamma(1/R)$. Although we are trying to control the meniscus size, it is still large on the solid electrodes compared to the stripped electrodes. That is principle of radius (R) is large. For large R, P is small from the Laplace equation. Smaller P means small de-wetting force. That means slow de-wetting or slow motion of the meniscus.

Not like in the conventional method, we apply only one force (F) in the L-junction. There is always a wetting boundary with a fixed curvature and only one de-wetting meniscus. Because of the wetting boundary is a very clear cut and angular stripped electrodes are smaller than solid electrodes, we are forcing to make an acute angle of the de-wetting meniscus. For an acute angle, the pressure difference $P_{in} - P_{out} < 0$ and is always negative. Further, the principle radius of the meniscus of acute angle is very small. For small R, P is large from the Laplace equation. Smaller P means large de-wetting force. That means fast de-wetting or fast motion of the meniscus.

5.4.5 Multiple Drop Dispensing at the Y-Junction

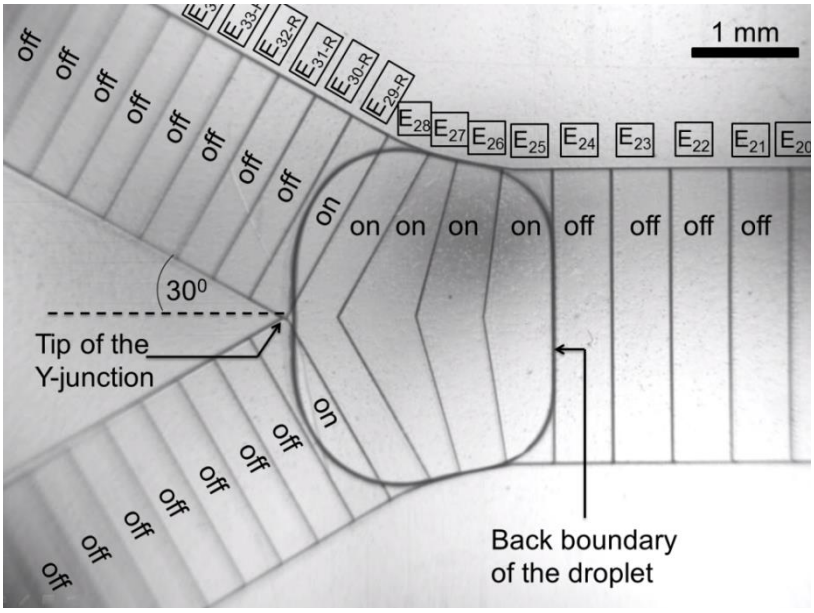

Figure 5.21 Droplet dispensed from the L-junction has arrived to the Y-junction. Stripped electrodes 24-28 are wetting

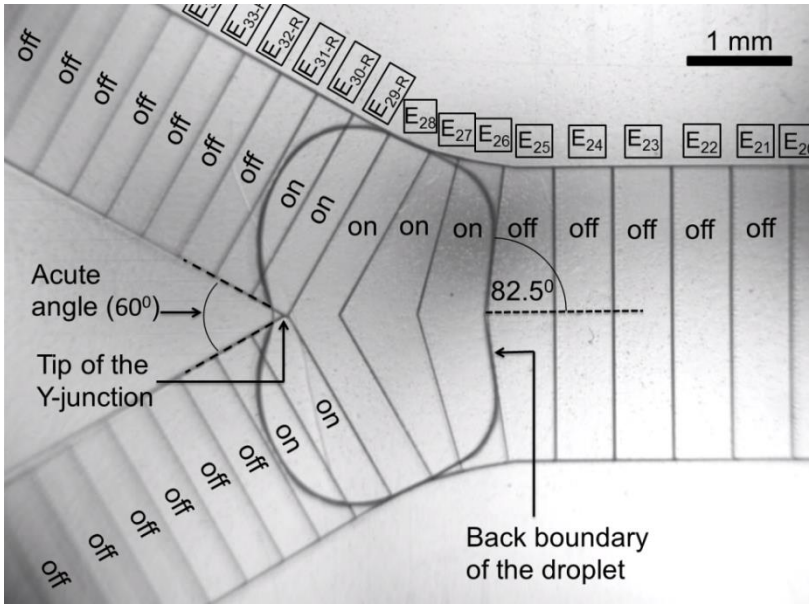

Figure 5.22 Liquid droplet at the beginning of Y-junction splitting

The angular edge of the stripped electrode ($\alpha = 82.5^0$) pushes the back boundary of the droplet towards the tip of the Y-junction. Front boundary of the droplet is pulled forward along the L and R branches by higher EWOD force. The inner boundary of the Y-junction ($\theta = 30^0$) hold the front boundary of the liquid drop at the middle.

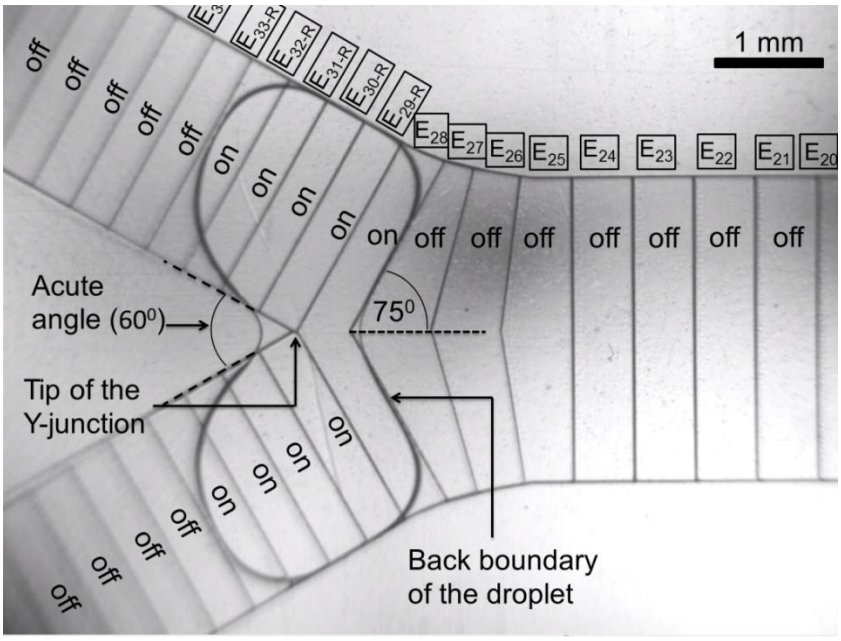

Figure 5.23 Formation of two droplets

As the two droplets are continued to be pulled by the *L* and *R* branches, higher pressure is developing at the middle of the back boundary of the liquid drop. As a result of that, liquid droplet becomes narrower at the middle.

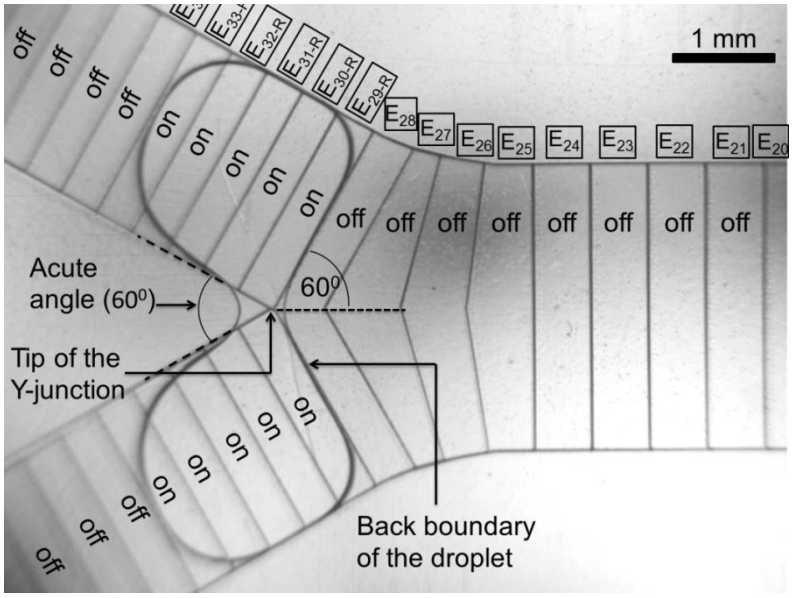

Figure 5.24 Already formed two droplets before the separation: fixed radius of curvature at the middle of the front meniscus

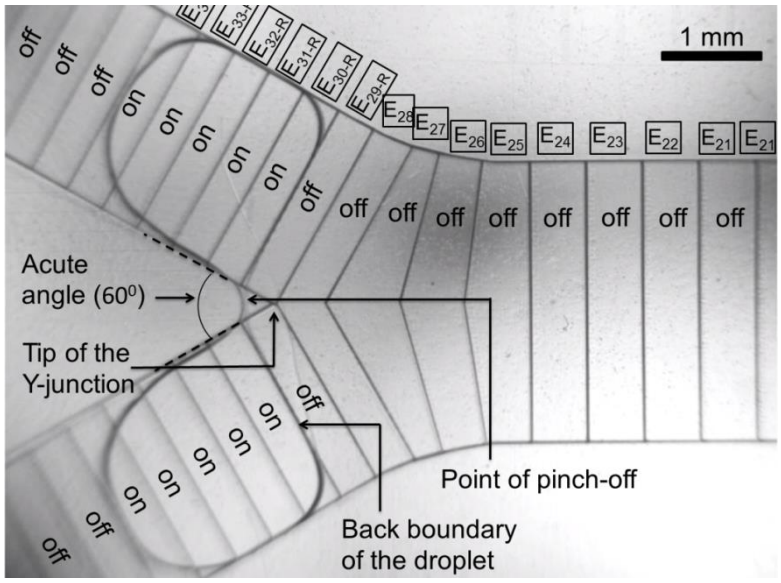

Figure 5.25 Pinch-off of the two droplets

As represented in the Figure 5.24, during the forward motion of the droplets, certain length of the front meniscus of the liquid drop aligns along the inner edges of the Y-junction (θ =

30^0). As a result of that, the radius of curvature of the front meniscus at the middle remains fixed throughout the motion. As the already formed droplets continued to be pulled forward along the *L* and *R* branches, back meniscus meets the fixed front meniscus at which pinch-off occurs

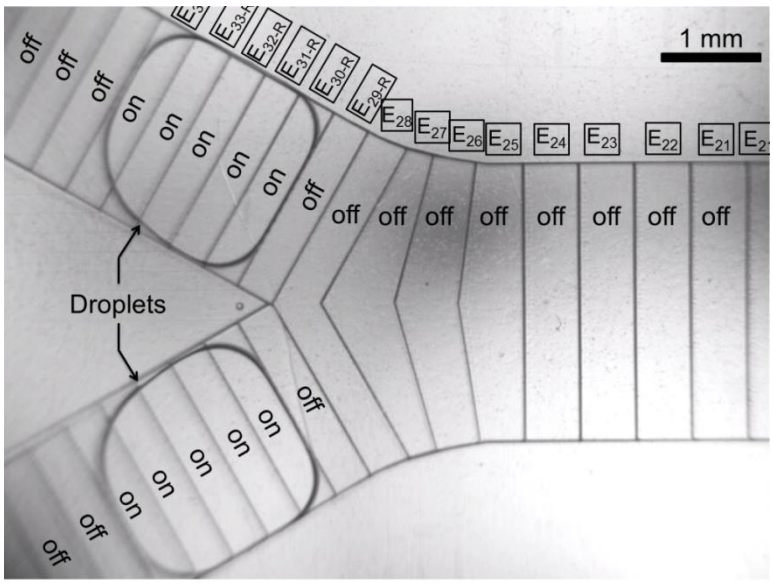

Figure 5.26 Created two droplets after separation

Table 5.3 Comparing the capability of drop splitting at both C-junction and Y-junction

Maximum speed of droplet splitting at the C-junction	Maximum speed of droplet splitting at the Y-junction
100 ms	5 ms

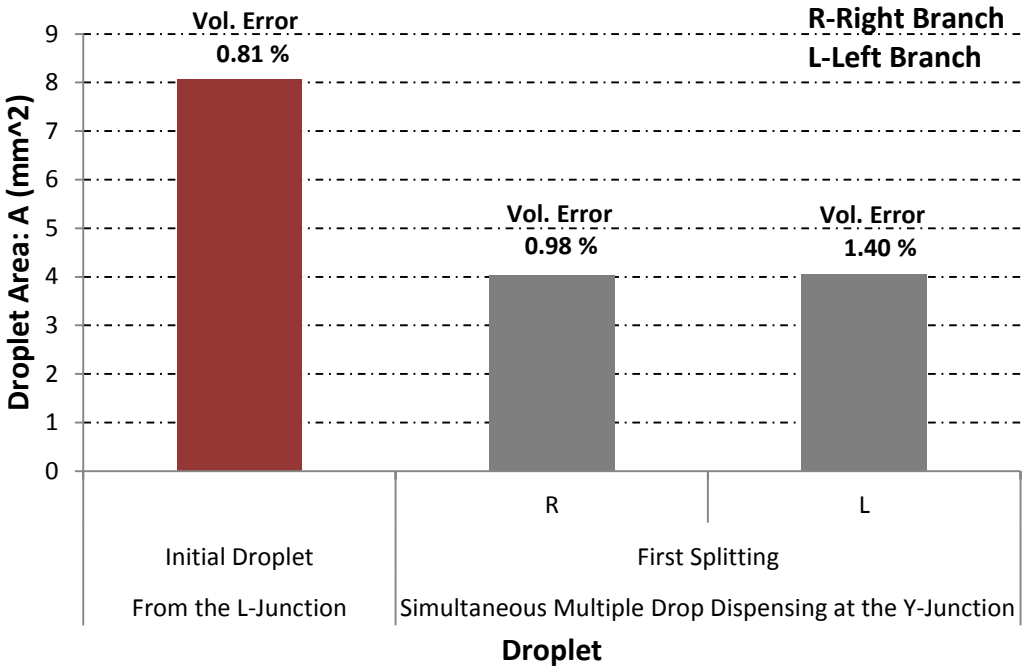

Figure 5. 27 Volume precision of one liquid droplet moving from the L-junction to the spreading zone

According to the above Figure 29, volume precision of the droplet dispensed from the L-junction is much higher. Not like the C-junction splitting, the volume variation of the unit droplet arriving to the spreading zone through the Y-junction is within acceptable range. Therefore, L-junction together with the Y-junction splitting demonstrates higher volume precision of the unit droplets, higher speed of drop dispensing and higher rate of reproducibility.

5.4.6 Comparing C-Junction with the Y-Junction

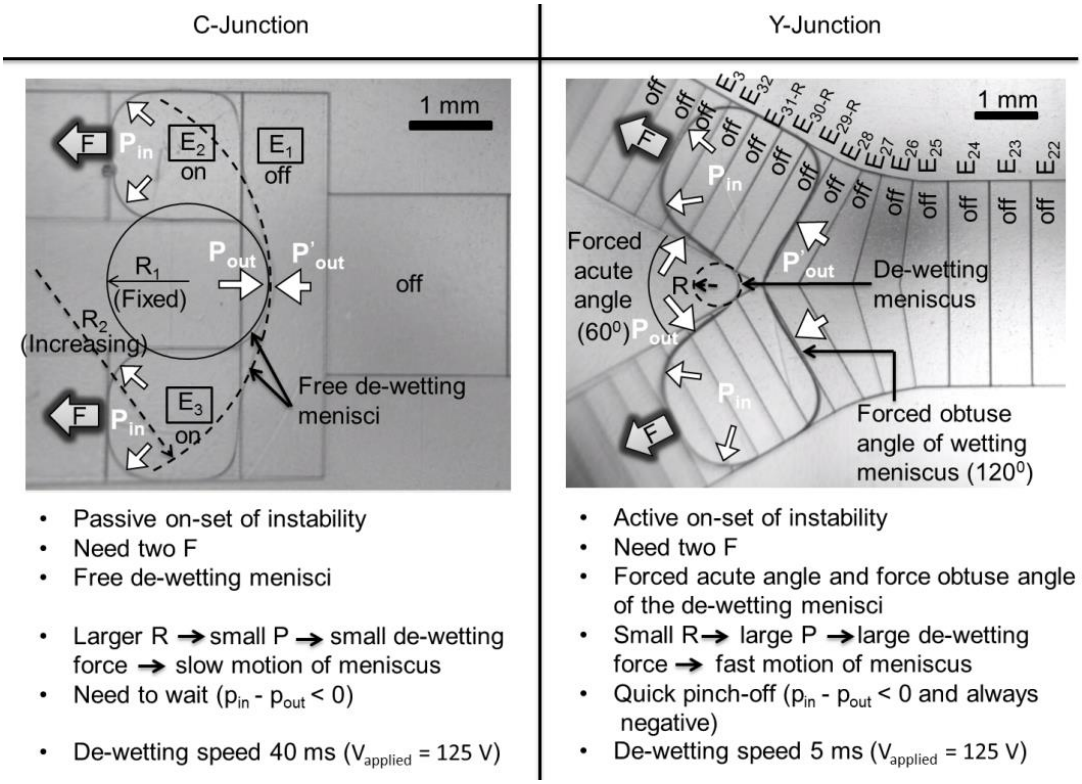

Figure 5.28 Comparison of droplet splitting at the Y-junction with the droplet splitting at the C-junction

In C-junction splitting, instability of the liquid column happens while two forces (F) are applied in the same direction. Curvature (R_1) of inner meniscus is fixed (solid circle). Curvature of the outer meniscus (R_2) is increasing while it is moving towards the inner meniscus (dashed arc). The problem of C-junction splitting is that it is passive on-set of instability. We do not know this instability is really happening or not. The liquid column becomes unstable if $P_{in} - P'_{out} < 0$, $P_{in} - P_{out} < 0$ and $P'_{out} - P_{out} < 0$. If the instability happens, we have to wait until the unstable menisci are setup. Once it is set up, outer meniscus is moving towards the inner meniscus until the liquid column finally gets cut. Since C-junction is designed with solid electrodes the meniscus size is large. That is principle radii of curvature (R_1 and R_2) are large. For large R, P is small

from the Laplace equation. Smaller P means small de-wetting force. That means slow de-wetting or slow motion of the meniscus.

In Y-junction splitting, the back boundary of the droplet is always wetting with obtuse angles (165^0, 150^0 and 120^0). The front meniscus is de-wetting. This front meniscus is forced to make an acute angle (60^0) by the inner edges of the Y-junction. For an acute angle, the pressure difference $P_{in} - P_{out} < 0$ and is always negative. Further, the principle radius of the meniscus of acute angle is very small. For small R, P is large from the Laplace equation. Smaller P means large de-wetting force. That means fast de-wetting or fast motion of the meniscus.

5.5 Conclusion

In this chapter, we report the liquid delivery capabilities of EWOD DMF towards high efficient cooling technology based on thin-film evaporations. The third challenge of EWOD coolant delivery part, which is increasing droplet arrival frequency to the SHNC spreading region while decreasing the droplet volume, is overcome successfully. To develop the droplet delivery system, a simultaneous multiple drop generating method called C-junction splitting is introduced. To further improve the droplet delivery system, a novel reservoir called L-junction reservoir and a novel simultaneous multiple drop generating method called Y-junction splitting are introduced. Not like the previous TCC reservoir, the L-junction reservoir dispenses droplets at high rate of reproducibility while maintaining the higher volume accuracy. At the Y-junction, the droplets dispensed from the L-junction split into two unit droplets in the same speed with higher volume accuracy. Therefore, L-junction together with the Y-junction are suitable for steady state drop delivery for longer time with a higher volume accuracy and higher frequency.

CHAPTER 6

CONCLUSION AND SUMMARY

In this study, we report completion of three essential requirements of the EWOD DMF towards the thin-film evaporative cooling platform: (1) dispensing coolant droplets from the reservoir with highly identical volume, (2) fast motion of coolant droplets to the hotspot to avoid dry-out (3) increasing the droplet arrival frequency to the spreading zone while decreasing the droplet volume. First, to enhance the volume precision and consistency of the coolant droplets, a novel design of reservoir called TCC reservoir with rectangular drop dispensing site is introduced. By optimizing the layout of the reservoir electrodes, the cutting length and the tail formation is minimized. A consistent point of pinch-off is achieved by controlling the menisci formation along the orthogonal direction to the symmetric axis of the reservoir. This reservoir demonstrates a very high average volume precision of ± 3.7 %.

To improve the volume precision further, the rectangular drop generating site of the TCC reservoir is replaced by circular and angular one. This drop generating site is patterned inside the T-electrode such that the cutting length and the tail formation are completely eliminated. The point of pinch-off is properly controlled and exactly located. The volume error of the droplet is reduced down to zero. This modified reservoir demonstrated a much higher volume precision of 0.083 % which is 50 times higher than that obtained from the rectangular drop generating site and TCC reservoir. Experimental results are compared with numerically simulated results and they show considerable agreement.

Second, to enhance the speed of coolant droplets, three major parameters that affect the speed of drop motion are studied; 1) effect of surface roughness, 2) electrode size, and 3) electrode geometry. To study the effect of surface roughness, PCB based EWOD substrate and

glass based EWOD substrate are tested. EWOD device based on PCB has large surface roughness (as large as ~ 8 μm) and waviness. These factors prevent the drop motion at high speed. Therefore, EWOD device on glass plate are suggested to remove those factors. To study the effect of electrode size, drop motion on electrodes with different sizes ($2 \times 2\ mm^2\ and\ 3 \times 3\ mm^2$) is tested. Higher speed of drop motion is achieved for larger electrodes.

It is found experimentally that the switching time corresponding to the maximum speed is 50 ms and this value is not dependent on the electrode size. To study the effect of electrode geometry, two electrode geometries are tested; 1) square electrodes, and 2) a set of 5 rectangular strips of electrodes. Much higher EWOD force is exerted on the droplet, with the second geometry of electrodes, hence, ten times faster speed (400 mm/s) of drop motion was achieved.

Finally, to enhance the coolant droplet arrival frequency to the spreading zone (e.g. hot spot), a novel technique of simultaneous dispensing of multiple drops, called C-junction splitting, is introduced. Using this technique, the droplet arrival frequency to the heated section is increased while the droplet volume that arrives to the heated section is decreased. The particular design that we tested in this study reduced the unit drop volume four times smaller than the volume of a drop generated from a TCC reservoir. However, in this method, drops arriving to the spreading zone have considerable volume variation (~10 %). Further, the rate of droplet splitting at the C-junction is very slow (10 drops per second). Moreover, time to generate a unit drop from a TCC reservoir is long so that only 3 droplets per second could be generated. Therefore, the droplet delivery system developed by C-junction splitting together with the TCC reservoir is not capable enough to satisfy the expected cooling requirements.

As a solution for the above issue, a novel reservoir called L-junction reservoir and a novel simultaneous multiple drop dispensing method called Y-junction splitting are introduced. Drop dispensing at L-junction is significantly faster so that it can dispense 90 droplets per second while maintaining the higher volume precision (< 5 %). At the Y-junction, the droplet

dispensed from the L-junction splits into two unit droplets in the same speed with higher volume precision.

In future, we plan to develop and characterize a fully completed and automated EWOD DMF system for SHNC thin film evaporation using L-junction drop dispensing and Y-junction splitting.

REFERENCES

[1]. Syms,R.R.A., Yeatman, E.M., Bright, V.M., and Whitesides, G.M., Surface Tension-Powered Self-Assembly of Microstructures- The State-of-the-Art, Journal of Microelectromechancal Systems, Vol. 12, No.4, 2003, Page 387-417.

[2]. Lu,Z., Chen, P.C.Y. and Lin, W., *Force Sensing and Control in Micromanipulation, IEEE Transactions on Systems, MAN, and Cybernetics-Part C: Applications and Reviews, Vol.36, No.6, November 2006, Page 713-724.*

[3]. Lee, J., Moon, H., Fowler, J., Schoellhammer, T. and Kim,C.J., *electrowettting and electrowetting-on-dieletric for microscale liquid handling*, Sensors and Actuators A 95 (2002) 259-268.

[4]. Pratap, V., Moumen, N. and Subramanian, R.S., *Thermocapillary Motion of a Liquid Drop on a Horizontal Solid Surface,* Langmuir 2008, 24, 5185-5193.

[5]. Sammarco, T.S. and Burns, M.A., *Thermocapillary Pumping of Discrete Drops in Microfabricated Analysis Devices*, Reactors, Kinetics, and Catalysis, February 1999 Vol. 45, No. 2, page 350-366

[6]. Saeki, F., Baum, J., Moon, H., Yoon, J.Y., Kim, C.J. and Garrell, R.L., *Electrowetting on Dielectrics (EWOD): Reducing Voltage Requirements for Microfluidics*

[7]. Wan, Z.L., Feinerman, A., Zeng,H.J. and Friedman, G., *Electrocapillary Piston Motion and a Prototype of Phase-Manipulating Micromirror,* Journal of Microelectromechanical Systems, Vol. 13, No. 4, 2004, Page 620-627.

[8]. Berge, B. and Peseux, J., *Variable focal lens controlled by an external voltage: An application of electrowetting,* The European Physical Journal E, 3, 159–163 (2000)

[9]. Verheijen, H.J.J. and Prins, M.W.J., Reversible Electrowetting and Trapping of Charge: Model and Experiments, Langmuir 1999, 15, 6616-6620, Page 6616-6620.

[10]. Walker, S.W. and Shapiro, B*., Modeling the Fluid Dynamics of Electrowetting on Dielectric (EWOD)*, Journal of Microelectromechanical Systems, Vol. 15, No. 4, 2006, Page 986-1000

[11]. Lee. J., Moon, H., Fowler, J., Kim, C.J. and Schoellhammer, T., *Addressable Microliquid Handling by Electric Control of Surface Tension*, in Proc, IEEE Int. Conf. MEMS, Interlaken, Switzerland, Jan 2001, Page 499-502

[12]. Moon, H., Cho, S.K., Garrell, R.L. and Kim, C.J., Low voltage electrowetting-on-dielectric, Journal of Applied Physics, Vol. 92, No. 7, 2002, Page 4080-4087.

[13]. Yi, U.C. and Kim, C.J., *Characterization of electrowetting actuation on addressable single-side coplanar electrodes*, Journal of Micromechanics and Microengineering, 16 (2006) Page 2053–2059

[14]. Pollack, M.G., Fair, R.B. and Shenderov, A.D., *Electrowetting-based actuation of liquid droplets for microfluidic applications,*Applied Physics, Vol. 77, No. 11, 2000, Page 1725-1726.
[15]. Gong, Jian and Kim, C.J., *All-electronic droplet generation on-chip with real-time feedback control forEWOD digital microfluidic,* Lab on a Chip, 2008,**8**, Page 898-906

[16]. Digilov, R., Charge-Induced Modification of Contact Angle: The Secondary Electrocapillary Effect, Langmuir, 2000, 16, Page 6719-6723

[17]. Cho, S.K., Moon, H. and Kim,C.J., Crating, Transporting, Cutting, and Merging Liquid Droplets by Electrowetting-Based Actuation for Digital Microfluidics Circuits, Journal of Microelctromechanical Systems, 2003, Vol. 12, No. 1, Page 70-80.

[18]. Gong, J., Fan, S.K. and Kim, C.J., Portable Digital Microfluidics Platform with Active but Disposable Lab-On-Chip, IEEE, 2004, Page 355-358

[19]. Cheng, J.T. and Chen, C.L., Active thermal management of on-chip hot spots using EWOD-driven droplet microfluidics, Exp Fluids (2010) 49:Page 1349–1357

[20]. Chakrabarty, K., Design, Testing, and Applications of Digital Microfluidics-Based Biochips, Proc. 18th International Conference, 2005

[21]. Fair, R.B., Khlystov, A., Tailor, T.D., Ivanov, V., Evans, R.D., Srinivasan, V., Pamula, V.K., Pollack, M.G., . Griffin, P.B., Drexel, J.Z., Chemical and Biological Applications of Digital-Microfluidic Devices, Biochips, 2007, Page 10-24

[22]. Glassman B.S., Spray cooling for land, sea, air and space based applications, a fluid management system for multiple nozzle spray cooing and a guide to high heat flux heater design, Master of Science Thesis, Department of Mechanical, Materials and Aerospace Engineering, University of Central Florida, (2005).

[23]. Paik, P.Y., Pamula, V.K. and Chakrabarty, K., Adaptive Cooling of Integrated Circuits Using Digital Microfluidics, IEEE Transactions on Very Large Scale Integration (VLSI) Systems, Vol. 16, No. 4, 2008, Page 432-443.

[24]. Moon, H., Bindiganavale, S., Nanayakkara, Y., and Armstrong, D.W., Digital Microfluidic Device Using Ionic Liquid for Electronic Hotspot Cooling, Proc 7th International ASME Confenerce on ICNMM2009, Pohang, South Korea, 2009.

[25]. Pamula, V.K. and Chakrabarty, K., Cooling of Integrated Circuits Using Droplet-Based Microfluidics, Proceeding of ACM Great Lakes Symposium on VLSI, pp. 84 – 87, 2003.

[26]. Anderson J.L. and Armstrong, D.W., High-stability ionic liquids. A new class of stationary phases for gas chromatography, Analytical Cemistry, 2003, 75(18):4851-8.

[27]. Castro, C.A.N., Lourenco, M.J.V., Ribeiro, A.P.C., Langa, E. and Vieira, S.I.C., Thermal Properties of Ionic Liquids and IoNanofluids of Imidazolium and Pyrrolidinium Liquids, J. Chem. Eng. Data 2010, 55, 653–661

[28]. Nikapitiya, N.Y.J.B. and Moon, H., Thermal Conductivity Enhancement of Room Temperature Ionic Liquids (RTILs) with Various Magnetic Nanoparticles. Proc. ASME 2012 3rd MNHMT2012, Atlanta, Georgia, 2012.

[29]. Pautsch, A.G., Shedd,T.A. and Nellis, G.F., Thickness Measurements of the Thin Film in Spray Evaporative Cooling, Inter Society Conference on Thermal Phenomena,2004, Page 70-76

[30]. Incropera F.P. and Dewitt D.P., Fundamentals of Heat and Mass Transfer. 5th ed. New York: John Wiley & Sons (2002).

[31] S. Tan, Computer Simulation of a Spray Cooling System with FC-72, PhD thesis, University of Central Florida, Orlando, Florida, 2001.

[32]. Gong, J. and Kim, C.J., Two-Dimensional Digital Microfluidic System by Multi-Layer Printed Circuit Board, IEEE, 2005, Page 726729

[33]. Ren, H., Srinivasan, V., and Fair, R.B., Design and testing of an interpolating mixing architecture for electrowetting-based drop- let on-chip chemical dilution, In: 12th International conference- Inter Conf on solid-state sensors, actuators and microsystems. Digest of Technical Papers, (2003a), pp 619–622

[34]. Wang, W., Jones, T.B. and Harding, D.R., On-Chip Double Emulsion Droplet Assembly Using Electrowetting-On-Dielectric and Dielctrophoresis, Fusion Science and technology, Vol. 59, 2001, Page. 240- 249.

[35]. J.Berthier et al, Sensors and Acyuators A, 127, 283, (2006)

[36]. Fair, R.B., Digital microfluidics: is a true lab-on-a-chip possible?, Microfluid Nanofluid (2007) 3:245–281

[37]. Gong, Jian and Kim, C.J., *All-electronic droplet generation on-chip with real-time feedback control forEWOD digital microfluidic,* Lab on a Chip, 2008,**8**, Page 898-906

[38]. Dittrich, P.S. and Manz, A., Lab-on-a-chip: microfluidics in drug discovery, Nat. Rev., Drug Discovery, 2006, Page 210-218.

[39] Ren, H. and Fair, R.B., MicroNano Liter Droplet Formation and Dispensing by Capacitance Metering and Electrowetting Actuation, WA4, Assembly, patterning and manipulation on the nanoscale, IEEE-Nano 2002, pp. 369-372.

[40]. Gong, J., Fan, S.K. and Kim, C.J., Portable Digital Microfluidics Platform with Active but Disposable Lab-On-Chip, Proceedings of 17th IEEE International Conferen e on Microelectromechanical Systems, Masstricht, Netherlands, 2004, Page 355-358.

[41]. Gong, J. and Kim, C.J., Two dimensional Digital Microfluidic System by Multi-layer Printed Circuit Board, Proceedings of 18th IEEE International Conference on Microelectromechanical Systems, Miami USA, 2005, Page 726-729.

[42]. Gong, J. and Kim, C.J., Characterization and Design of Digitizing Process for Uniform and Controlable droplet volume in EWOD Digital Microfluidics, Proceedings of Hilton Head 2006: A Solid State Sensors and Microsystems Workshop, Hilton Head Island, SC, USA, 2006, Page 159-162.

[43]. Gong, J. and Kim, C.J., Real-Time Feedback Control of Droplet generationfor EWOD Digital Microfluidics, Preceedings of 10th International Conference on Miniaturized Systems for Chemistry and Life Sciences, Tokyo, Japan, Page 1046-1048.

[44]. Ren, H., Srinivasan, V. and Fair, R.B., Automated electrowetting- based droplet dispensing with good reproducibility. Proceedings of MicroTAS 2003: (2003b), Page 993–996

[45]. Ren, H., Electrowetting-based sample preparation: an initial study for droplet transportation, creation and on-chip digital dilution, 2004, Ph.D. Tthesis, Duke University

[46]. Cho, S.K., Kim, C.J., Particle separation and concentration control for digital microfluidic systems, Proc IEEE Micro Electro Mech Syst (MEMS), 2003, Page 686–689

[47]. Yi, U.C., Kim, C.J., “Soft printing of droplets pre-metered by electrowetting”, Sens. Actuators A, Phys., vol.114, no.2/3, pp.347-354, Sep. 2004

[48]. Gong, J. and Kim, C.J., Direct-Referencing Two-Dimensional-Array Digital Microfluidics Using Multilayer printed Circuit board, Journal of Microelectromechanical Systems, Vol. 17, No.2, April 2008

[49]. Pautsch, A.G., Shedd,T.A. and Nellis, G.F., Thickness Measurements of the Thin Film in Spray Evaporative Cooling, Inter Society Conference on Thermal Phenomena,2004, Page 70-76

[50]. Incropera F.P. and Dewitt D.P., Fundamentals of Heat and Mass Transfer. 5th ed. New York: John Wiley & Sons (2002).

[51] S. Tan, Computer Simulation of a Spray Cooling System with FC-72, PhD thesis, University of Central Florida, Orlando, Florida, 2001.

BIOGRAPHICAL INFORMATION

Jagath B. Yaddessalage received his BS degree in July 2007 from the Department of Physics, University of Kelaniya, Sri Lanka. His Bachelor's thesis is to design an economical computer-interfaced current source and a measure unit. He has been a PhD student in the Department of Mechanical and Aerospace Engineering at the University of Texas at Arlington since spring 2009. His current research interest is developing new techniques to improve the volume precision and enhance the speed and frequency of the droplets in the EWOD device. In future, he will be developing a fully automated and controllable coolant delivery system based on EWOD and characterizing thin film evaporation on SHNC.